Architecture and Power Balancing Strategies of Multifrequency Microgrid

A

Thesis Submitted

in Partial Fulfilment of the Requirements

for the Degree of

DOCTOR OF PHILOSOPHY

By

Rajdip Dey

Department of Electronics and Electrical Engineering

Indian Institute of Technology Guwahati

Guwahati - 781039, India

July 2022

Certificate

This is to certify that the thesis entitled "**Architecture and Power Balancing Strategies of Multifrequency Microgrid**", submitted by **Rajdip Dey**, a research scholar in the *Department of Electronics and Electrical Engineering, Indian Institute of Technology Guwahati*, for the award of the degree of **Doctor of Philosophy**, is a record of an original research work carried out by him under my supervision and guidance. The thesis has fulfilled all requirements as per the regulations of the institute and has reached the standard needed for submission. The results embodied in this thesis have not been submitted to any other University or Institute for the award of any degree or diploma.

Dated:

Guwahati.

Dr. Shabari Nath
Associate Professor
Dept. of Electronics and Electrical Engg.
Indian Institute of Technology Guwahati
Guwahati - 781039, Assam, India.

Acknowledgement

I would like to convey my earnest gratitude to my thesis supervisor Dr. Shabari Nath. Her persistent guidance, extensive support, and continuous encouragement throughout the years have acted as a catalyst for my research journey to be fruitful. It would not be possible to achieve the desired current form of my research work without her precious time and foresight of work.

I am also thankful to my doctoral committee members Prof. Chitralekha Mahanta, Dr. Praveen Tripathy, and Dr. A. Ravindranath for their productive and immense guidance for ensuring the quality of my thesis and assuring timely completion of my research.

I would like to thank all the faculty members of the Electrical Engineering department of NIT Durgapur for their help and cooperation in my thesis work. I want to thank Dr. Tushar Kanti Bera for giving permission to use his hardware laboratory and for helping me with the vast knowledge of hardware set-ups.

My gratitude seems very little to my father Nitya Ranjan Dey, my mother Ila Dey, my teacher Sankar Roy and my brother Subhadip Dey for their continuous support in all ways. The backbone of this entire journey is my wife Anindita Roy. Her immense support in all my hard times, her extreme sincerity, and her respect to my research work have kept myself on track.

Every course ends up with some good friends and valuable colleagues who make harder things easier and be part of the rest of my life. I would prefer to mention the names like Gayatri Nayak, Deepak Kumar, Wasim Akram, Vivek Joshi, Deepankar Kumar, Kumar Abhinav, Ramyani Chakrabarty, Pramith Nandi, Nishant Anurag, Nupur, Paban Barua, and Archit for providing me all kind of support at any time. Apart from this, there are so many people involved in my research journey to whom I am thankful and respectful for the rest of my life.

Above all, I am grateful to God for showering never-ending blessings and countless opportunities to accomplish my research work.

Abstract

A new type of microgrid called multifrequency microgrid (MFMG) is investigated in this thesis. It is formed based on the superposition theorem, orthogonal power flow theory, and frequency selectivity criteria. It is a unique system where different frequency voltages and currents are present on the multifrequency (MF) bus and different frequency powers maintain orthogonality and transmit simultaneously through the MF bus without mixing. Frequency selectivity criteria states that the consumers can choose any available frequency power from the MF bus based on their requirements. MFMG has several advantages over traditional AC or DC microgrids like higher efficiency, higher transmission capacity, higher degree of functionality, and higher flexibility. This research work focuses on the basic architecture, converters, and control strategies of MFMG.

MFMG concept has been explored very little in the literature. The basic architecture and converter for MFMG is still not defined. In this thesis, the basic architecture of MFMG is defined where a voltage source converter named DC/MF converter acts as the building block. The DC/MF converter is used as grid side, grid feeding, grid forming, load side, and battery side converter, and all control strategies are explained. The DC/MF converter structure is proposed and modelling of the DC/MF converter is performed with the state space analysis method. Different controllers are designed using the transfer functions of the small signal model of the DC/MF converter to control the output voltage and current. The modelling and controller designs are verified by open loop hardware and closed loop simulation results.

The presence of different frequency powers on the MF bus and frequency selective power transmission create different new active and reactive power imbalance situa-

tions which are not present in traditional microgrids. No power balancing strategy is discussed in the literature for MFMG. In this thesis, all new active and reactive power imbalance cases are discussed and the conditions are identified to balance different frequency active and reactive powers in MFMG for grid connected and islanded modes. New power balancing strategies are proposed here to solve all power imbalance cases based on the power balancing conditions. The power balancing strategies are verified by the circuit simulation of MFMG in the Matlab Simulink environment.

An energy storage system (ESS) needs to be integrated with MFMG due to the uncertainty and intermittency of renewable sources. In this thesis, an algorithm is proposed to coordinate the ESS and different renewable sources to balance different frequency load power demands of MFMG for optimum power generation through communication under a cooperative framework. The framework is constructed based on the assumption that any load prefers to absorb power from the closest source for minimum power loss and cost. The categorization of different source load pairs is done based on the physical distance by different frequencies and accordingly, the algorithm is structured. An 8 bus MFMG is simulated to evaluate the algorithm for different power imbalance cases in the Matlab Simulink environment.

Contents

List of Figures

List of Tables

List of Common Abbreviations

ACMG	AC microgrid
BESS	Battery energy storage system
CONV	Converter
DCMG	DC microgrid
DIPFC	Distributed interline power flow controller
DL	Domestic load
DPFC	Distributed power flow controller
ESR	Equivalent series resistance
ESS	Energy storage system
EV	Electric vehicle
FC	Fuel cell
FFT	Fast Fourier transform
GCF	Gain crossover frequency
GI	Grid interactive
IL	Industrial load
IPFC	Interline power flow controller
LC	Load controller
MF	Multifrequency
MFMG	Multifrequency microgrid
MFMGCCS	Multifrequency microgrid central controller system
MOSFET	Metal oxide semiconductor field effect transistor
MT	Micro turbine

PCC	Point of common coupling
PID	Proportional integral derivative
PSDMS	Power system distribution management system
PV	Photo voltaic
PWM	Pulse width modulation
RMS	Root mean square
SC	Source controller
SSM	Small signal model
SOC	State of charge
SOH	State of health
SVPWM	State vector pulse width modulation
TF	Transfer function
WT	Wind turbine

List of Symbols

$C_A,\ C_B,\ C_C$	Filter capacitor of DC/MF converter
$C_{B1},\ C_{B2}$	Filter capacitor of battery side converter
C_{BESS}	Charge of the battery
C_G	Filter capacitor of grid side converter
C_{GF}	Filter capacitor of grid forming converter
C_{in}	Input side capacitor of DC/MF converter
$C_{L1},\ C_{L2}$	Filter capacitor of load converter
d	Duty cycle of DC/MF converter
D	DC value of the duty cycle of DC/MF converter
$\hat{d}$	Perturbation of duty cycle of DC/MF converter
f_{Cr-Cm}	Compensator gain crossover frequency
f_S	Switching frequency
I_{BESS}	Output current of battery side converter
I_{BESS-A}	Output current of 'A' phase of battery side converter
I_G	Output current of grid side converter
$I_{G1},\ I_{G2}$	Components of output current of grid side converter
I_{G-A}	Output current of 'A' phase of grid side converter
$I_{G-d},\ I_{G-q}$	Direct and quadrature axis component of I_G
I_{GFE}	Output current of grid feeding converter
I_{GFE-A}	Output current of 'A' phase of grid feeding converter

$I_{GFE-d},\ I_{GFE-q}$	Direct and quadrature axis component of I_{GFE}
I_{GI-A}	Output current of 'A' phase of grid interactive converter
I_{GI-A-e}	Error in output current of 'A' phase of grid interactive converter
I_{GI-A-f}	f^{th} frequency component of I_{GI-A}
$I_{GI-A-f-d},\ I_{GI-A-f-q}$	Direct and quadrature axis component of I_{GI-A-f}
I_{in}	Input current of DC/MF converter
i_L	Inductor current of DC/MF converter
$i_L(t)$	Instantaneous inductor current of DC/MF converter
$\hat{i_L}$	Perturbation of inductor current of DC/MF converter
I_L	Input current of load side converter
I_{L-A}	Input current of 'A' phase of load side converter
I_{Lx}	Load current of x^{th} bus
I_{Lx-f}	f^{th} frequency component of I_{Lx}
I_M	Output current of DC/MF converter
$i_M(t)$	Instantaneous output current of DC/MF converter
I_{M-A}	Output current of 'A' phase of DC/MF converter
$I_{M-d},\ I_{M-q}$	Direct and quadrature axis component of I_M
$I_{M-f-diff}$	f^{th} frequency current difference between source and load at MF bus
I_{S-f}, I_{L-f}	f^{th} frequency source and load current
I_{S-f-d}, I_{S-f-q}	Direct and quadrature axis component of I_{S-f}
$I_{S-f-d-max}, I_{S-f-q-max}$	Maximum value of direct and quadrature axis component of I_{S-f}
$I_{S-f-max}$	f^{th} frequency maximum available source current
$K_B^P,\ K_B^R$	Proportional constant of battery side controller
$K_B^I\ K_B^S$	Integral constant of battery side controller
K_{G-V}^P	Proportional constant of voltage loop of grid side controller
K_{G-V}^I	Integral constant of voltage loop of grid side controller

K_{G-I}^{P}	Proportional constant of current loop of grid side controller
K_{G-I}^{I}	Integral constant of current loop of grid side controller
K_{GF}^{P}	Proportional constant of grid forming controller
K_{GF}^{I}	Integral constant of grid forming controller
K_{GFE}^{C}	Compensator constant of grid feeding controller
K_{PW}	PWM gain of controller
$L_A,\ L_B,\ L_C$	Filter inductor of DC/MF converter
L_{B1}	Filter inductor of battery side converter
L_G	Filter inductor of grid side converter
L_{G-A}	Filter inductor of 'A' phase of grid side converter
L_{GF}	Filter inductor of grid forming converter
L_{GF-A}	Filter inductor of 'A' phase of grid forming converter
L_{GFE}	Filter inductor of grid feeding converter
L_{GFE-A}	Filter inductor of 'A' phase of grid feeding converter
L_{L1}	Filter inductor of load converter
$P_1,\ Q_1$	Active and reactive power of single frequency system
$P_3,\ Q_3$	Active and reactive power of three frequency system
$p_3(t),\ q_3(t)$	Instantaneous active and reactive power of three frequency system
$P_0,\ P_{25},\ P_{50}$	Active power of DC, 25 Hz, 50 Hz frequency
P_{BESS}	Battery power
$P_{BESS-max}$	Maximum battery power
P_{BESS-f}	f^{th} frequency component of battery power
P_{ESS}	Energy storage system power
PM_d	Desired phase margin of controller
$P_G,\ Q_G$	Grid active and reactive power
$P_{G-diff},\ Q_{G-diff}$	Active and reactive power differences at grid

$P_{G-f},\ Q_{G-f}$	f^{th} frequency component of grid active and reactive power
$P_L,\ Q_L$	Active and reactive power load demand
$P_{L-f},\ Q_{L-f}$	f^{th} frequency load active and reactive power
P_{LT}	Total load power of MFMG
$P_{Lx},\ Q_{Lx}$	Load active and reactive power of x^{th} bus
$P_{Lx-f},\ Q_{Lx-f}$	f^{th} frequency component of P_{Lx}, and Q_{Lx}
$P_{M-A},\ Q_{M-A}$	Active and reactive power at A phase of MF system
$P_{M-A-f},\ Q_{M-A-f}$	f^{th} frequency active and reactive power component at A phase
P_{M-f-S} , Q_{M-f-S}	f^{th} frequency source active and reactive power at MF bus
$P_{M-f-L},\ Q_{M-f-L}$	f^{th} frequency load active and reactive power at MF bus
$P_{M-f-S-new}$	Changed value of P_{M-f-S}
$P_{M-f-L-new}$	Changed value of P_{M-f-L}
$P_{M-f-S-var}$	Variation in P_{M-f-S}
$P_{M-f-L-var}$	Variation in P_{M-f-L}
$P_{M-f-diff},\ Q_{M-f-diff}$	f^{th} frequency active and reactive power difference at MF bus
$P_{n+1},\ Q_{n+1}$	Active and reactive power of (n+1) frequency system
$P_{S-f},\ Q_{S-f}$	f^{th} frequency source active and reactive power
P_{ST}	Total source power of MFMG
$P_{Sx},\ Q_{Sx}$	Source active and reactive power of x^{th} bus
P_{Sx-av}	Maximum available source active power of x^{th} bus
$P_{Sx-f},\ Q_{Sx-f}$	f^{th} frequency component of P_{Sx}, and Q_{Sx}
$P_{Sx-BESS}$	Battery power component of the source power of x^{th} bus
$Q_{25},\ Q_{50},\ Q_{100}$	Reactive power of 25 Hz, 50 Hz, 100 Hz frequency
R	Load resistance of DC/MF converter
$R_a,\ R_b,\ R_c$	Resistances of Schmitt trigger circuit
R_S	Current sensor resistance of average mode current control

r	Capacitive ESR of DC/MF converter
$s_1(t)$	Instantaneous power of single frequency system
$s_2(t)$	Instantaneous power of double frequency system
$s_{n+1}(t)$	Instantaneous power of (n+1) frequency system
T_S	Total switching time
$v_1(t),\ i_1(t)$	Instantaneous voltage and current of single frequency system
$v_2(t),\ i_2(t)$	Instantaneous voltage and current of double frequency system
$V_{AB},\ V_{BC},\ V_{CA}$	Line voltage of the MF system
$V_{AN0},\ I_{A0}$	DC voltage and current of 'A' phase of the MF system
$V_{AN25},\ I_{A25}$	25 Hz voltage and current of 'A' phase of the MF system
$V_{AN50},\ I_{A50}$	50 Hz voltage and current of 'A' phase of the MF system
V_{BESS}	Battery voltage
v_C	Capacitor voltage of DC/MF converter
$v_C(t)$	Instantaneous capacitor voltage of DC/MF converter
$\hat{v_C}$	Perturbation of capacitor voltage of DC/MF converter
V_{dc}, I_{dc}	DC voltage and current present on the bus of MF system
V_{in}	Input voltage of DC/MF converter
$v_{in}(t)$	Instantaneous input voltage of DC/MF converter
$\hat{v_{in}}$	Perturbation of input voltage of DC/MF converter
V_L	Load voltage
V_{L-A}	'A' phase load voltage
V_{L-DC}	DC bus voltage of load side converter
V_M	Output voltage of DC/MF converter
$v_M(t)$	Instantaneous output voltage of DC/MF converter
$\hat{v_M}$	Perturbation of output voltage of DC/MF converter
V_{M-A}	'A' phase output voltage of DC/MF converter

V_{M-A-e}	Error in V_{M-A}
$V_{M-d},\ V_{M-q}$	Direct and quadrature axis component of V_M
V_{M-f-d}	f^{th} frequency direct axis voltage component of V_M
V_{M-f-q}	f^{th} frequency quadrature axis voltage component of V_M
V_{M-A-f}	f^{th} frequency component of 'A' phase MF voltage
$V_{M-A-f-d}$	Direct axis component of V_{M-A-f}
$V_{M-A-f-q}$	Quadrature axis component of V_{M-A-f}
$v_{n+1}(t),\ i_{n+1}(t)$	Instantaneous voltage and current of double frequency system
V_n, I_n	RMS voltage and current of n^{th} frequency present on the MF bus
V_{P0}, I_{P0}	DC voltage and current component in each phase of MF system
V_{P25}, I_{P25}	25 Hz voltage and current component in each phase of MF system
V_{P50}, I_{P50}	50 Hz voltage and current component in each phase of MF system
V_R	Peak voltage of external ramp signal
v_S	Switched voltage of DC/MF converter
V_S	Source voltage
$V_{th+},\ V_{th-}$	Upper and lower limit of threshold voltage of hysteresis controller
ω_{cr-co}	Controller gain crossover frequency
ω_{P-GFE}	Compensator pole frequency
$\omega_{P,Q}$	Chosen frequency power at load side
ω_{Z-GFE}	Compensator zero frequency
ϕ_{in}	Phase angle of n^{th} frequency current of MF system
ϕ_{vn}	Phase angle of n^{th} frequency voltage of MF system
$\phi_{vn} - \phi_{in}$	Phase angle difference of n^{th} frequency voltage and current waveform
θ_{25}	phase angle between 25 Hz voltage and current in MF system
θ_{50}	phase angle between 50 Hz voltage and current in MF system
$\Delta(H)$	Hysteresis band

1

Introduction

Contents

1.1 Introduction

The current power distribution system faces several challenges related to renewable sources integration, quality of power, and load increment [5]. From the last decade the application of renewable energy sources is increasing rapidly but there are some limitations to connect the sources to the existing grid. Microgrids are a proper way to connect all local loads and renewable sources without any new major construction [6]. Based on the availability of the grid, a microgrid can be operated in grid connected or islanded mode [7]. In grid connected mode, the bus frequency and voltage are regulated by the main grid. In islanded mode, a microgrid behaves like a separate entity and can produce, control, and distribute power locally [8]. Microgrid has several advantages like higher efficiency, superior load handling strategy, and better ability to connect renewable sources [9]. A microgrid has a positive environmental impact on reducing carbon emission by utilising renewable energy sources. Different types of storage systems are connected to the microgrid to increase the stability and reliability of the system [10].

The main components of a microgrid are distributive energy sources, power storage systems, fixed and flexible loads, converters, controllers, smart switches, protection and communication devices. PCC is the point of common coupling between grid and microgrid which has a switch. By opening the switch, a microgrid can change from grid connected mode to islanded mode. Three different types of microgrids are reported in the literature called AC, DC, and hybrid microgrid [11]. In an AC microgrid, all sources and loads are connected to a common AC bus. The structure of an AC microgrid is presented in Fig. 1.1 (a). Any 50 Hz source, all AC loads, and the grid are directly connected to the bus. Any other frequency AC sources are connected by an AC/DC and DC/AC converter combination. Any DC source and load are connected by a DC/DC and DC/AC converter combination to the bus. DC microgrid has several advantages over AC microgrid like higher efficiency, higher stability, simpler control strategy, and no synchronization issue [2]. In Fig. 1.1 (b), the DC microgrid structure is shown. Any AC source or load can be connected by an AC/DC converter whereas any DC source or load can be connected by DC/DC converter to the bus. The grid is connected by a DC/AC

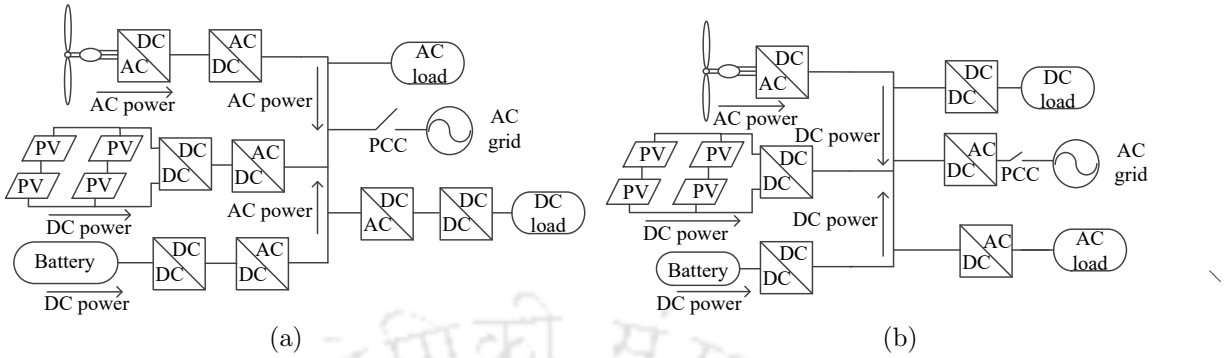

Figure 1.1: (a) Structure of AC microgrid [1]. (b) Structure of DC microgrid [2].

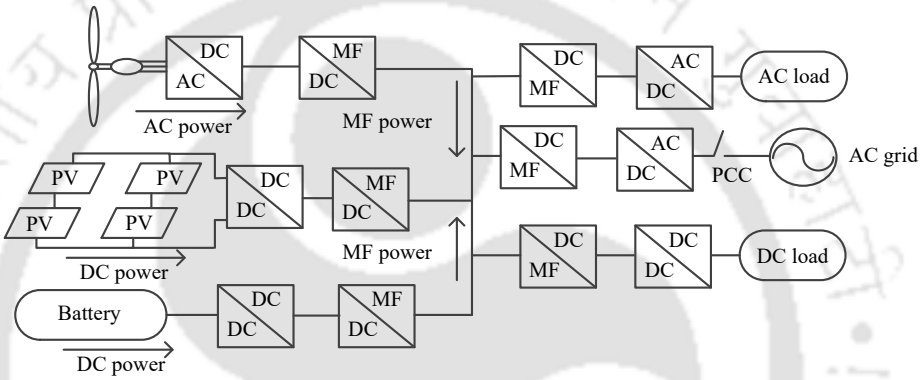

Figure 1.2: Structure of multifrequency microgrid (MFMG).

converter. The hybrid microgrid is proposed by merging AC and DC microgrid [12]. The hybrid microgrid has both the AC and DC bus. The AC sources and loads are connected to the AC bus and DC sources and loads are connected to the DC bus by proper converters. So AC+DC microgrid has high efficiency due to less number of conversions.

As all conventional power system works in AC supply so most of the microgrids are AC microgrid. DC microgrid has safety and protection issues [13], whereas stability, control, and synchronization are the biggest concerns for AC microgrid [14]. A hybrid microgrid requires distinct buses for AC and DC connections hence system cost increases [15]. This thesis discusses a unique type of microgrid called multifrequency microgrid (MFMG). Unlike a hybrid microgrid, it accommodates different frequency elements on a single conductor. MFMG has several new characteristics and can remove the disadvantages of conventional microgrids by proper use of power electronics converters.

An MFMG (Fig 1.2) is a new type of microgrid where the MF bus carries multiple frequency

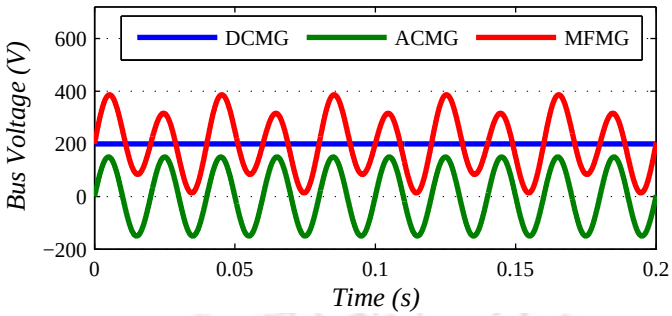

Figure 1.3: Bus voltage of DC, AC, and MFMG.

voltages and currents. A voltage source inverter named as DC/MF converter is operated as the building block of MFMG. It has been noticed that if different frequency components are superimposed on a single conductor, different frequency active powers become orthogonal to each other and create separate channels to transfer without mixing. A user can choose any frequency power channel available on the multifrequency bus as the load side converter behaves like an active power filter. So this system is superior to other microgrid systems. The bus voltage or current equation of MFMG is presented in equation 1.1, where x is bus voltage or current (Fig. 1.3). This equation is explained in detail in chapter 2.

$$x(t) = X + \hat{x_1} sin(2\pi f_1 t - \phi_1) + \hat{x_2} sin(2\pi f_2 t - \phi_2) + ... + \hat{x_n} sin(2\pi f_n t - \phi_n) \tag{1.1}$$

This system allows several independent source load interactions to happen simultaneously on a single transmission line with the help of different frequency power channels. Power electronic converters convert the source power to the multifrequency (MF) form required for the microgrid bus, and MF bus power can be converted to the form required by the load as shown in Fig. 1.4.

In most of the retail power markets in India, there is only one distribution company and hence there is no competition [16], [17]. These power markets can not include more than one distribution company due to the construction of new transmission lines. Like a telecommunication system, customers have no personal choice among the distribution companies in the power system which is not desirable. MFMG has been introduced with a new feature that different

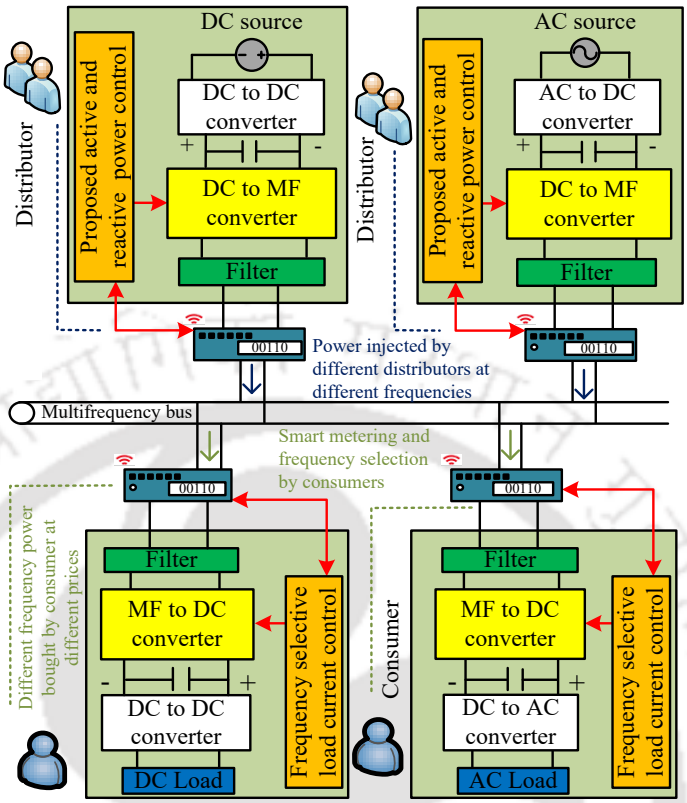

Figure 1.4: Structure and control of multifrequency microgrid (MFMG).

power generation companies can sell their power through different assigned frequency channels on the MF bus and consumers can subscribe to any company based on the requirements. It is analogous to the present subscription of different TV channels by users. Users can identify and subscribe to a certain kind of power or a certain power generation company by choosing the proper frequency channel. A zoomed version of MFMG is presented in Fig. 1.4, with two sources and two loads. It can be noticed that two different distributors send different powers at different frequencies to the MF bus. Smart meters are used to measure different source and load powers. At load side, the customers can buy different powers from different distributors at different prices by selecting the proper frequency channels.

1.2 Advantages of Multifrequency Microgrid

All MF systems have several new characteristics which MFMG can use and create several advantages over the traditional microgrids.

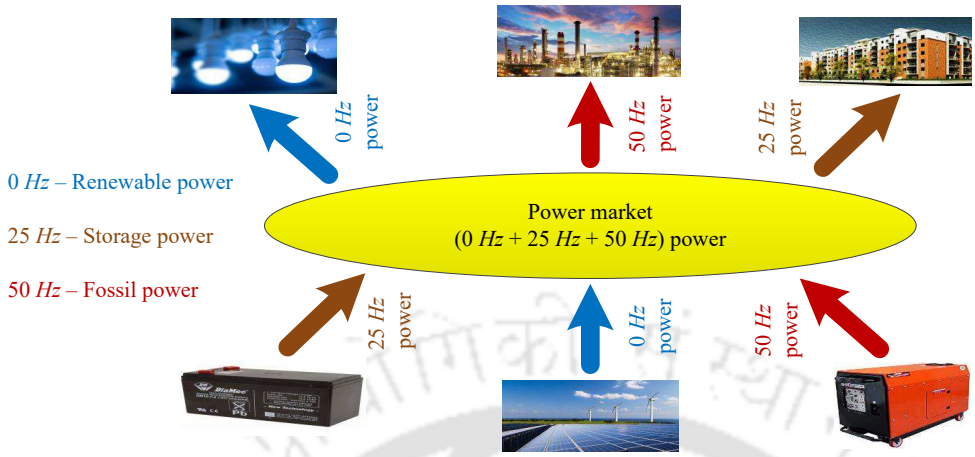

Figure 1.5: Structure of open power market.

(i) Several operational frequencies exist in the MF bus which enables the decoupled power flow. MFMG has a higher degree of functionality and flexibility in control by utilizing the full potential of power electronics converters than any traditional AC or DC microgrid [18].

(ii) AC power system can not reach its thermal limit of the conductor due to the stability limit. Maintaining the same voltage level, different frequency AC and DC currents can be superimposed on 50 Hz AC current to increase the transmission capacity of the system [19].

(iii) The bus voltage amplitude at its fundamental frequency can be increased by keeping the voltage peak constant by adding other harmonics to the voltage waveform [20]. The current in the system decreases which increases efficiency, and reduces the size of the converter and cables. So, the cost of investment is also reduced [21].

(iv) In multifrequency microgrid, different powers can be categorized by using different frequencies. Specific frequencies can be used for renewable power, fossil power, and storage power as they are different in terms of availability and reliability. Power selectivity in multifrequency microgrid can create an open market in the distribution system. Generation companies can use different assigned frequency channels to broadcast their powers and customers can select different frequency channels depending upon their needs. Using this

concept future power market can be constructed. In Fig. 1.5, a power market structure is presented where three generation companies use three different frequencies to send fossil, renewable and storage power and customers can choose any frequency channel depending upon their requirement.

1.3 Literature Review

1.3.1 Structure and converter of microgrid

The architectures and converters of AC, DC, and hybrid microgrids are narrated in different pieces of literature. The AC microgrid structure is explained in [1] to achieve stability for any kind of load. A scalable DC microgrid architecture is presented in [22] which can be used for rural electrification. DC microgrid structure, its interaction with the AC grid, and different grounding schemes are described in [2]. In [23], the architecture and operation of a hybrid microgrid are explained. A novel hybrid microgrid structure with a central storage system is shown in [24] with simulation results. A comprehensive review of the microgrid architectures is presented in [25] based on stability and control aspects. In [26] a primitive unified AC-DC microgrid structure is proposed whose bus has both DC and 50 Hz components.

A three phase isolated converter is proposed in [27] which can be used for any microgrid integration with the main grid. The modified SVPWM technique is also explained for the bidirectional converter operation. The design of the three phase AC/DC converter for AC microgrid application is narrated in [28] which is verified by experimental results. In [29], a novel DC/DC converter operation is explained which can be used for DC microgrid. A back to back converter structure is explained in [30] for the hybrid microgrid. The structure and the operation of a coupled interlinking converter is shown in [31] for a hybrid microgrid. In [32], the selection of grid side converter is done based on the reliability of the converter. A unified AC-DC converter structure is proposed in [26] for a microgrid whose bus has two different frequencies (DC, 50 Hz).

1.3.2 Power management of microgrid

Active power balance is necessary for a microgrid to share the total load demand between parallelly connected source inverters and keep the voltage and frequency stability in the bus in both grid connected and islanded mode [9]. To get active power balance in AC microgrid, there are different communication based power sharing strategies like concentrated control [33], distributed control [34] and decentralized control [35]. Different droop control methods without any communication for AC microgrid are described in [36]. A communication based decentralized control and autonomous control schemes of DC microgrid are presented in [37,38]. Different droop control methods are used [39] to balance active power in the DC microgrid. An alternative droop control scheme for a microgrid with both AC and DC characteristics is presented in [40]. In [41], different active power management problems are described for hybrid microgrid and a coordinated power sharing method is proposed. Reactive power control is essential in a microgrid to maintain voltage stability, system efficiency and power quality [42]. Master slave control strategy is used in [43] to control reactive power in an islanded AC microgrid. In [44], a communication based decentralized reactive power control method is narrated. Droop control methods are narrated in several pieces of literature [45] to get reactive power balance in AC microgrid. A distributed [46] and a decentralized [47] reactive power control strategy are employed in the hybrid microgrid to control the reactive power. Droop control method without communication for reactive power balance in a hybrid microgrid is conferred in [40]. The different active and reactive power imbalance situations which are created due to presence of different frequency components in MFMG are not conferred in any literature. There is no existing method to balance the different frequency active and reactive powers of any MF systems.

1.3.3 Energy storage system integration with microgrid

ESS integration with microgrid is one key research topic and several new strategies are introduced in recent years to operate an ESS with AC, DC, or hybrid microgrid [48]. Solar and wind power varies throughout the day. In the noon time, solar irradiation is maximum

and at night time, no solar power is available. The wind power of a wind turbine depends upon the wind speed which varies throughout the day. So without the help of an energy storage system, the solar and wind sources cannot supply a sensitive load which needs reliable power. Different types of storage systems like flywheel [49], chemical battery [50], and super capacitor [51] are conferred in different literature. Lithium ion batteries are mostly used as an ESS in a microgrid due to higher energy to weight ratio, no memory effect, and lower self discharge rate [52]. For AC microgrid, different power balancing strategies like droop control [53], distributed control [54], decentralized control [55], and fuzzy logic control [56] are explained to integrate an ESS. Different power sharing method like droop control [57], decentralized control [58], and distributed control [59] between DC microgrid and an ESS are reported in literature. In hybrid microgrid distributed control [60], autonomous control [61], adaptive control [62] strategies are used for the operation of an ESS. An ESS can be integrated with a cluster of microgrids by using a coordinated control strategy [63]. However, no literature explains the control and management of ESS with MFMG. A new power balancing strategy is required to operate the ESS and MFMG sources together so that different frequency active power loads can be delivered.

1.3.4 Different Multifrequency Systems

The basic idea of the superposition of different frequencies in a single conductor is old. In [19] a superposed AC+DC power transmission system is described and different applications with advantages are explained. The implementation was very complex as thyristor converters were not proper for this kind of application. So this idea did not get any attention at that time. In the last two decades, power electronic converters are widely used with the development of Si based IGBT and MOSFET. Different new fast control strategies and power electronic switches are invented which can make MF operation possible. Recently several MF systems like distributive power flow controller [64], wireless power transfer [65], and modular multilevel converter [66] are proposed where MF operation provides several advantages. The impact of superposed elements (50 Hz AC and its odd harmonics) on converters, power cables, protection,

Table 1.1: List of the existing literature on MFMG

Reference No.	Work presented in the paper
[67]	More than one frequency voltages and currents are used in an islanded system. Impact of MF power transfer on cables, protection system, communication system, loads, and transformers are analyzed.
[26]	An AC-DC microgrid idea is proposed with primitive architecture. An H bridge AC-DC converter is designed for the load side whose control got affected if load frequency changes.
[69]	A MF power distribution system is explained with two different frequencies (DC, 50 Hz) sources and loads. At load side passive filters are used which increases the size and limits the flexibility of power management.
[70]	Here the structure and control strategy of load side converter of MF system are presented. The load side converter can choose different frequency powers in different time frames.
[18]	This paper shows the possibility of MF power transfer in presence of a smart transformer in a distribution system. The impact of MF system on the grid is also discussed.
[68]	The feasibility of transmitting power at multiple frequencies is validated experimentally.

power line communication systems, and loads are observed and discussed in [67, 68]. The first AC+DC microgrid concept is presented in [26] with a primitive architecture. In [69], some passive filters are used at the load side to filter out the required frequency power from the AC+DC bus. The design and control of the load side converter of an MF system are presented in [70], where users have the ability to choose among different frequency available powers. The hardware realization of the load side converter is presented in [68]. In [18], the MF power transfer is made possible with the help of a smart transformer in a distribution system. All previous research works on MFMG are listed in Table 1.1. Two MF systems named DPFC, and DIPFC are briefly described here for a better understanding of the properties of MF systems.

1.3.4.1 Distributed Power Flow Controller

Distributed power flow controller (DPFC) is derived from a unified power flow controller (UPFC) which provides fast-acting reactive power compensation on high-voltage electricity transmission networks. Reactive power is generated internally in the series converter and active power is supplied through the DC link of the shunt converter. The shunt converter maintains

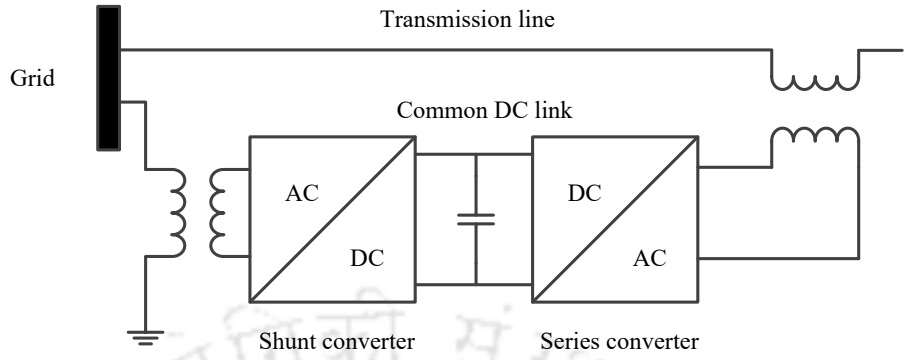

Figure 1.6: UPFC structure [3].

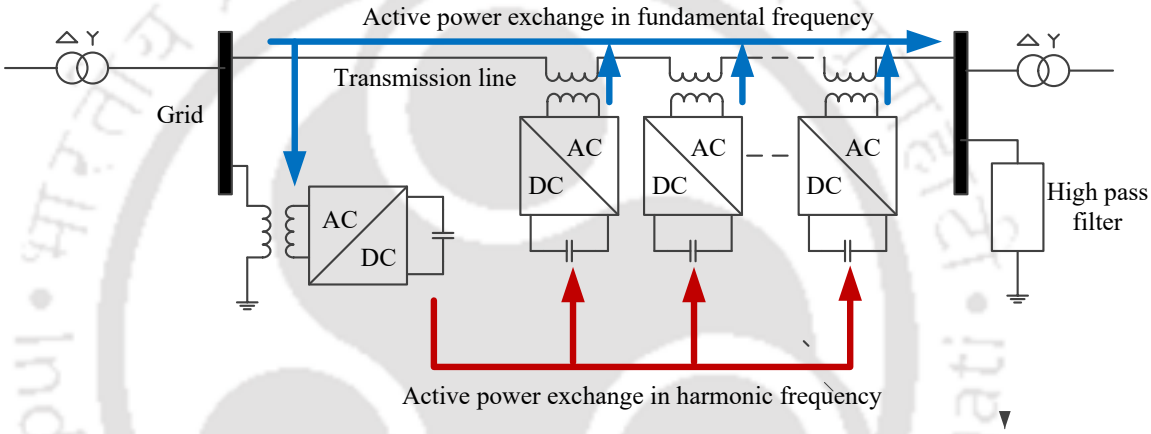

Figure 1.7: Active power flow in DPFC in fundamental frequency (blue) and harmonic frequency (red) [3].

the voltage of the common DC bus by taking active power from the transmission line (Fig. 1.6). DPFC has the same structure of UPFC without common DC link between series and shunt converter [3]. The active power exchange between series and shunt converter occurs through the distribution line in third harmonic frequency. DPFC also uses the distributed FACTs concept where many small single phase inverters are employed instead of one big three phase converter. Each converter has its own DC capacitor to provide the required active power to the transmission line. Besides the converters, DPFC needs one high pass filter on the other side of the transmission line and two star-delta transformers on both sides of the line. The third harmonic frequency will pass through the neutral of the transformer and can make a close loop for the third harmonic current through the ground.

The transmission line is the common connection between the shunt and the series devices.

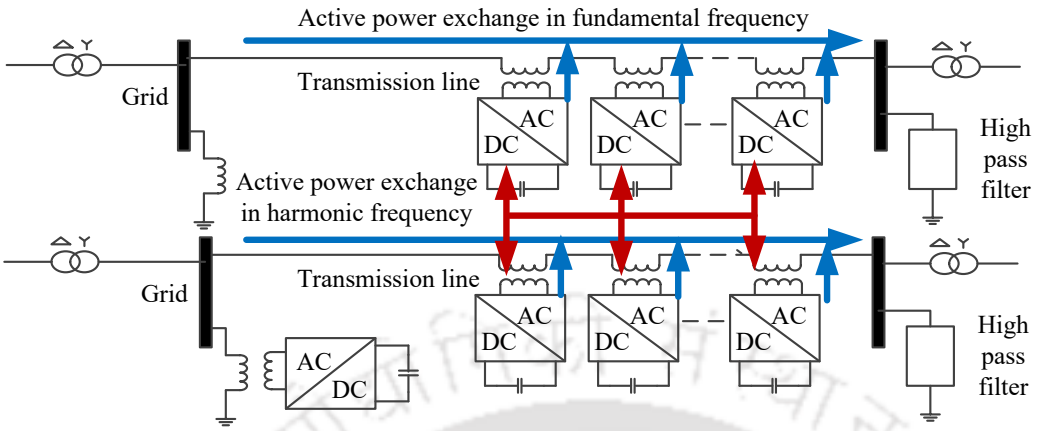

Figure 1.8: Active power flow in DIPFC in fundamental frequency (blue) and harmonic frequency (red) [4].

So they can exchange active power in between them through the transmission line. By applying the orthogonal power flow theory the shunt converter can absorb active power from the grid at the primary frequency and can inject the power back to the series converter at the harmonic frequency. The DPFC series converters generate a voltage at the harmonic frequency to absorb the active power from shunt converters according to the amount of required power and serve this harmonic frequency active power to the transmission line at the next fundamental frequency cycle. In DPFC, the third harmonic loop is mainly used to balance the capacitor voltage of the series and shunt converter. In primary frequency, the series converter delivers active power to the transmission line, so the capacitor voltage of the series converter decreases. In primary frequency, the shunt converter absorbs active power from the grid so its capacitor voltage increases. In the third harmonic loop, shunt converter delivers active power to the series converter and maintains the capacitor voltage as shown in Fig. 1.7. Assuming a lossless converter, the active power generated at the fundamental frequency is equal to the power absorbed from the third harmonic frequency. So using the MF concept, the DC link capacitor connection between the series and shunt converter is removed which reduces cost and increases reliability.

1.3.4.2 Distributed Interline Power Flow Controller

It is the distributed version of the interline power flow controller (IPFC) [4]. IPFC generally employs two or more series converters which are connected to different lines of a multi-line transmission system to control the active and reactive power in a multi-line system. Each converter can generate reactive power and compensate reactive power of its own line. Active power is also provided by a converter to its own line which is supplied through the common DC link of the other converter which takes active power from a different line to balance the DC bus voltage. By using the distributed FACTs concept, DIPFC consists of many small single phase series converters. In fundamental frequency, the converter compensates active power to its own line from its DC bus capacitor and the capacitor voltage decreases. Now in the third harmonic frequency, it takes active power from another series converter of a different line and balances the DC bus voltage. The other converter takes active power from the other line in the next fundamental frequency. So the sum of active power injected by all series converters at the fundamental frequency is zero. So here also the MF concept is used and the DC link capacitor is removed.

1.4 Gaps in the Existing Literature and Problem Formulation

The followings are the gaps in the existing literature :

- *The basic laws of MFMG are not defined :* The basic laws behind MFMG are superposition theorem, orthogonal power flow theory, and frequency selectivity criteria. However, the orthogonal power flow theory for reactive power and frequency selectivity criteria are still not discussed in any literature. These two theories need to be explored to understand the working of MFMG.

- *The basic structure and modular converter of MFMG is not designed :* The basic architecture and converters of traditional microgrids don't fit with MFMG. The basic architecture of MFMG is still unexplored. In some literature, AC-DC microgrid architecture is pro-

posed where the bus has only two different frequencies (DC, 50 Hz). In MFMG, every source is connected to the multifrequency (MF) bus through a converter. The converter converts the source frequency power to the desired frequency power and send to the MF bus. The source side and load side converters are proposed for AC-DC microgrid but they don't work in MFMG where more than two different frequency elements are present. The controller design procedure of any of these converters is not discussed in any literature.

- *Power balancing strategy of MFMG is not proposed :* Active and reactive power balance is necessary to maintain the frequency and voltage of a system. Different active and reactive power balancing strategies are proposed in different literatures for AC, DC, and hybrid microgrids. As different frequency active and reactive powers are present in the MF bus so, different new active and reactive power imbalance cases occur in MFMG which is still unexplored. Based on the cases a proper source side active and reactive power control strategy needs to be defined.

- *ESS integration with MFMG is not explained :* ESS is now an integral part of any microgrid system as it increases the stability and reliability of the system. In literature, different integration strategies of ESS are explained for AC, DC, and hybrid microgrid. However, these strategies are not applicable to MFMG as the ESS absorbs and supplies different frequency active powers. No literature explains the integration and operation strategy of the ESS with MFMG.

Based on the gaps in the existing literature, the following are the problem formulation of the thesis :

(i) To develop the architecture, and basic converter structure for MFMG.

(ii) To propose control strategies of the DC/MF converter for grid feeding, grid forming, and grid interactive operation. To propose a load side control strategy to achieve frequency selective criteria.

(iii) To propose control algorithms to balance different frequency active and reactive powers of MFMG in grid connected and islanded modes.

(iv) To integrate ESS with MFMG and explain the operation of the ESS unit to supply different frequency active powers.

1.5 Objectives and Main Contributions of the Thesis

MFMG has various advantages over traditional microgrids. However, the MFMG concept is not discussed in any literature. To set up the MFMG, the primary objective is to define the architecture, power converters, and control strategies of converters of the MFMG. The active and reactive power of any electrical system need to be balanced to maintain the bus voltage magnitude and frequency [71]. The presence of different frequency powers on the MF bus and the frequency selective power distribution create several power mismatch problems in MFMG which are not present in any AC, DC, or hybrid microgrid. For the operation of MFMG in grid connected and islanded mode, different frequency active and reactive powers need to be balanced for all these cases. So the second objective is to design an active and reactive power balancing algorithm for all the cases. The addition of ESS with MFMG increases the reliability and stability of the system but the integration is challenging due to the presence of different frequency active powers in MFMG which is the third objective. Based on the objectives the main contributions of the thesis are,

(i) *The basic laws of MFMG are studied :* The orthogonal power flow theory is studied mathematically for single phase and three phase MF systems. For frequency selective power transmission, a new control strategy is proposed for load side converter. Finally, the theory is proved through the simulation of two different MF load profiles.

(ii) *The architecture and basic converter of MFMG are proposed :* This work introduces the basic architecture of the MFMG. A new DC/MF converter is proposed as the basic converter of MFMG. The small signal modelling of the converter is executed based on the state space equations. The converter is studied by open loop hardware results.

(iii) *Different control strategies of the DC/MF converter are explained :* Different control strategies have been proposed for grid side, grid forming, and grid feeding operation of DC/MF converter in the microgrid. Based on the modelling of the converter, controller designs of the DC/MF converter are performed for all these control strategies. The control strategies and controller designs are validated by closed loop simulation result of the DC/MF converter.

(iv) *A power balancing strategy is proposed for MFMG :* The problem of different frequency power imbalances in MFMG, due to frequency selective power transmission is analyzed for grid connected and islanded modes. Different power unbalance cases are discussed and the conditions to balance active and reactive power at different frequencies are identified for an MF system for all the cases. Different control methods are introduced for grid connected and islanded modes of MFMG to solve the problem of active and reactive power imbalance for different cases. The proposed methods are verified by simulation in Matlab Simulink environment of 7 and 9 bus MFMGs, which consist of three different frequency sources and loads (DC, 25 Hz, 50 Hz) for both grid connected and islanded modes with three different cases.

(v) *Integration of ESS with MFMG is explained :* The integration and control strategy of the ESS are explained to supply different frequency active powers to the MFMG. Different new active power imbalance cases which occur due to the integration of ESS with MFMG are properly discussed and the active power balancing conditions for all these cases are defined. Based on the power balancing conditions, a cooperative active power balancing algorithm is proposed for MFMG with an ESS for both grid connected and islanded modes. The performance analysis of the algorithm is done by simulating an 8 bus MFMG in the Matlab Simulink environment for different power imbalance cases.

1.6 Orientation of the Thesis

The orientation of the thesis is as follows:

- Chapter 2 discusses the orthogonal power flow theory and frequency selectivity criteria for any MF systems. These theories are proven mathematically and through simulation results.

- Chapter 3 introduces the architecture and basic converter structure of MFMG. Different control strategies of DC/MF converter to act as grid side, grid forming, grid feeding, load side, and battery side are explained. The modelling of the DC/MF converter is done and accordingly, different controllers are designed.

- Chapter 4 deals with the active power balancing problems of MFMG. The active power balancing criteria are defined for MFMG in grid connected and islanded modes. An active power control strategy is explained to balance the different frequency active powers of MFMG.

- The reactive power balancing problem of MFMG is described in chapter 5. Different new reactive power imbalance cases are discussed for grid connected and islanded modes of MFMG and accordingly reactive power balancing strategy is designed.

- Chapter 6 presents the integration technique of an ESS with MFMG. A cooperative power balancing algorithm is structured for the proper operation of MFMG with ESS.

- Chapter 7 confers the conclusion of the thesis and provides the scope for future works.

2

Orthogonal Power Flow Theory and Frequency Selectivity Criteria

Contents

2.1 Introduction

Orthogonal power flow theory and frequency selectivity criteria are the basic laws behind the formation of any MF system. Orthogonal power flow theory conveys that if different frequency voltages and currents are present in any system, then the different frequency powers are orthogonal to each other and can pass through a single conductor without mixing. So by using different frequencies, different active and reactive power channels can be created on a single conductor for MF power flow. MF systems have another unique feature termed as frequency selectivity criteria. This criteria states that a consumer can absorb power at any available frequency from the MF bus based on the requirement. Different frequency powers can be categorized based on cost, reliability, quality, availability, or distance. For this operation, the control of load side converter is done in a way that it can select and absorb power at any available frequency.

It has been found that if a source and a load are tuned to a different frequency than the rest of the system then they can exchange power with each other without interfering with the system [64, 66]. Thus a frequency selective power channel is created inside any MF system. By virtue of superposition theory, many power channels can be superimposed on a single conductor. So different generation companies can categorize their power and distribute different types of powers through different frequency channels of the conductor. Consumers can choose any available frequency channel as per their requirement at the load side. As different frequency currents are passed through the conductor so the electromagnetic field of the currents interact with each other. The proximity effect results in the increment of the apparent resistance of the conductor due to the presence of different currents in its vicinity. Different frequency currents has different skin effects on the conductor. High frequency current has higher skin effect on the conductor. Due to skin and proximity effects the AC resistance of the wire increases [72]. So total loss of the system increases. Based on orthogonal power flow theory and frequency selectivity criteria, a new power market can be designed where the sellers and customers can identify each other and can monitor the real-time transaction. In this chapter first, the orthog-

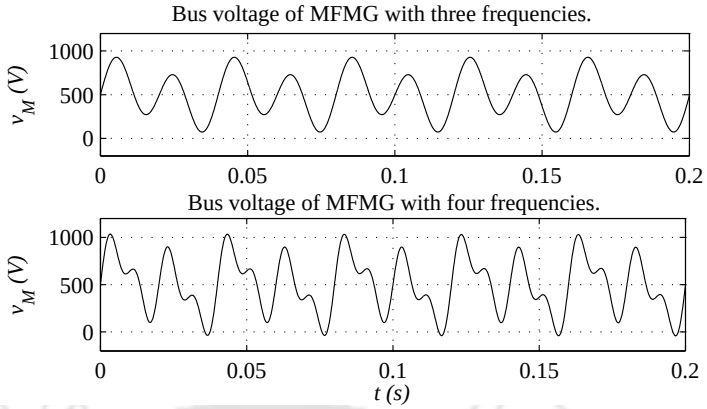

Figure 2.1: Multifrequency bus voltage with three $(500+\sqrt{2}\ 100\ \sin(157t)+\sqrt{2}\ 230\ \sin(314t))$, and four $(500+\sqrt{2}\ 100\ \sin(157t)+\sqrt{2}\ 230\ \sin(314t)+\sqrt{2}\ 150\ \sin(628t))$ frequencies.

onal power flow theory is proved through mathematical calculation and simulation. Then the frequency selectivity criteria is defined for MFMG and based on this theory, a new power distribution concept is explored. A new load side converter control strategy is proposed to achieve the frequency selectivity criteria. Finally, an MFMG system is simulated with the proposed load side control and the theory is verified.

2.2 Multifrequency Bus Voltage and Current Equations

Multifrequency microgrid is a special type of microgrid where different frequency voltages and currents are present on the bus. To find out the active and reactive power exchange in MFMG first, the bus voltage and current equations need to be defined. The voltage ($v_{n+1}(t)$) and current ($i_{n+1}(t)$) equations contain different frequency terms and are presented in equations 2.1, 2.2.

$$v_{n+1}(t) = V_{dc} + \sum_{n=1}^{n=\infty} \sqrt{2} V_n \sin(n\omega t - \phi_{vn}) \tag{2.1}$$

$$i_{n+1}(t) = I_{dc} + \sum_{n=1}^{n=\infty} \sqrt{2} I_n \sin(n\omega t - \phi_{in}) \tag{2.2}$$

Here, the MF bus contains $(n+1)$ numbers of different frequency elements. V_{dc}, I_{dc} are the DC voltage and current present on the bus, V_n, I_n are the RMS value of n^{th} frequency voltage and current waveforms, ω is the angular frequency, and $(\phi_{vn} - \phi_{in})$ is the phase angle between

n^{th} frequency voltage and current waveforms. The bus voltage waveforms for three and four frequency microgrids are shown in Fig. 2.1. For this thesis, it is considered that the MF bus carries three different frequency voltages and currents (DC, 25 Hz, and 50 Hz). As most of the microgrids use 50 Hz and DC, so those two frequency has been chosen. There are a few systems (Amtrak traction system, Niagara falls system, telephone exchange of Japan) where 25 Hz is used. So the third frequency is chosen as 25 Hz. The voltage ($v_M(t)$) and current ($i_M(t)$) equations for this MFMG are,

$$v_M(t) = V_{dc} + \sqrt{2}V_{25}\sin(157t - \phi_{v25}) + \sqrt{2}V_{50}\sin(314t - \phi_{v50}) \tag{2.3}$$

$$i_M(t) = I_{dc} + \sqrt{2}I_{25}\sin(157t - \phi_{i25}) + \sqrt{2}I_{50}\sin(314t - \phi_{i50}) \tag{2.4}$$

For proper operation of MFMG, it is needed that different frequency active and reactive powers should not mix with each other and different frequency active and reactive powers should flow through different frequency channels on the MF bus. This condition can only be maintained if different frequency active and reactive powers are orthogonal to each other. Based on the orthogonality, another theory is formed named frequency selectivity criteria by which the users can choose any available power channel from the MF bus based on their needs.

2.3 Orthogonal Power Flow Theory

In this section, the orthogonal power flow theory is proved. To prove the orthogonality of different frequency powers in an MF system, first the instantaneous power of a single frequency system and double frequency system is compared. For this single frequency system, the voltage ($v_1(t)$) and current ($i_1(t)$) waveforms are taken as per equation 2.5.

$$v_1(t) = \sqrt{2}V\sin(\omega t),\ i_1(t) = \sqrt{2}I\sin(\omega t + \phi) \tag{2.5}$$

Where V and I are the RMS value of voltage and current, ω is the angular frequency and ϕ is the phase angle. The instantaneous power ($s_1(t)$) of this single frequency system is calculated

and presented in equation 2.6.

$$s_1(t) = v_1(t)i_1(t) = 2VI\sin(\omega t)\sin(\omega t + \phi) = VI\cos(\omega t) - VI\cos(2\omega t + \phi) \tag{2.6}$$

The instantaneous power has one average value and an oscillatory component. So, there is a net power exchange between the sources. In this same fashion, the instantaneous power is calculated for another system where the voltage and current sources have two different frequencies. The voltage ($v_2(t)$) and current ($i_2(t)$) waveforms of the system are given in equation 2.7.

$$v_2(t) = \sqrt{2}V\sin(\omega_1 t),\ \ i_2(t) = \sqrt{2}I\sin(\omega_2 t + \phi) \tag{2.7}$$

$$s_2(t) = VI\cos((\omega_1 - \omega_2)t + \phi) - VI\cos((\omega_1 + \omega_2)t + \phi) \tag{2.8}$$

This instantaneous power equation ($s_2(t)$) contains two oscillatory terms. So the average power exchange between the sources is zero. As the sources have different frequencies so there is no interaction between the sources. So in a double frequency system, two different frequency powers are orthogonal.

Another way to prove orthogonal power flow theory is to calculate the active and reactive power for a multifrequency system and from those equations, orthogonality can be shown. With help of a single-frequency single-phase system, the active and reactive power for (n+1) frequency system is calculated here. For a single-phase single-frequency system, the voltage and current waveforms are shown in equation 2.5. The instantaneous power equation for a single frequency single phase system is,

$$s_1(t) = v_1(t)i_1(t) = VI\cos\phi(1 - \cos 2\omega t) - VI\sin\phi\sin 2\omega t \tag{2.9}$$

Which can be written as,

$$s_1(t) = P_1(1 - \cos 2\omega t) - Q_1\sin 2\omega t \tag{2.10}$$

Where $s_1(t)$ is the instantaneous power, P_1, and Q_1 are the active and reactive power of the system. Based on this next, the active and reactive powers are found for an MF system. For the 'n+1' frequency system the voltage and currents are defined in equations 2.1, 2.2. For this

MF voltage and current, the instantaneous power is calculated and presented in Equation 2.11.

$$s_{n+1}(t) = V_{dc}I_{dc} + V_{dc}\sum_{n=1}^{n=\infty}\sqrt{2}I_n\sin(n\omega t - \phi_{in}) + I_{dc}\sum_{n=1}^{n=\infty}\sqrt{2}V_n\sin(n\omega t - \phi_{vn}) + \sum_{n=1}^{n=\infty}\sqrt{2}V_n\sin(n\omega t - \phi_{vn})\sum_{n=1}^{n=\infty}\sqrt{2}I_n\sin(n\omega t - \phi_{in}) \quad (2.11)$$

By simplifying and neglecting higher order terms,

$$s_{n+1}(t) = V_{dc}I_{dc} + \sum_{n=1}^{n=\infty}V_nI_n\cos\phi_n\left(1-\cos(2n\omega t - 2\phi_{vn})\right) - \sum_{n=1}^{n=\infty}V_nI_n\sin\phi_n\sin(2n\omega t - 2\phi_{vn}) \quad (2.12)$$

By comparing equation 2.12 with equation 2.10, the average active and reactive power equations for MF system are,

$$P_{n+1} = \sum_{n=1}^{n=\infty}V_nI_n\cos\phi_n,\ \ Q_{n+1} = \sum_{n=1}^{n=\infty}V_nI_n\sin\phi_n \quad (2.13)$$

This active and reactive power equation does not contain any cross-frequency terms. Equation 2.13 shows that the MF active and reactive powers are the algebraic sum of individual frequency active and reactive powers. So different frequency powers maintain their magnitude in the MF system and do not mix with each other. At the load side they can be separated by the use of a proper filter. Sources with different frequencies do not exchange any active or reactive power and have a null average interaction. So orthogonal power flow theory is mathematically proved here. If two elements are tuned at a different frequency than the rest of the system then they can exchange power with each other but not with other elements of the system. By this, a power channel is created between those two elements. Using the superposition theorem, many such power channels can be created on the MF bus.

To prove the orthogonality of different frequency power through simulation, two different frequency voltage and current sources (25 Hz, 50 Hz) are connected in parallel, and accordingly the instantaneous active and reactive power of the system is measured in the Matlab Simulink environment. The instantaneous power is averaged by using a mean block. It can be noticed from Fig. 2.2, that when voltage and current sources are of the same frequency, active and reactive power exchange happen. If the voltage and current sources are of different frequencies,

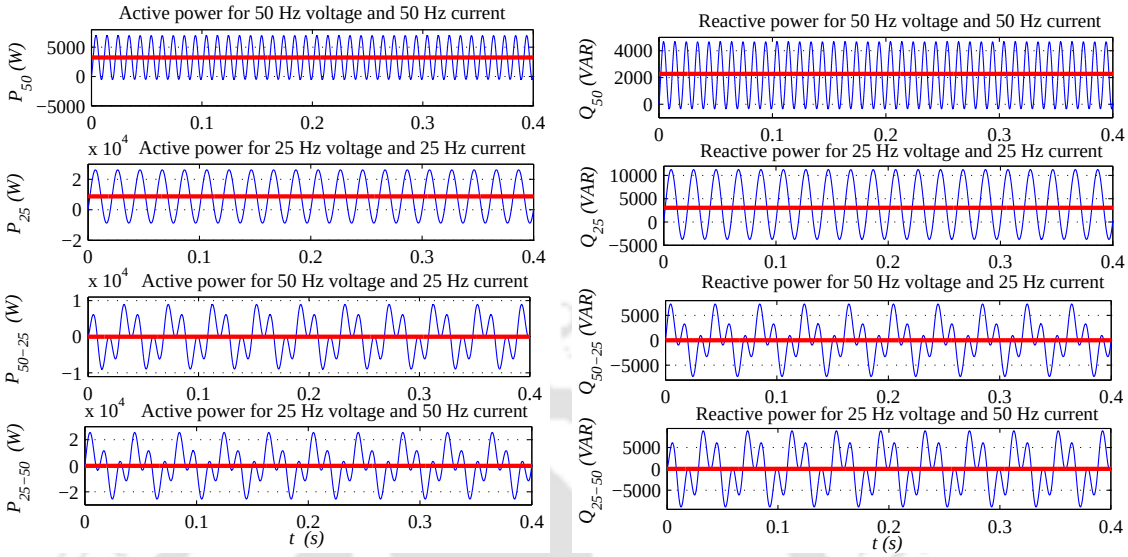

Figure 2.2: Instantaneous (blue) and average (red) (a) active power exchange between the 50 Hz voltage source and 50 Hz current source (P_{50}), 25 Hz voltage source and 25 Hz current source (P_{25}), 50 Hz voltage source and 25 Hz current source (P_{50-25}), 25 Hz voltage source and 50 Hz current source (P_{25-50}). (b) reactive power exchange between the 50 Hz voltage source and 50 Hz current source (Q_{50}), 25 Hz voltage source and 25 Hz current source (Q_{25}), 50 Hz voltage source and 25 Hz current source (Q_{50-25}), 25 Hz voltage source and 50 Hz current source (Q_{25-50}).

then there is null interaction between the sources. These simulation results prove orthogonality of different frequency active and reactive powers in any MF system.

2.4 Frequency Selectivity Criteria

In MFMG, the load side converters have the ability to absorb a certain frequency channel power from the MF bus. Different source powers can be categorized based on source availability, reliability, quality, and distance. The customers can choose between several available power channels as per their requirements. This unique characteristic of MFMG is termed frequency selectivity criteria. A new control technique is required for load side converters to follow the frequency selectivity criteria. Based on frequency selectivity criteria, a new distribution system can be formed.

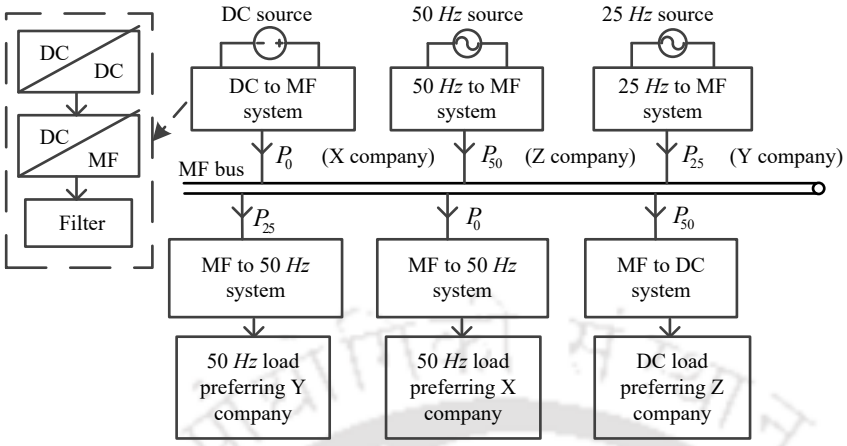

Figure 2.3: Multifrequency power distribution system.

2.4.1 Multifrequency Power Distribution

There is no option for the customers to identify and choose between power distribution companies in today's power system. In most of the retail power markets in India, only one power distribution company is present. A new power system where customers have more decision making ability is highly commendable like a telecommunication system. For this type of operation, dedicated source-load connections are required. To implement this idea in AC, DC, or hybrid microgrid, a huge number of new constructions are needed and the system becomes very complex. For this operation, the MF distribution system is designed which has several frequency voltages and currents superimposed on the bus, and frequency selective power transmission capability at the load side. Here different generation companies can distribute their powers through different power channels on the MF bus and consumers can choose between those power channels based on their needs. These generation companies can distribute different types of powers from different sources and have different prices. By using orthogonal power flow theory and frequency selective criteria, this operation is possible in any MF system.

Here one MF distribution system is designed (Fig. 2.3). The MF bus contains DC, 25 Hz, and 50 Hz powers. Three different generation companies are present in the distribution system. 'X' company has a renewable DC solar source, which is not available during the night but the source power is very cheap due to high subsidies and tax reductions. 'Y' company has a 50 Hz

fossil fuel source, which is available throughout the 24 hours and has a medium cost. 'Z' company has 25 Hz storage source power which has a high power quality and high price. The storage power of the 'Z' company is actually DC power. In MFMG, there is a DC/MF converter connected to every source. This source converter changes the DC power to the 25 Hz power and sends it to the MF bus.Two 50 Hz and one DC loads are connected to the MF bus. The load side DC/MF converter acts like a power filter for this frequency selective power transmission. It can be seen that the two 50 Hz load users choose different power generation companies power. One 50 Hz load is choosing 'Y' company (25 Hz power channel) and another 50 Hz load is choosing 'X' company (DC power channel). The DC load chooses the 'Z' company (50 Hz power channel) due to better availability. So in this system consumers and sellers can identify and select each other in real-time. Based on this a better power market structure can be formed.

2.4.2 Multifrequency Load Profiles

Frequency selectivity criteria is the fundamental theory behind MFMG and need to be validated. For this, MFMG loads need to be simulated with the new load side converter control. For this simulation, some standard MF load profiles are needed which are not available in any literature. MF loads can consume a mixture of different frequency powers at a time and can shift between different power channels throughout a day. So, two different load profiles are designed here based on customer preference and availability of the powers. It is assumed that the renewable source (DC) is solar and available only in the daytime. The fossil power source (50 Hz) is available through out the day and can increase power generation during peak load time. The storage power (25 Hz) is only available during peak load time.

2.4.2.1 User Taking Different Frequency Channel Powers Alternatively at Different Time Frames

A consumer can take power from a certain frequency channel at a time but can shift between different power channels to get lower charges and better availability. A 4 kW rated load profile is shown in Fig. 2.4 (a). As solar power (DC) is available in the day time and cheap, a

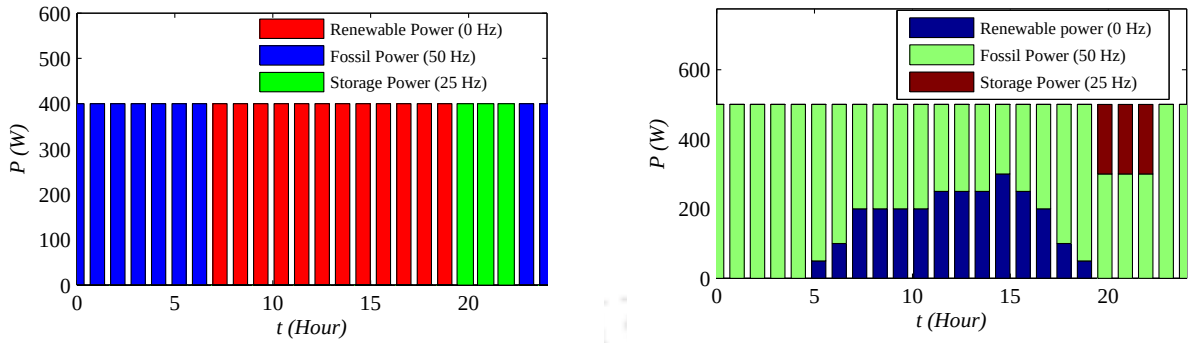

(a) (b)

Figure 2.4: Multifrequency load profile of (a) user taking different frequency channel powers alternatively at different time frames. (b) user taking mixture of different frequency channel powers simultaneously at same time frame.

consumer can take 4 kW solar power from 06:00 to 18:00. 18:00 to 21:00 is the peak load time so, a consumer can take storage power (25 Hz) of 4 kW during this time. During night time (21:00-06:00), the customer can take the fossil power (50 Hz) as this is the only power available during this time.

2.4.2.2 User Taking Mixture of Different Frequency Channel Powers Simultaneously at Same Time Frame

Another type of MF load profile of 6.5 kW is conferred in Fig. 2.4 (b). Here a consumer can take a mixture of more than one companies power at a time. In the daytime (06:00-18:00), a consumer can take whatever solar power (DC) is available. It is considered that only 3 kW DC power is available at this time. So, the consumer takes another 3.5 kW fossil power (50 Hz) to fulfill 6.5 kW load demand. The load absorbs a mixture of DC and 50 Hz frequency currents. In the peak load time (18:00-21:00), it is considered that only 3.5 kW fossil power (50 Hz) is available. So the consumer takes the remaining 3 kW storage power (25 Hz) during this time. Rest of the time (21:00-06:00), the consumer consumes 6.5 kW fossil power (50 Hz). Based on these two profiles, the MF distribution system is simulated in Matlab Simulink to verify frequency selectivity criteria.

Table 2.1: 50 Hz load power and DC load power references for simulation

Load power	$0 - 0.75$ (s)	$0.75 - 2.25$ (s)	$2.25 - 2.75$ (s)	$2.75 - 3$ (s)
P_{L5}	4 kW 50 Hz	4 kW DC	4 kW 25 Hz	4 kW 50 Hz
P_{L3}	6.5 kW 50 Hz	3 kW DC +3.5 kW 50 Hz	3.5 kW 50 Hz +3 kW 25 Hz	6.5 kW 50 Hz

2.4.3 Control Technique for Frequency Selective Power Transmission

For frequency selective power transmission the load side converter structure and control strategy need to be defined. To implement frequency selectivity criteria, a back to back converter structure is used at the load side. The load converter system can select any frequency available power and convert that power to the required load frequency. For any 50 Hz load, an MF/DC converter and DC/AC converter are connected at the load side. In MF/DC converter, hysteresis control is applied to select different frequency currents from the MF bus. By providing proper active and reactive power reference any frequency power channel can be chosen. The MF/DC converter converts the MF power to DC power and DC/AC converter converts the DC power to 50 Hz power. The load side converter structure and control strategy are properly explained in chapter 3, load side converter subsection.

2.4.4 Simulation Results

An MFMG system with three different frequency sources (DC, 25 Hz, 50 Hz), and multi-frequency loads (DC, 50 Hz) are simulated in Matlab Simulink to verify the control strategy for frequency selectivity criteria. The simulated bus structure of MFMG is shown in chapter 4 Fig. 4.4. The 50 Hz load (P_{L5}) is connected by an MF/DC and DC/AC converter at bus 5 and the DC load (P_{L3}) is connected by an MF/DC and DC/DC converter at bus 3. All simulation parameters are shown in Table 4.4 of chapter 4. The load side control is done based on the load profiles shown in Fig. 2.4. As per the load profiles, the active and reactive power reference of the MF/DC converter is changed and accordingly load absorbs the selected frequency power. The MF bus contains three different frequency voltages and is maintained at 600 V DC+ 210 V 50Hz+ 50 V 25Hz.

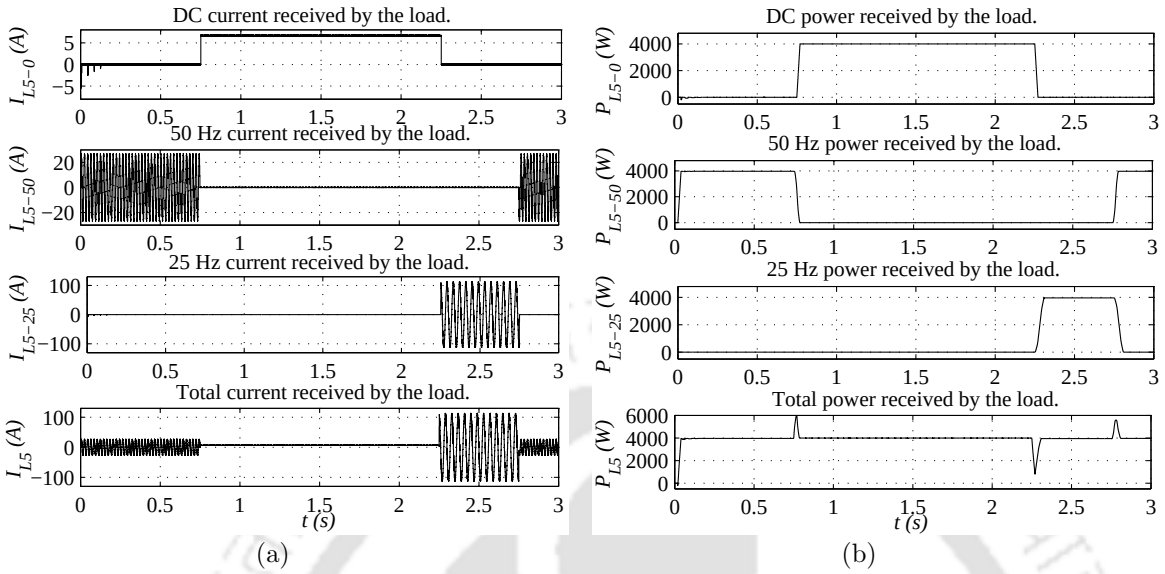

Figure 2.5: (a) Different frequency current segments and total current of 50 Hz load which maintains first MF load profile. (b) Different frequency power segments and total power of 50 Hz load which maintains first MF load profile.

The first profile is simulated on 50 Hz load where consumer chooses only one frequency power at a time but can shift between different frequency power channels throughout the day. According to Fig. 2.4 (a), the 50 Hz load chooses different power generation companies at different time frame of a day. The reference load powers are presented in Table 2.1. First, the reference load current is calculated based on different frequency power reference and bus voltage. Accordingly, the MF/DC converter absorbs those frequency powers to maintain the load profile. The load is a constant 4 kW 50 Hz load. Here total simulation time has been taken as 3 s. The simulation results are presented in Fig. 2.5 (a). As per the load profile, the first $0 - 0.75$ s, the 50 Hz load takes 50 Hz power. In between 0.75 $s - 2.25$ s, load takes DC power and DC/AC converter converts that to 50 Hz power. In between 2.25 $s - 2.75$ s, only the 25 Hz power is available, so the load absorbs 25 Hz power. The reference currents to achieve the 4 kW load are 19 A 50Hz, 6.6 A DC, and 80 A 25Hz. It can be noticed from Fig. 2.5 (a) that in between $0 - 0.75$ s, the different load current segments are, $I_{L5-0} = 0$, $I_{L5-50} = 19$ A, and $I_{L5-25} = 0$. So the 4 kW load is fulfilled by 50 Hz source power. In between 0.75 $s - 2.25$ s, the different load current segments are $I_{L5-0} = 6.6$ A, $I_{L5-50} = 0$, and $I_{L5-25} = 0$. In this time period, the 4 kW load power is supplied by the DC source. In between 2.25 $s - 2.75$ s, the

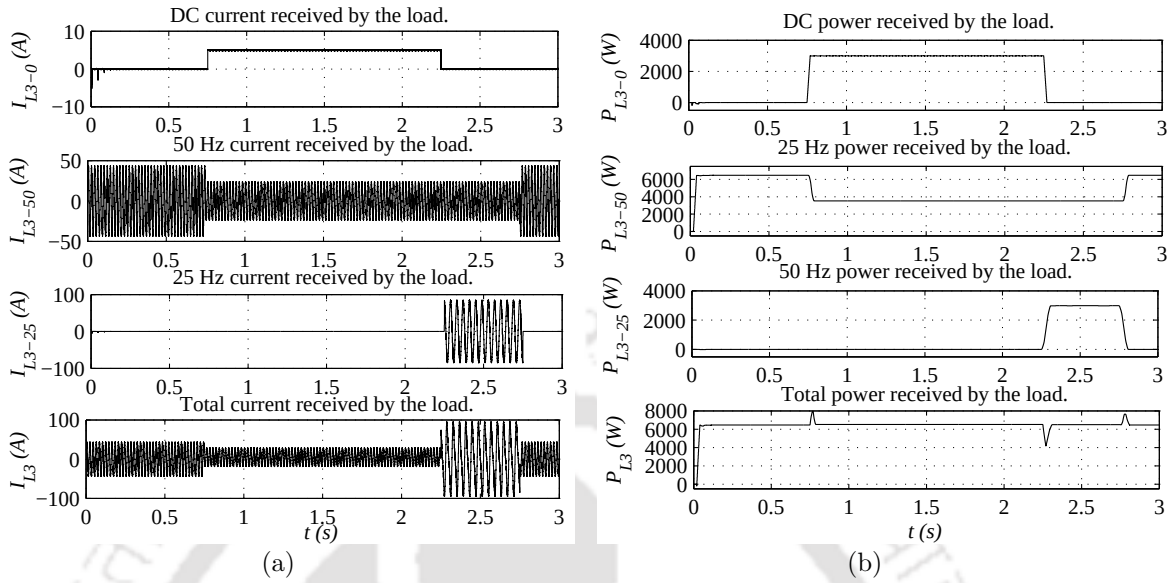

Figure 2.6: (a) Different frequency current segments and total current of DC load which maintains second MF load profile. (b) Different frequency power segments and total power of DC load which maintains second MF load profile.

different load current segments are $I_{L5-0} = 0$, $I_{L5-50} = 0$, and $I_{L5-25} = 80\ A$. So here the load is supplied by 25 Hz source. Different frequency load power segments are conferred in Fig. 2.5 (b). The total load power is calculated by algebraically adding all these segments ($P_{L5} = P_{L5-0} + P_{L5-50} + P_{L5-25}$). It can be observed that total load power is kept constant at 4 kW throughout the $0 - 3\ s$ time. The load can shift between different frequency channels and the control strategy is functioning properly for frequency selectivity criteria.

The other DC load is simulated with the second load profile where the consumer can choose between a mixture of different frequency powers at a time and can shift between different frequency powers throughout a day. The load is a constant 6.5 kW load. According to the second load profile (Fig. 2.4 (b)), the reference powers for the DC load is presented in Table 2.1. The DC load chooses a mixture of different power generation companies at the same time frame of a day. As per the load profile, for the first $0-0.75\ s$, the DC load takes 6.5 kW 50 Hz power. In between $0.75\ s - 2.25\ s$, the load takes whatever DC power is available and with this takes 50 Hz power to fulfill the load power (3 kW DC+3.5 kW 50 Hz). In between $2.25\ s-2.75\ s$, the load chooses a mixture of 25 Hz and 50 Hz power (3.5 kW 50 Hz+3 kW 25 Hz). According to the bus voltage, different frequency reference currents are calculated and sent to the hysteresis

controller. The controller controls the input current of the MF/DC converter and accordingly load profile is maintained. The reference current segment for 50 Hz is 30.95 A for the first 0.75 s and last 0.25 s and 16.86 A in between 0.75 $s-2.75$ s. The reference current segment for DC is 5 A in between 0.75 $s-2.25$ s and for 25 Hz is 60 A in between 2.25 $s-2.75$ s to attain 6.5 kW load. The different frequency segments of the load current are presented in Fig. 2.6. In between $0-0.75$ s, the different load current segments are, $I_{L3-0}=0$, $I_{L3-50}=30.95$ A, and $I_{L3-25}=0$. So the 6.5 kW load is fulfilled by only 50 Hz source power. In between 0.75 $s-2.25$ s, the different load current segments are $I_{L3-0}=5$ A, $I_{L3-50}=16.86$ A, and $I_{L3-25}=0$. In this time period, the 6.5 kW load power is supplied by the DC and 50 Hz sources combinedly. In between 2.25 $s-2.75$ s, the different load current segments are $I_{L3-0}=0$, $I_{L3-50}=16.86$ A, and $I_{L3-25}=60$ A. So here the load is supplied by 50 Hz and 25 Hz sources. The total bus current is formed with these three segment currents i.e. $I_{L3}=I_{L3-0}+I_{L3-50}+I_{L3-25}$. In Fig. 2.6 (b), different frequency load power segments for DC load are presented. The total load power is calculated by algebraically adding all these segments ($P_{L3}=P_{L3-0}+P_{L3-50}+P_{L3-25}$). It can be observed that total power remains constant (6.5 kW) throughout the operation but the consumer is choosing a mixture of power channels at different time frames to achieve the load power. So the control strategy is achieving frequency selectivity criteria with the second load profile.

2.5 Conclusion

In this chapter, the orthogonal power flow theory is mathematically proved for single-phase and three-phase MF systems. So it is concluded that different frequency active and reactive powers can flow through a conductor without mixing and creates different frequency power channels. A new power distribution concept is explored where the consumers can select any available power channel from the bus as per their requirements. For this frequency selective power transmission, a control strategy is designed for load side converter. The strategy is verified by simulating an MFMG system based on two MF load profiles. The load currents match with the reference and the loads take power according to the load profiles. It is observed that

MFMG is achieving frequency selectivity criteria for both load profiles with the new distribution strategy.

Note: Major part of this chapter is reproduced from my publications:

1. R. Dey and S. Nath, "Orthogonality of different frequency reactive powers in multifrequency system," in *proceedings of National Power Electronics Conference (NPEC)*, 2021, pp. 1–6.

2. R. Dey and S. Nath, "A new power distribution concept for multifrequency microgrid," in *proceedings of IEEE 12th Energy Conversion Congress Exposition - Asia (ECCE-Asia)*, 2021, pp. 491–496.

3

Architecture and Power Converters of Multifrequency Microgrid

Contents

3.1 Introduction

To establish a microgrid first, the architecture of the microgrid needs to be decided. As no MFMG architecture is available in the literature, in this chapter the architecture of MFMG is introduced with three different frequency (DC, 25 Hz, 50 Hz) sources and loads. A new modular converter named DC/MF converter is proposed here which acts as the building block of MFMG. The DC/MF converter can be strategically controlled and used as grid side, grid forming, grid feeding, grid interactive, battery side, or load side converter. The DC/MF converter model is required to understand the behaviour of the system in the open loop. For modelling of converters, two traditional strategies generally have been used which are the circuit averaging method [73] and the state space averaging method [74]. Here, the state space averaging method is adopted to model DC/MF converter. As the equivalent series resistance (ESR) of filter capacitor generates extra dynamic terms in the TF, so in this work only the capacitive parasite component is considered. Ultimately, small signal modelling is done to generate the TF. The closed loop operation of the DC/MF converter is required to use it as grid side, grid forming, grid feeding, grid interactive, battery side, or load side converter. From the small signal model (SSM), different controllers are designed for closed loop output voltage and current control of the DC/MF converter. In this chapter first, the architecture is defined with the modular DC/MF converter. Then by using the modular converter different control strategies are defined for grid connected and islanded mode operations. Next, the structure of the DC/MF converter is proposed and a small signal model of the converter is generated. The converter structure is verified by hardware experiment of DC/MF converter operation in open loop with input variations. By using the transfer functions derived from the SSM, controller designs are performed to control the output voltage and current of the DC/MF converter in closed loop. Finally, the controller designs are verified by the closed loop simulation results.

3.2 Architecture of Multifrequency Microgrid

For the operation of the MFMG, the architecture of the MFMG need to be defined first. Based on the architecture, different power management strategies can be formulated. In this section, the architecture is proposed for the MFMG. By using the modular DC/MF converter, different control strategies are also described.

The key difference between the proposed architecture with the conventional architecture is that three different frequency voltage and current components are present in the proposed architecture. DC, 25 Hz, and 50 Hz are chosen as base frequencies of the MFMG architecture. Here an 8 bus MFMG architecture is proposed with three different frequency (DC, 25 Hz, and 50 Hz) sources and loads. The grid is connected through a switch at point of common coupling (PCC) with the MFMG. MFMG can be operated in islanded mode by opening the switch. The main components of the architecture are different frequency sources and loads, grid, battery, and different converters. All sources and loads are connected to the MF bus by power electronic interfaces. In the literature, there is no standard voltage available for the MF bus. It has been found that 500 V DC is used as the bus voltage in DC microgrid [2], and 230 V (RMS) is used as the bus voltage of AC microgrid [1] to keep the line loss modest. So in this thesis, the MF bus voltage is chosen as 500 V $DC+$ 100 V $25Hz+$ 230 V $50Hz$. A basic voltage source converter named DC/MF converter connects all sources and loads to the MF bus. All DC loads and sources are connected by a DC/DC and DC/MF converter. All AC sources and loads are connected by AC/DC and DC/MF converters. All source side converter works as grid feeding converter to supply the power to the MFMG. In islanded mode, the grid interactive converter works as a grid forming converter to maintain the MF bus voltage. The main grid is connected with the MFMG by DC/AC and DC/MF converter. This combination of converters works as grid side converter. The ESS is connected to the MF bus by a bidirectional DC/DC converter and DC/MF converter. The block diagram of the DC/MF converter is shown in Fig. 3.1 (a). The input of the converter is DC voltage whereas the output of the converter is MF voltage (DC+25 Hz+50 Hz). The output voltage of the DC/MF converter is switched

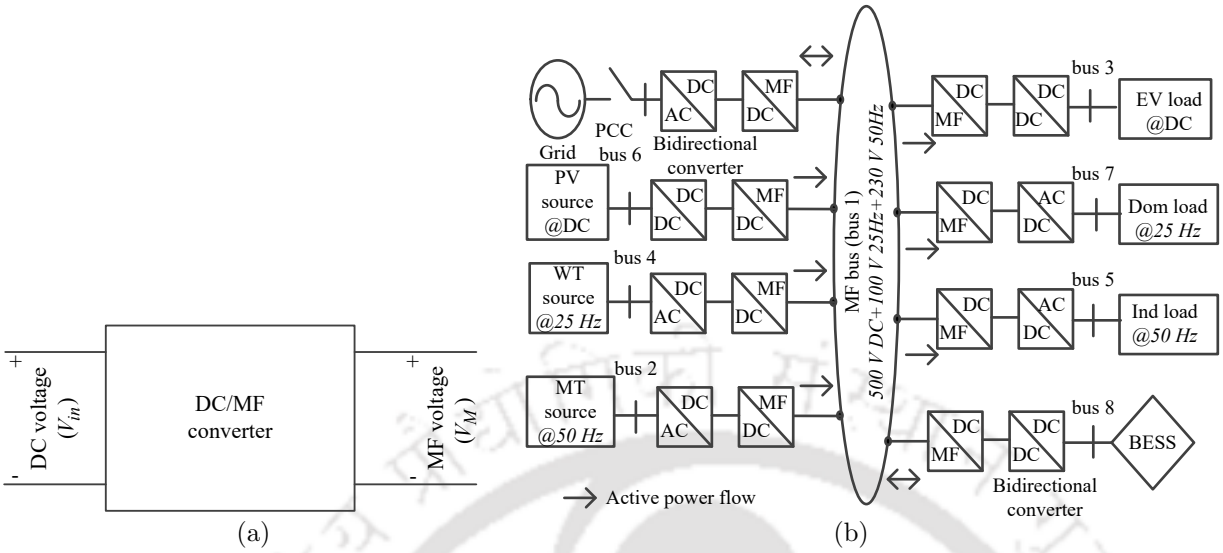

Figure 3.1: (a) DC/MF converter block diagram. (b) Basic architecture of MFMG.

MF voltage. To convert the switched voltage to the desired frequency, some passive filter is required. In Fig. 3.1 (b), the bus structure with MFMG is presented with practical sources and loads. One photo voltaic (PV) unit, two wind turbines (WT), and a micro turbine (MT) act as DC, 25 Hz, and 50 Hz sources respectively. One of the WT's converters behaves like a grid interactive converter. The electric vehicle charging station (EV) is operated as a DC load. Similarly, the domestic load (DL) and industrial load (IL) are operated at 25 Hz and 50 Hz respectively. The DL and IL are non-sensitive loads and can be shredded during a power crisis. The battery rating is chosen as 50 kW, 480 V, 0.8 kWh for 6 hours.

3.2.1 Different Converters of Multifrequency Microgrid

In grid connected mode, the grid is connected to the MF bus by grid side converter. In islanded mode, the MF bus voltage is maintained by grid forming converter, and the load power is supplied by the grid feeding converters. Different MF loads are connected to the MF bus by load side converters. For all the converters same DC/MF converter structure is used and different control strategies are employed on DC/MF converter to control it as grid side, grid forming, grid feeding, grid interactive, or load side converter. All control strategies are shown here using the modular DC/MF converter.

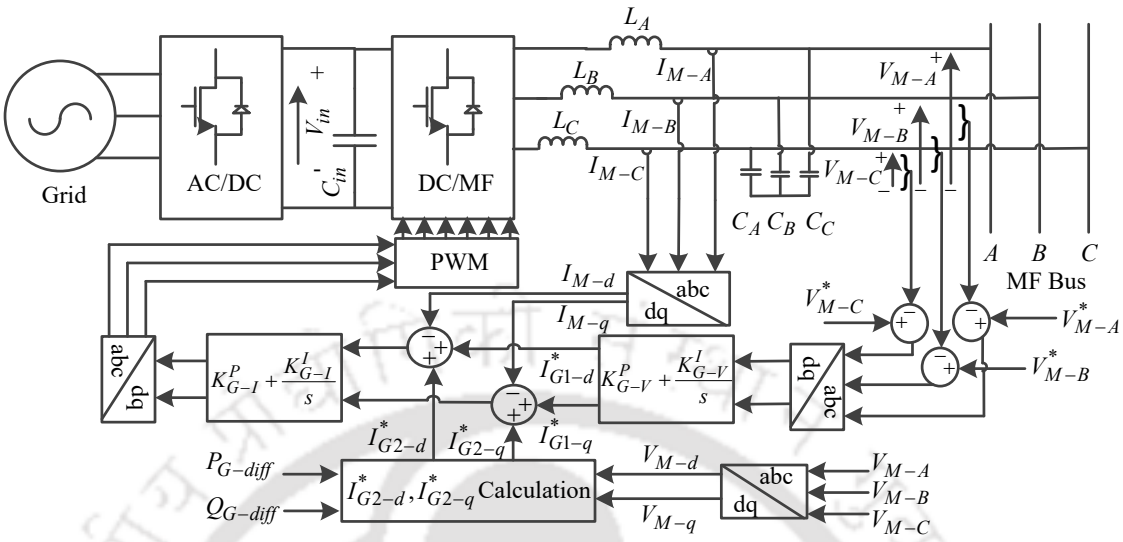

Figure 3.2: Control strategy for DC/MF grid side converter.

3.2.1.1 Grid Side Converter

In grid connected mode, the grid side converter balances the MF bus voltage and with this, the grid maintains the power balance of the microgrid. So the output voltage and current both need to be controlled by the DC/MF converter. For this, a double loop average mode current control method is implemented. The 50 Hz grid power can be converted to other frequency power as per MFMG requirements and sent to the MF bus. The grid side AC/DC converter converts the 50 Hz power to DC and DC/MF converter converts the DC power to multifrequency powers. The input voltage of the grid side DC/MF converter is V_{in}. As the output of the DC/MF converter is switch voltages and currents so LC filters are connected to the output terminal of DC/MF converter. From Fig. 3.2, it can be seen that the controller has two loops. The inner loop maintains the output current and the outer loop maintains the output voltage. First, the output voltage (V_M) is sensed and compared with the reference voltage (V_M^*). A PI controller is used to generate the current reference (I_{G1}^*) from the error signal. Next, I_{G2}^* is calculated based on a flowchart to balance different frequency powers in MFMG which is presented in chapter 4. The active and reactive power references (P_{G-diff}, Q_{G-diff}) are given to the flowchart, and accordingly the reference current is calculated. These two reference currents are added and compared to the output current (I_M) of the grid side

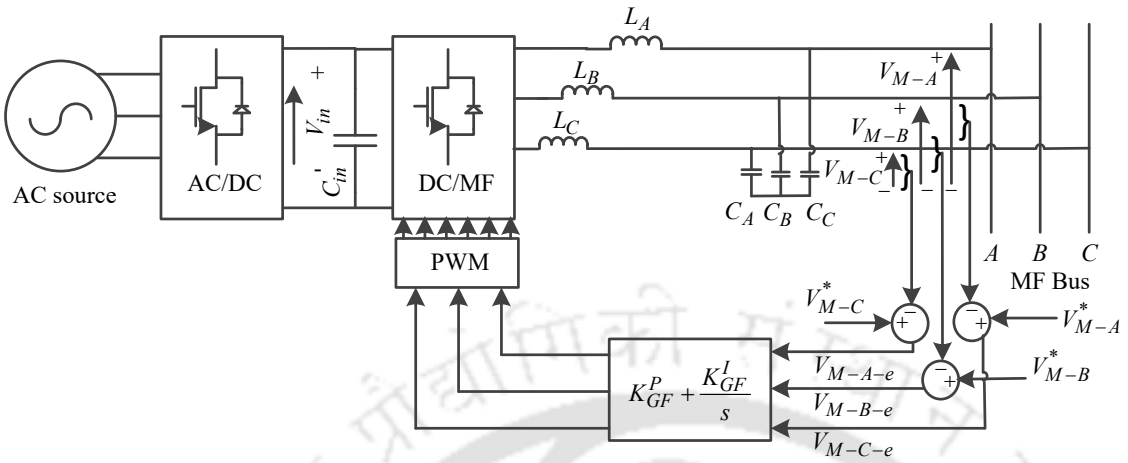

Figure 3.3: Control strategy for DC/MF grid forming converter.

converter. The error signal is sent to a PI controller to generate the modulating signal. This signal is sent to a PWM block to generate the switching pulses for DC/MF converter.

3.2.1.2 Grid Forming Converter

The grid forming converter is a source side converter and controlled as a voltage source and operated in parallel with other grid feeding converters. In islanded mode, the grid forming converter controls the MF bus voltage. The grid forming structure is created by the back to back connection of a DC/MF and either AC/DC or DC/DC converter based on the source frequency. The required input voltage (V_{in}) of DC/MF converter is created by the source side AC/DC or DC/DC converter. The output voltage of the DC/MF converter is switched so, LC filters are connected to generate required MF voltage at output. To control the output voltage, the PWM voltage control technique is used as shown in Fig. 3.3 due to lower switching loss. The reference bus voltage (V^*_M) is compared with the converter output voltage (V_M) and the error result is sent to a PI controller to obtain the reference for the PWM block. PWM block generates the switching signals to maintain the MF bus voltage.

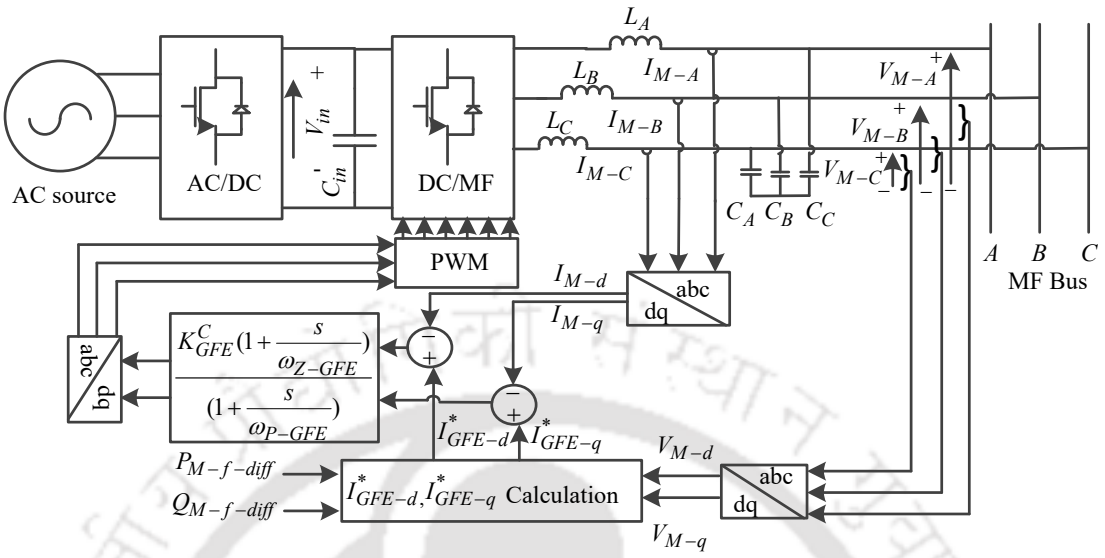

Figure 3.4: Control strategy for DC/MF grid feeding converter.

3.2.1.3 Grid Feeding Converter

Grid feeding converters are source side converters and send active and reactive power to the MF bus from the sources with respect to a fixed voltage and frequency. In MFMG operation, these converters are controlled as current sources. Grid feeding converters balance different frequency active and reactive powers of MFMG, so the output currents of these converters need to be controlled. The grid feeding converter structure is formed by the back to back connection of DC/MF converter and either AC/DC or DC/DC converter based on source frequency. The 50 Hz AC or DC source power is converted to DC power by the source side converter and this DC power is converted to MF power by DC/MF converter. The output current of the DC/MF converter is switched so, L filters are connected to the output to get the desired frequency current output. The inner loop of average mode current control is employed hare as shown in Fig. 3.4. If a power imbalance situation happens in MFMG, then $P_{M-f-diff}$ and $Q_{M-f-diff}$ are calculated and fed back to the power balancing flowchart presented in chapter 4. The flowchart calculates the direct and quadrature axis reference currents (I^*_{S-n-d}, I^*_{S-n-q}) for grid feeding converters. Finally, dq/abc transformation is done to calculate the three phase reference current (I^*_{GFE}). This reference current is compared with the output inductor current (I_M) and the error

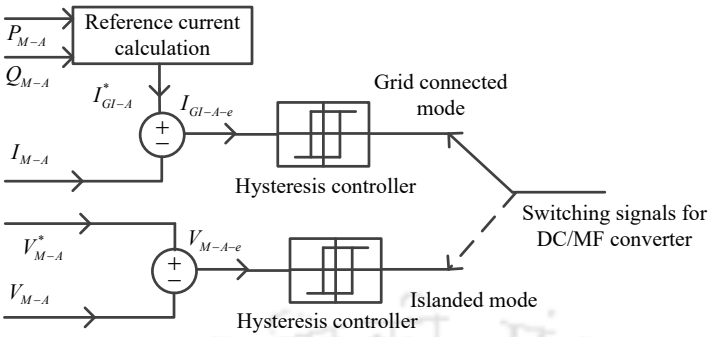

Figure 3.5: Control strategy for DC/MF grid interactive converter.

signal is passed through a controller to generate the reference modulating signals. Finally, the PWM block generates the switching signals for the converter.

3.2.1.4 Grid Interactive Converter

The grid interactive converter can be operated in either voltage control mode or current control mode. In islanding mode, the grid interactive converter acts as a grid forming converter and balances the bus voltage. In grid connected mode it behaves like a grid feeding converter and sends power to the bus. This converter has a unique capability to generate power of different frequencies in different phases to balance single phase loads. The control structure of grid interactive converter is shown in Fig. 3.5. In islanded mode, hysteresis voltage control is adopted to maintain the output voltage of the DC/MF converter. The reference MF bus voltage (V^*_M) contains frequency elements of DC, 25 Hz, and 50 Hz. The output voltage (V_{M-A}) of the converter is sensed and compared with the reference value. The voltage error (V_{M-A-e}) is passed through the hysteresis controller to create the switching signals. When different single phase loads are connected to the MF bus, power imbalance cases happen in different phases. To balance these cases the output current of each phase of grid interactive converter needs to be controlled separately. For this operation, a separate hysteresis controller is employed in each phase of the converter. For each phase, the deficit amount of different frequency active ($P_{M-A} = \sum^f P_{M-A-f}$) and reactive power ($Q_{M-A} = \sum^f Q_{M-A-f}$) are added and total deficit power is calculated. It is fed to the reference current calculation box to generate the reference currents for the hysteresis controller. For this, first the direct and quadrature axis current

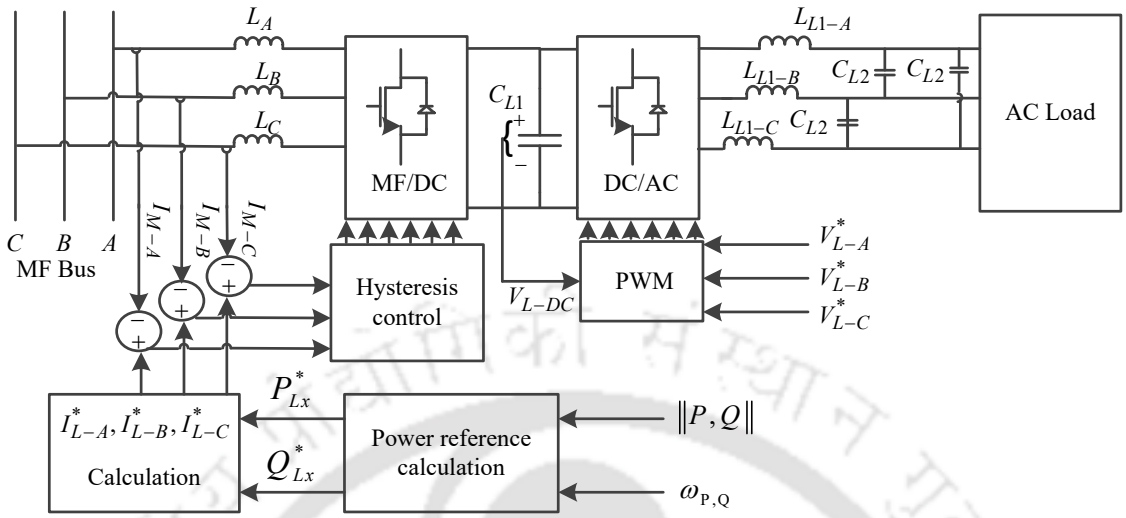

Figure 3.6: Control strategy for DC/MF load side converter.

reference of each phase is calculated as per equations (3.1, 3.2). The dq/abc conversion is done with help of a phase locked loop (PLL), and the reference for each phase current is calculated by, $I^*_{GI-A} = \sum^f I^*_{GI-A-f}$. The output current of the converter in each phase is sensed and compared with the calculated reference value. Finally, the compared result is sent through a hysteresis controller to create the switching signals.

$$I^*_{GI-A-f-d} = \frac{2}{3}\left(\frac{P^*_{M-A-f}V_{M-A-f-d} + Q^*_{M-A-f}V_{M-A-f-q}}{V^2_{M-A-f-d} + V^2_{M-A-f-q}}\right) \tag{3.1}$$

$$I^*_{GI-A-f-q} = \frac{2}{3}\left(\frac{P^*_{M-A-f}V_{M-A-f-q} - Q^*_{M-A-f}V_{M-A-f-d}}{V^2_{M-A-f-d} + V^2_{M-A-f-q}}\right) \tag{3.2}$$

3.2.1.5 Load Side Converter

In an MFMG, the customers are able to select any frequency available power from the MF bus. A new control strategy is required to achieve this frequency selective power transmission. A back to back converter control structure is employed to control the load voltage and current as presented in Fig. 3.6. For any AC load, one DC/MF converter and one DC/AC converter are used to connect the load to the MF bus. To control the load voltage, the output load voltage (V_L) is sensed and scaled by measured DC link voltage (V_{L-DC}). This signal is compared with

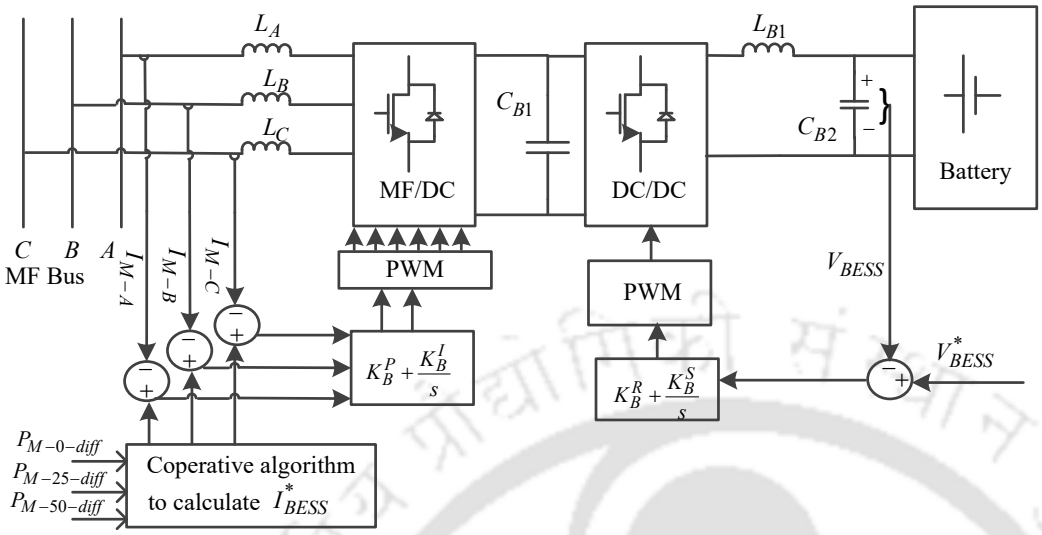

Figure 3.7: Control strategy for DC/MF battery side converter.

a triangular waveform to produce the required gate pulses for the converter. On the load side, LC filters are used to maintain the load voltage. The power frequency channel selection is done by the hysteresis controller in DC/MF converter. Here for the reference power, any magnitude (P, Q) and any available frequency ($\omega_{P,Q}$) can be chosen. Accordingly, the reference current (I_L^*) is calculated and the hysteresis controller selects that certain frequency current as the load current (I_M). So, a load-side user can select any power channel according to his need from the multifrequency bus by choosing the appropriate frequency for the reference load power. Here the DC/MF converter acts as a filter for a certain frequency channel. In the input side of the DC/MF converter L filters are connected to filter out the input current harmonics. For DC load DC/MF and a DC/DC converter are used and accordingly control is done.

3.2.1.6 Battery Side Converter

In MFMG, the BESS is connected by a back to back converter structure to control the active power flow and voltage of the battery. The control strategy of BESS is conferred in Fig. 3.7. The output current of the battery is controlled by DC/MF converter. Here average current control method is applied and accordingly PI controller design is performed. The reference current of the battery side converter is determined by a cooperative algorithm which is properly discussed

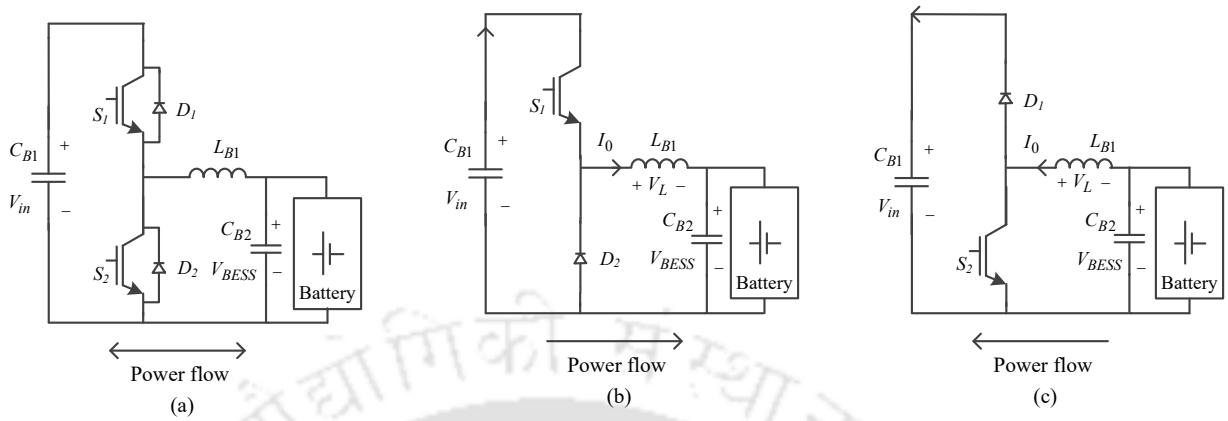

Figure 3.8: (a) Bidirectional DC-DC converter structure. (b) Bidirectional DC-DC converter in buck mode. (c) Bidirectional DC-DC converter in boost mode.

in chapter 6. I^*_{BESS} can be positive or negative depending on the charging or discharging mode. Output current (I_M) is sensed and compared with the reference output current of the algorithm. This error is sent to a designed PI controller to create the modulating signal. This signal is compared with a sawtooth carrier waveform of 10 kHz frequency to generate the switching signals. A bidirectional DC-DC converter maintains the battery voltage at C_{B2}. Based on the charging or discharging mode, the voltage at C_{B1} is changed. So to maintain the battery voltage at 480 V, the bidirectional DC-DC converter is required. If $C_{B1} < C_{B2}$ then it works in boost mode otherwise works in buck mode. Here voltage mode control strategy is used to control the voltage of the converter. The voltage of the battery (V_{BESS}) is sensed and compared to the reference battery voltage (V^*_{BESS}). The error signal is passed through a PI controller to generate the required modulating signals. The PI controller design is done by the loop shaping method.

In bidirectional DC-DC converter, power flows in both forward and reverse directions. When S_1 is switched on and S_2 is switched off, forward current flows through S_1 and D_2. The battery is acted as a load to form a buck converter circuit and got charged through this process. When S_2 is switched on and S_1 is switched off, reverse current flows through S_2 and D_1. The battery is acted as a source to form a boost converter circuit and got discharged through this process. Here a sample bidirectional DC-DC converter is simulated in Matlab Simulink. The input

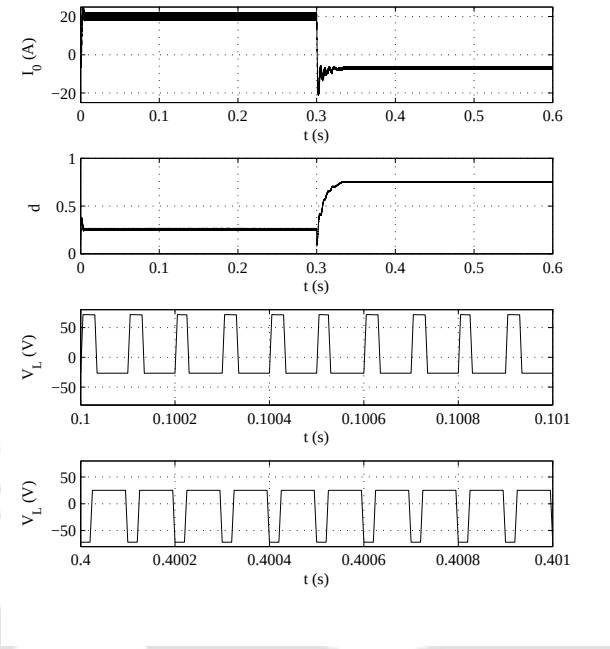

Figure 3.9: Output current, duty ratio, inductor voltage in buck mode, and inductor voltage in boost mode of bidirectional DC-DC converter.

voltage of the converter is taken as 100 V, and the battery voltage is taken as 24 V. The reference current of the converter is 20 A for 0-0.3 s and -7 A for 0.3-0.6 s. So from 0-0.3 s, the converter should act as a buck converter and the battery is charged whereas in 0.3-0.6 s, the converter should act as a boost converter and the battery is discharged. The simulation results are shown in Fig. 3.9. It can be seen from the result the output current is following the reference current. Between 0-0.3 s, the duty ratio is 0.25 ($\frac{V_{BESS}}{V_{in}}$) and between 0.3-0.6, the duty ratio is 0.75 ($\frac{V_{BESS}-V_{in}}{V_{BESS}}$). When the converter works in buck mode (0-0.3 s) the inductor voltage varies between 76 ($V_{in} - V_{BESS}$) and -24 ($-V_{BESS}$). When the converter works in boost mode (0.3-0.6 s) the inductor voltage varies between 24 (V_{BESS}) and -76 ($V_{BESS} - V_{in}$).

3.3 Basic Converter Structure of Multifrequency Microgrid

It can be noticed from the architecture that DC/MF converters are the building block of MFMG. It is a modular converter which can be used for grid side, grid forming, grid feeding,

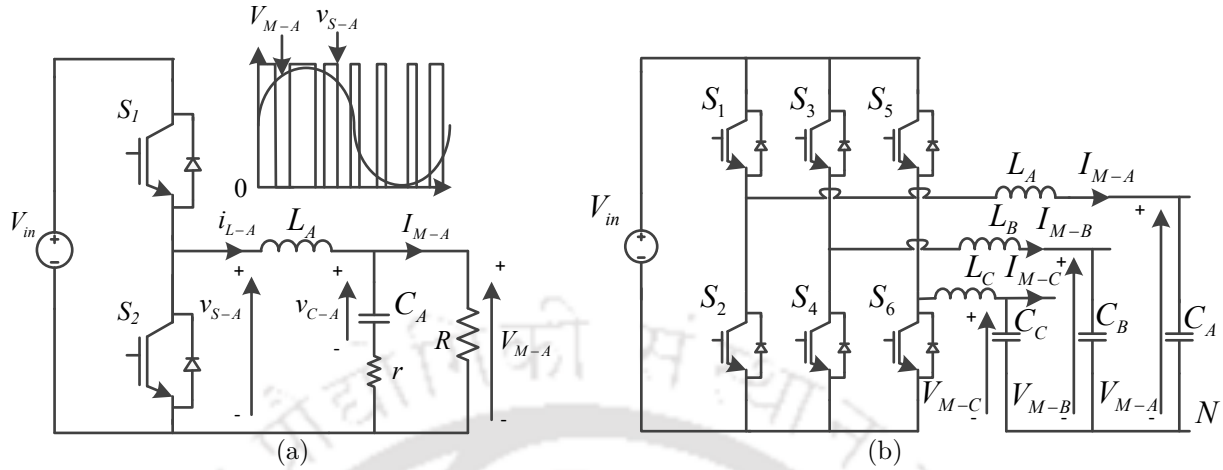

Figure 3.10: (a) One phase of DC/MF converter. (b) DC/MF converter.

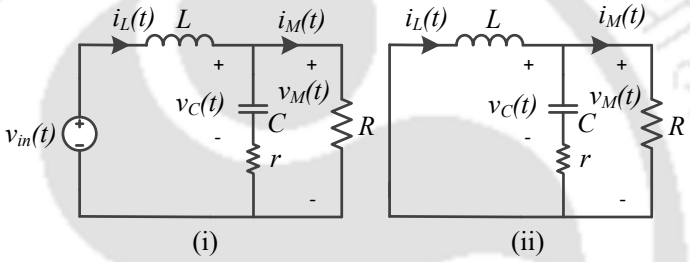

Figure 3.11: (i) Equivalent circuit of converter in dT_S mode (ii) Equivalent circuit of converter in $(1-d)T_S$ mode.

grid interactive, or load side converter. In this section, the structure of the DC/MF converter is proposed. From the structure, the SSM is obtained by using state space modelling. The structure is verified by open loop hardware and simulation results.

3.3.1 DC/MF Converter

On the input side of the converter, DC voltage is applied and the output is the mixture of DC and AC quantities. The structure is similar to one leg of a DC/AC converter. This one-leg structure can produce switched AC+DC voltage. An LC filter is connected at the output side to generate desired frequency outputs. For this chapter, the control of DC/MF converter is done in a way that it produces DC, 50 Hz, and 25 Hz components. The total converter structure is presented in Fig. 3.10. The circuit comprises of an input voltage V_{in}, two switches S_1 and S_2, and one load side LC filter where the capacitor has one effective series resistance (r). A load resistance R is connected at the output. The duty cycle for S_1 is d and for S_2 is

$(1-d)$. The switched output voltage is v_S and the filtered output is V_M, which has all three frequency components. Based on the switching conditions, the switching period is divided into two modes. In mode I $(0 < t < dT_S)$, S_1 is on and S_2 is off. In mode II $(dT_S < t < T_S)$, S_1 is off and S_2 is on. The equivalent circuit diagrams of these two modes are conferred in Fig. 3.11. By connecting three single phase DC/MF converter, three phase DC/MF converter structure is created.

3.3.2 Modelling of DC/MF Converter

The DC/MF converter model is required to understand the the behaviour of the system in the open loop. For modelling of converters, state space averaging method is adopted here. By using inductor volt-sec balance and capacitor charge balance criteria, the state space equations for each mode are derived. Here the modelling of DC/MF single phase converter is presented. All switches are considered ideal, the ESR of the inductor is neglected. Only the capacitive parasite component is considered. The average load current is obtained as half of the ripple load current.

3.3.2.1 State Space Equations for Different Switching Mode

For DC/MF converter, inductor current (i_L) and capacitor voltage (v_C) are taken as state variables, input voltage (V_{in}) and duty ratio (d) are considered as input variables and output voltage (V_M) is taken as output variable. The state space equations for two modes are,

$$\dot{x} = A_1 x + B_1 u,\ y = C_1 x + E_1 u \quad for\ 0 < t < dT_S \tag{3.3}$$

$$\dot{x} = A_2 x + B_2 u,\ y = C_2 x + E_2 u \quad for\ dT_S < t < T_S \tag{3.4}$$

Where the vector notation of different variables are, $x = [i_L\ v_C]^T$, $u = [V_{in}\ d]^T$ and $y = [V_M]$. The different coefficient matrices are,

$$A_1 = \ A_2 = \begin{bmatrix} -\frac{rR}{L(r+R)} & -\frac{R}{L(r+R)} \\ \frac{R}{C(r+R)} & -\frac{1}{C(r+R)} \end{bmatrix}$$

$$B_1 = \begin{bmatrix} \frac{1}{L} \\ 0 \end{bmatrix}$$

$$B_2 = \begin{bmatrix} 0 \\ 0 \end{bmatrix}$$

$$C_1 = C_2 = \begin{bmatrix} \frac{rR}{(r+R)} & \frac{R}{(r+R)} \end{bmatrix}$$

$$E_1 = E_2 = \begin{bmatrix} 0 & 0 \end{bmatrix}$$

3.3.2.2 Averaged State Space Model

As there are two different switching modes so coefficient matrices can be different for these two modes. To get coefficient matrices for the whole switching period, averaged state space technique can be used. The averaged equations are,

$$A_{av} = dA_1 + (1-d)A_2 \tag{3.5}$$

$$B_{av} = dB_1 + (1-d)B_2 \tag{3.6}$$

$$C_{av} = dC_1 + (1-d)C_2 \tag{3.7}$$

$$E_{av} = dE_1 + (1-d)E_2 \tag{3.8}$$

All averaged coefficient matrices are,

$$A_{av} = A_1 = A_2 \tag{3.9}$$

$$B_{av} = \begin{bmatrix} \frac{d}{L} \\ 0 \end{bmatrix}$$

$$C_{av} = C_1 = C_2 \tag{3.10}$$

$$E_{av} = E_1 = E_2 \tag{3.11}$$

3.3.2.3 Small Signal Perturbation and Linearisation

To define different TFs, a linearised and time invariant DC/MF converter model is required. For this, small signal perturbation and linearisation method is used. The state space equations become,

$$\dot{X} + \dot{\hat{x}} = (X + \hat{x})[A_1(d + \hat{d}) + A_2(1 - d - \hat{d})] + (U + \hat{u})[B_1(d + \hat{d}) + B_2(1 - d - \hat{d})] \quad (3.12)$$

$$Y + \hat{y} = (X + \hat{x})[C_1(d + \hat{d}) + C_2(1 - d - \hat{d})] + (U + \hat{u})[E_1(d + \hat{d}) + E_2(1 - d - \hat{d})] \quad (3.13)$$

The final small signal equation can be calculated by neglecting the DC and non linear terms.

$$\dot{\hat{x}} = A_{av}\hat{x} + B_{av}\hat{u} + [(A_1 - A_2)X + (B_1 - B_2)U]\hat{d} \quad (3.14)$$

3.3.2.4 Open Loop Transfer Function

The output voltage to input voltage TF of the converter is defined as,

$$\frac{\hat{v_M}(s)}{\hat{v_{in}}(s)} = C(sI - A)^{-1}B \quad (3.15)$$

Putting all the matrix values the final equation becomes,

$$\frac{\hat{v_M}(s)}{\hat{v_{in}}(s)} = \frac{Rd(1 + srC)/(R + r)LC}{s^2LC(R + r) + s(L + rRC) + R} \quad (3.16)$$

To design a controller for voltage mode control, the duty cycle (d) to output voltage (v_M) TF needs to be obtained. Here this TF is calculated by doing Laplace transformation of equation 3.14. The TF is,

$$\frac{\hat{v_M}(s)}{\hat{d}(s)} = C(sI - A)^{-1}F \quad (3.17)$$

$$F = (A_1 - A_2)X + (B_1 - B_2)U \quad (3.18)$$

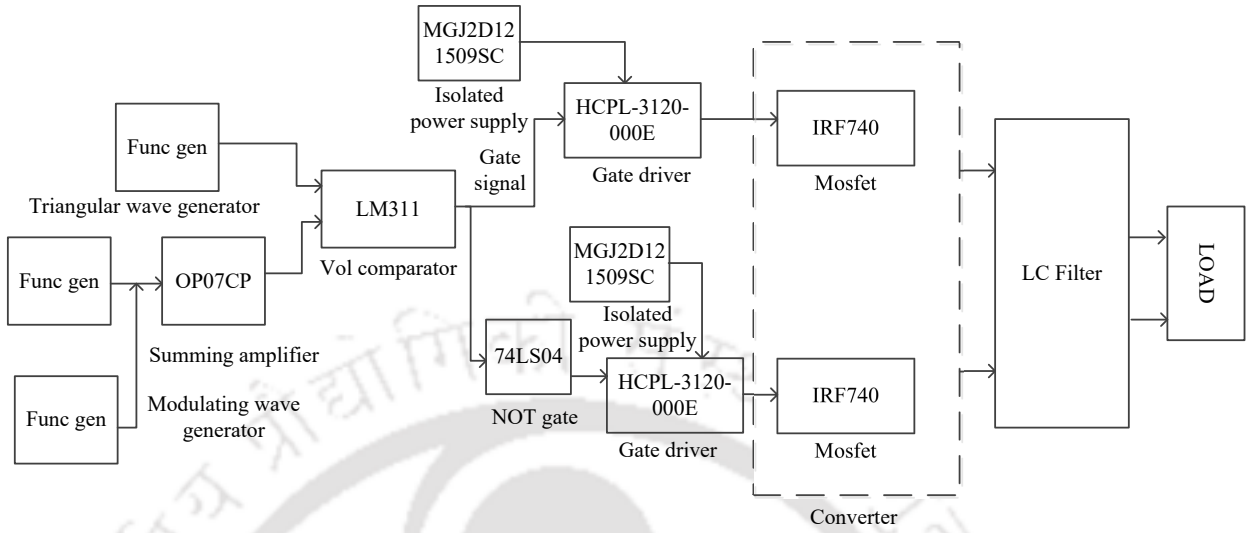

Figure 3.12: Block diagram of hardware set-up.

After calculating and simplifying the equation, the TF becomes,

$$\frac{\hat{v_M}(s)}{\hat{d}(s)} = \frac{RV_{in}(1+srC)/(R+r)LC}{s^2LC(R+r)+s(L+rRC)+R} \tag{3.19}$$

For output current control of the converter average mode current control method is used. To design controller for current control mode, duty cycle (d) to inductor current (i_L) TF is obtained.

$$\frac{\hat{i_L}(s)}{\hat{d}(s)} = \frac{V_{in}(1+(r+R)Cs)}{s^2LC(R+r)+s(L+rRC)+R} \tag{3.20}$$

3.3.3 Hardware Experiment to Operate DC/MF Converter in Open Loop

The structure of the DC/MF converter is verified by open loop hardware and simulation results. For hardware results, here a DC/MF converter prototype (Fig. 3.13) is developed with power electronics elements. The input voltage, duty ratio, and load resistance is varied and accordingly the output voltage of the the DC/MF converter is measured. To validate the structure of the DC/MF converter, the hardware results are compared with the simulation results. The block diagram of the experimental setup is shown in Fig. 3.12. The prototype can be divided into power and control circuits. The power circuit consists of two power MOSFETs,

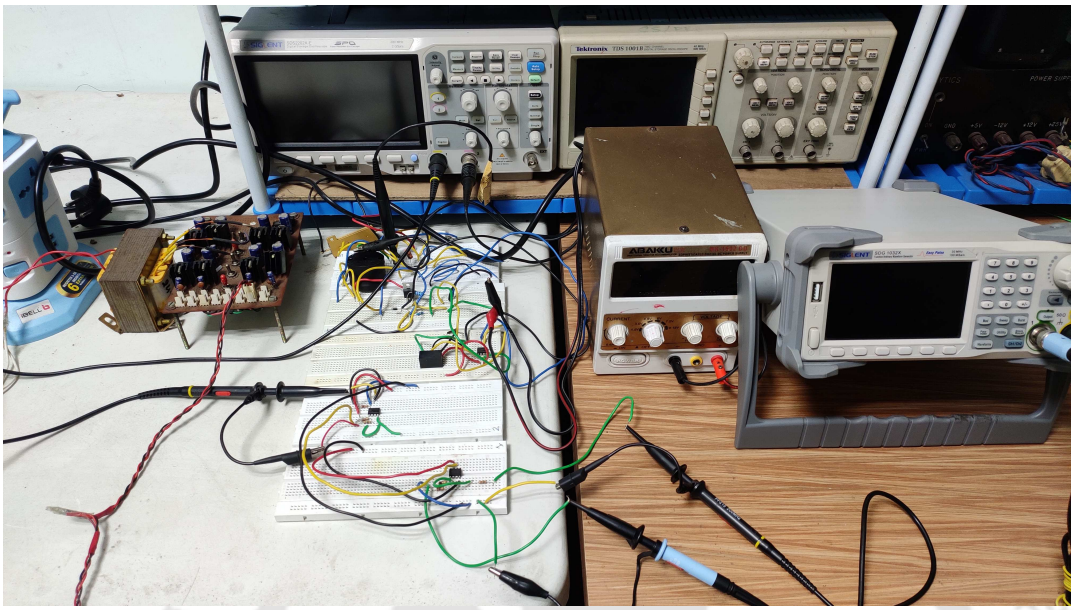

Figure 3.13: Hardware set-up to operate the DC/MF converter in open loop.

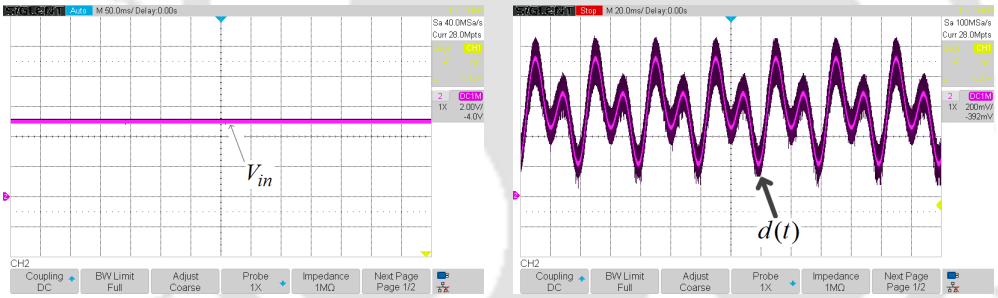

(a) (b)

Figure 3.14: (a) Input voltage of DC/MF converter. (b) Modulating signal of DC/MF converter.

one inductor, one electrolytic capacitor, and one load resistance. The gate signals of the two switches are created from the control circuit. To create MF voltage and current at the output, the modulating signal needs to be an MF waveform. Two different function generators are used to create DC, 25 Hz, and 50 Hz signals. These signals are superimposed through a summing amplifier to create the MF modulating waveform as shown in Fig 3.14. Here two different modulating signals are created by varying the DC, 25 Hz, and 50 Hz signals. Another function generator is used to create the triangular carrier waveform of 10 kHz frequency. A voltage comparator compares the modulating and carrier waveforms to generate the switching pulse. This signal is passed through a not gate to generate the complementary switching pulse. These gate signals are sent to the gate driver circuit to generate the gate signals for MOSFETs.

Table 3.1: List of components required for hardware setup

Component name	Part number	Specification
Transformer	-	$18-0-18\ V,\ 5\ A$
Diode	1N5408	$1000\ V,\ 3\ A$
5 V regulator	LM7805, LM7905	-
9 V regulator	LM7809, LM7909	-
12 V regulator	LM7812, LM7912	-
15 V regulator	LM7815, LM7915	-
Operational amplifier	LM311, OP07CP	-
Not Gate	74LS04	-
Isolated power supply	MGJ2D121509SC	-
Gate driver IC	HCPL-3120-000E	-
Power MOSFET	IRF740BPBF	$400\ V,\ 10\ A$
Inductor	1140-472K-RC	$4.6\ mH,\ 2\ A$
Electrolytic capacitor	100YXG1000MEFC18X40	$1000\ \mu F,\ 100\ V$
Resistor	RS01010R00FE12	$10\ \Omega,\ 10\ W$
Resistor	810F5R0E	$5\ \Omega,\ 10\ W$

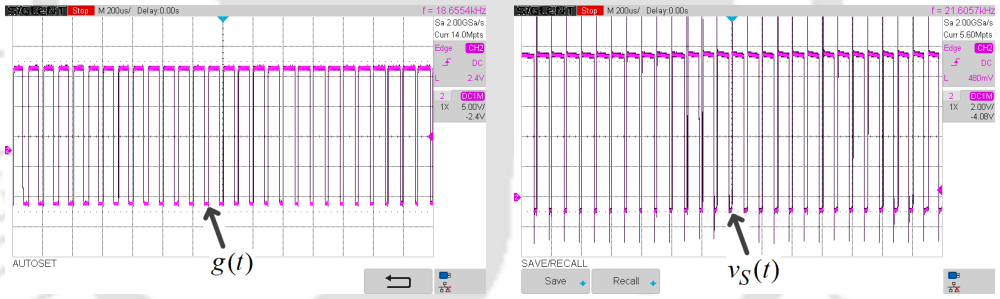

(a) (b)

Figure 3.15: (a) Gate signal ($g(t)$) of DC/MF converter. (b) Switched output voltage of DC/MF converter.

The input voltages of the gate driver circuits are supplied by isolated power supplies to remove the floating ground problem. The gate signal and output switched voltage are presented in Fig 3.15. It can be noticed that the gate signal varies between $+15\ V$ and $-9\ V$ as per the requirement. To supply the required input DC voltage to the ICs, a power supply circuit is designed which consists of a transformer and a rectifier circuit. Different voltage regulators are used to create $\pm 5\ V$, $\pm 9\ V$, $\pm 12\ V$, $\pm 15\ V$, and $\pm 18\ V$ DC supply. The different power electronic components of the experiment are presented in Table 3.1.

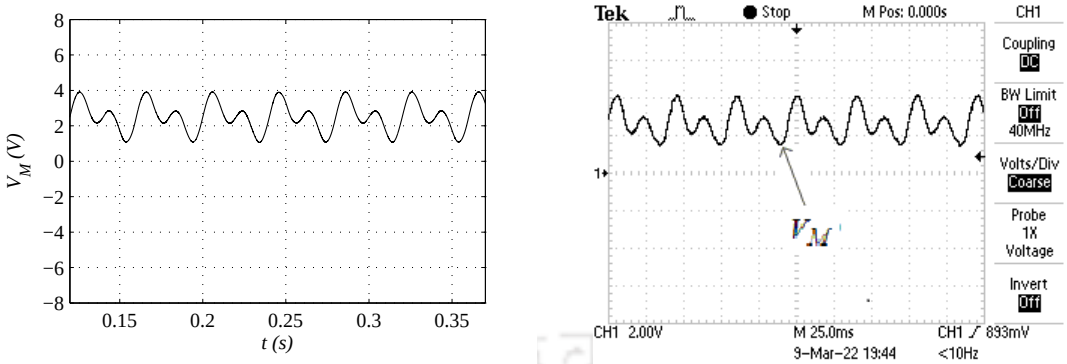

(a) (b)

Figure 3.16: (a) Simulation result (b) Hardware result of output voltage of DC/MF converter with $V_{in} = 5\ V,\ d = 0.5 + 0.15\ sin\ 314t + 0.15\ sin\ 157t$.

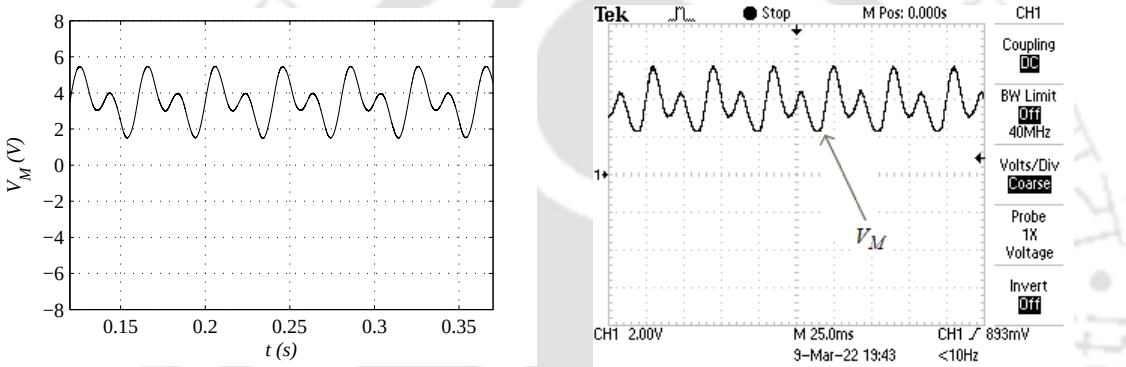

(a) (b)

Figure 3.17: (a) Simulation result (b) Hardware result of output voltage of DC/MF converter with $v_{in} = 7\ V,\ d = 0.5 + 0.15\ sin\ 314t + 0.15\ sin\ 157t$.

3.3.4 Simulation and Hardware Results of DC/MF Converter Operation in Open Loop

The hardware results are taken from the hardware set-up by using an oscilloscope. To verify the hardware result, a simulation model of DC/MF converter is prepared. The parameters of the simulation model are taken same as the hardware model. Finally, the hardware and simulation results are compared.

The DC/MF converter is tested in the open loop by varying input voltage, duty ratio, and load resistance. First, 5 V input voltage is given and the duty ratio is kept at $d = 0.5 + 0.15\ sin\ 314t + 0.15\ sin\ 157t$. The output voltage becomes 2.5 V DC+ 0.75 V 50 Hz+ 0.75 V 25 Hz which is shown in Fig. 3.16. So the DC/MF converter can generate MF voltage and current from a DC source. So the design of the converter and control strategy is perfect for the system.

Next, the input voltage is changed to 7 V. With this configuration, the output voltage is

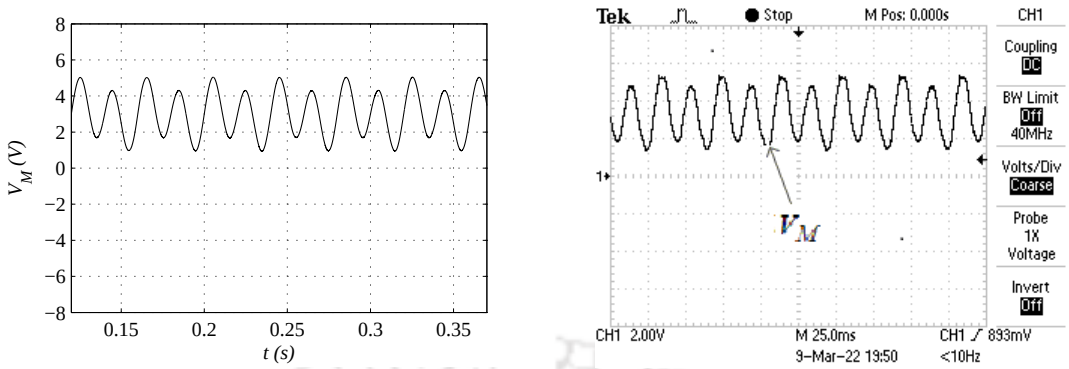

(a) (b)

Figure 3.18: (a) Simulation result (b) Hardware result of output voltage of DC/MF converter with $v_{in} = 5\ V,\ d = 0.6 + 0.3\ sin\ 314t + 0.1\ sin\ 157t$.

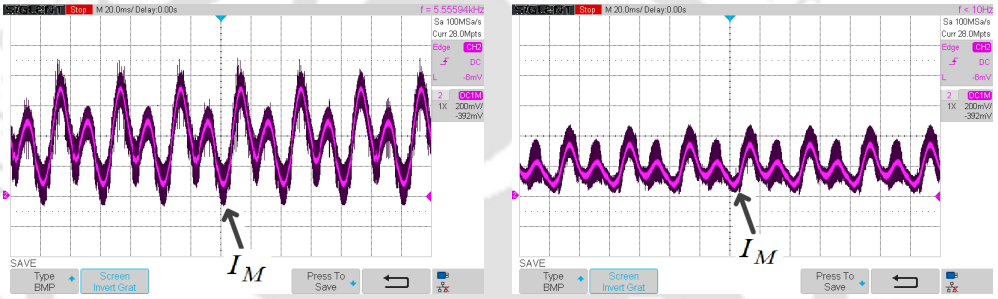

(a) (b)

Figure 3.19: (a) Output current of DC/MF converter with 5 Ω load. (b) Output current of DC/MF converter with 10 Ω load.

proportionally changed to 3.5 V $DC +$ 1.05 V 50 $Hz +$ 1.05 V 25 Hz. So the converter responds properly to the input voltage change as shown in Fig. 3.17.

Then the duty ratio is varied to $0.6 + 0.3\ sin\ 314t + 0.1\ sin\ 157t$ keeping $V_{in} =$ 5 V and the effect of the duty ratio to output voltage is observed. Fig. 3.18 presents that the output voltage changes to 3 V DC+ 1.5 V 50 $Hz +$ 0.5 V 25 Hz. The experimental results are compared with simulation results and it can be seen the experimental results are matching with simulation results. Next, the load resistance of the converter is changed from 5 Ω to 10 Ω. From Fig. 3.19, it can be noticed that the load current changes to maintain the same load voltage. In the experiment, the current is measured by using a 1 Ω resistance and voltage probes.

Table 3.2: Design specification of DC/MF converter

Parameter	value
Filter inductance (L)	0.1 mH
Filter capacitance (C)	250 μF
Load resistance (R)	5 Ω
Capacitive ESR (r)	0.1 Ω
Input voltage (V_{in})	1000 V
Controller gain crossover frequency (ω_{cr-co})	4 kHz
Controller desired phase margin (PM_d)	45°
Switching frequency (f_S)	100 kHz
PWM gain (k_{PW})	1
Current sensor resistance (R_S)	1 Ω

3.4 Controller Design of DC/MF Converter

For the operation of DC/MF converter with different control strategies in grid connected and islanded mode, the closed loop control of the converter is required. For close loop voltage and current control, different PI, type II compensator, and hysteresis controllers need to be designed. In this section, the design techniques of the PI controller, type II compensator, and hysteresis controller are presented.

3.4.1 PI Controller Design

Here the design of PI controller for voltage mode control is described first. Duty cycle (d) to output voltage (v_M) TF is required for voltage mode controller. In similar manner PI controller for current mode control can be designed based on the duty cycle (d) to inductor current (i_L) TF.

$$G_{PV}(s) = \frac{\hat{v_M}(s)}{\hat{d}(s)} = \frac{RV_{in}(1+srC)/(R+r)LC}{s^2LC(R+r)+s(L+rRC)+R} \tag{3.21}$$

Using the design specifications provided in Table 3.2, the final TF can be calculated.

$$\frac{\hat{v_M}(s)}{\hat{d}(s)} = \frac{98039(10000+s)}{0.000005s^2+0.0015s+5} \tag{3.22}$$

The root-locus plot of the duty cycle (d) to output voltage (v_M) TF of DC/MF converter is shown in Fig. 3.20 (a). The open loop TF has two poles and one zero. As all poles and zero are

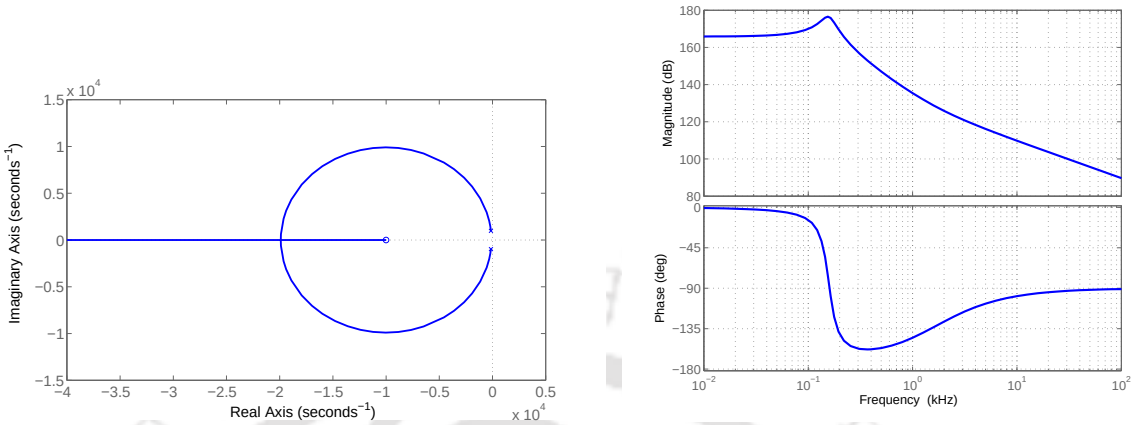

(a) (b)

Figure 3.20: (a) Root-locus plot (b) Bode plot of duty cycle (d) to output voltage (v_M) TF of DC/MF converter.

situated at the left half plane so the open loop system is stable. The bode plot of the plant is presented in Fig. 3.20 (b). The objective of the controller design is to maintain a decent phase margin at gain crossover frequency to make the total closed loop system stable. Here step by step design procedure is described.

(i) First the controller transfer function needs to be defined. The transfer function (G_{Co}) of controller is,

$$G_{Co}(s) = K_P + \frac{K_I}{s} \tag{3.23}$$

Where K_P is the proportional gain constant and K_I is the integral gain constant.

(ii) The magnitude and angle of the controller transfer function is, ($\omega_k = \frac{K_I}{K_P}$)

$$|G_{Co}| = \frac{K_P\sqrt{(\omega^2 + \omega_k^2)}}{\omega}, \angle G_{Co} = -90^\circ + \tan^{-1}(\frac{\omega}{\omega_k}) \tag{3.24}$$

(iii) From the characteristic equation of the total system, two criteria can be estimated with the desired phase margin (PM_d) of overall system.

$$|G_{Co}G_{PV}| = 1, \ \angle G_{Co}G_{PV} = -180^\circ + PM_d \tag{3.25}$$

(iv) The gain crossover frequency (ω_{Cr-co}) is chosen as 4 kHz from the bode plot of $G_{PV}(s)$.

Desired phase margin is chosen as 45° for the closed loop transfer function of total system. Putting these values, equations (3.26), (3.27) can be obtained.

$$\tan^{-1}(\frac{\omega_{Cr-co}}{\omega_k}) = -90^\circ + 45^\circ - \angle G_{PV_{\omega_{Cr-co}}} \tag{3.26}$$

$$K_P\sqrt{1+(\frac{\omega_k}{\omega_{Cr-co}})^2} = \frac{1}{|G_{PV}|_{\omega_{Cr-co}}} \tag{3.27}$$

(v) At 4 kHz, the magnitude and angle of the plant transfer function are calculated. They are,

$$|G_{PV}|_{4kHz} = 36.23,\ \angle G_{PV_{4kHz}} = -108^\circ \tag{3.28}$$

(vi) Using equations (3.26), (3.27), and (3.28) the value of K_P and K_I can be calculated. The final transfer function of controller is,

$$G_{Co}(s) = 0.022 + \frac{238.51}{s} \tag{3.29}$$

(vii) The total closed loop transfer function of the system is defined as,

$$C.L.T.F = k_{PW} * G_{Co}(s) * G_{PV}(s) \tag{3.30}$$

The bode plot of the C.L.T.F of voltage mode control is presented in Fig. 3.21 (a). It can be found that the gain crossover frequency of total system is 4 kHz and total phase margin of the closed loop system is 46°. So the controller design is satisfactory and it can control the output voltage DC/MF converter in a closed loop.

3.4.2 Type II Compensator Design

For current control of the DC/MF grid feeding converter, the inner loop of average mode current control is used. For this, a type II compensator needs to be designed. The duty cycle (d) to inductor current (i_L) transfer function ($G_{PI}(s)$) is,

$$G_{PI}(s) = \frac{\hat{i_L}(s)}{\hat{d}(s)} = \frac{V_{in}(1+s(R+r)C)}{s^2LC(R+r)+s(L+rRC)+R} \tag{3.31}$$

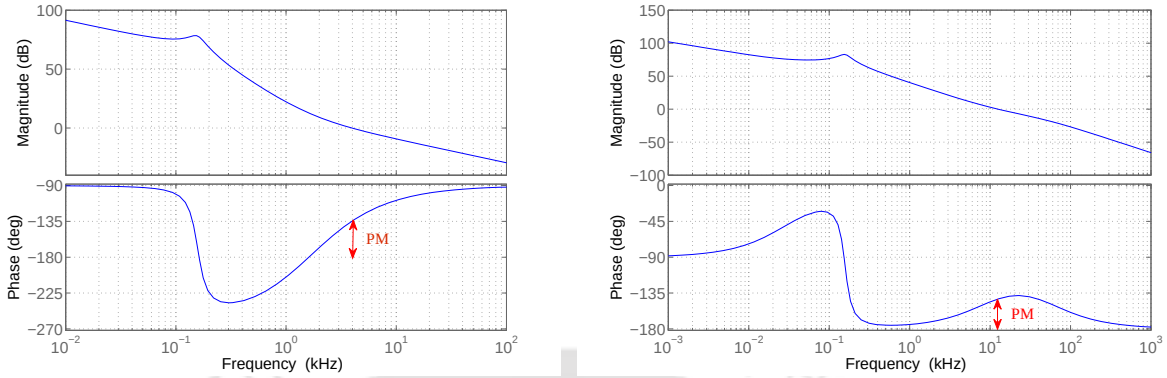

(a) (b)

Figure 3.21: (a) Bode plot of total closed loop transfer function for voltage mode control. (b) Bode plot of total closed loop transfer function for current mode control.

Using the values given in Table 3.2, the final transfer function can be calculated.

$$\frac{\hat{i_L}(s)}{\hat{d}(s)} = \frac{(5.1s + 1000)}{0.0000051s^2 + 0.0015s + 5} \tag{3.32}$$

The step by step type II compensator design is shown here.

(i) The compensator transfer function ($G_{Cm}(s)$) is defined as,

$$G_{Cm}(s) = \frac{K_C(1 + \frac{s}{\omega_Z})}{s(1 + \frac{s}{\omega_P})} \tag{3.33}$$

Where ω_Z, and ω_P are the zero and pole frequency of the compensator.

(ii) Different parameters of the compensator are calculated from equation (3.34).

$$f_{Cr-Cm} = \frac{V_{in} f_s}{2\pi V_R}, f_Z = \frac{f_{Cr-Cm}}{3}, f_P = \frac{f_s}{2}, K_C = \frac{V_{in} f_s L}{V_R R_s} \tag{3.34}$$

(iii) The closed loop transfer function of total system is,

$$C.L.T.F = R_s * k_{PW} * G_{Cm}(s) * G_{PI}(s) \tag{3.35}$$

The bode plot of the C.L.T.F of current mode control is presented in Fig. 3.21 (b). It can be found that the gain crossover frequency of the total system is 30 kHz and the total phase margin of the closed loop system is 39°. So the compensator design is satisfactory and it can

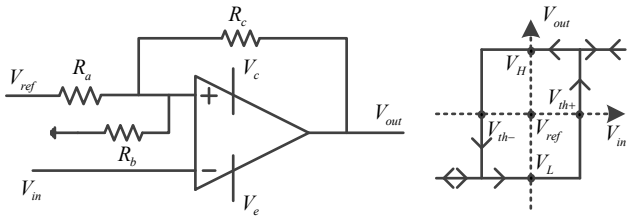

Figure 3.22: Inverting Schmitt trigger circuit and hysteretic characteristics curve.

control the output current DC/MF converter in a closed loop.

3.4.3 Hysteresis Controller Design

To control the output voltage and current of DC/MF converter, hysteresis control can be used due to several advantages. For this, a hysteresis controller is designed to control the output voltage and current of the DC/MF converter. An inverting Schmitt trigger circuit is used as a comparator with hysteresis band [75]. The circuit diagram is presented in Fig. 3.22. A positive feedback is applied on the non-inverting side. When the input voltage touches the upper threshold, the circuit automatically changes the threshold in opposite direction. By using equations 3.36, and 3.37, the upper and lower threshold values can be calculated. The hysteresis band (ΔH) is defined by the equation (3.38).

$$V_{th+} = \frac{R_{abc}V_{ref}}{R_b} + \frac{R_{abc}V_{out}}{R_c}, \; R_{abc} = \frac{1}{R_a} + \frac{1}{R_b} + \frac{1}{R_c} \tag{3.36}$$

$$V_{th-} = \frac{R_{abc}V_{ref}}{R_b} - \frac{R_{abc}V_{out}}{R_c} \tag{3.37}$$

$$\Delta H = V_{th+} - V_{th-} \tag{3.38}$$

The hysteretic characteristics curve is presented in Fig. 3.22. It can be noticed that when input voltage increases and crosses the upper threshold value (V_{th+}), the output voltage jumps up to an upper value (V_H) and remains constant. When the input voltage decreases and crosses the lower threshold value (V_{th-}), the output voltage jumps down to a lower value (V_L). The upper and lower output voltage limit can be controlled by controlling different parameters of Schimitt

Table 3.3: Simulation parameters of DC/MF converter

Parameter	value
V_{in}	1000 V
L, C	0.1 mH, 250 μF
K^P_{GF}, K^I_{GF}	1.6, 45
K^C_{GFE}	0.8
R	10 Ω

trigger circuit. The limits are calculated by using equations 3.39, and 3.40.

$$V_H = \frac{R_{abc}V_{ref}}{R_c} + \frac{R_{abc}V_c}{R_b} \tag{3.39}$$

$$V_L = \frac{R_{abc}V_{ref}}{R_c} - \frac{R_{abc}V_c}{R_b} \tag{3.40}$$

In this manner, the hysteresis voltage controller is designed. The hysteresis current controller can be designed by using the same procedure.

3.5 Simulation Results of Closed Loop Control of DC/MF Converter

In this section, the controller designs are verified by the closed loop simulation results of the DC/MF converter. To control the output voltage, the voltage mode control technique is used, and to control the output current of the DC/MF converter, average mode current control and hysteresis control techniques are used. All these control techniques are simulated on the DC/MF converter. The controllers are designed as per described methods and presented in Table 3.3.

3.5.1 Voltage Mode Control

First, the DC/MF converter is simulated with the designed PI controller for voltage mode control for different cases.

(i) Case 1: Output voltage control with reference voltage variation - Here the reference output voltage is chosen as 600 V DC+ 210 V 50 Hz (RMS)+ 50 V 25 Hz (RMS) for

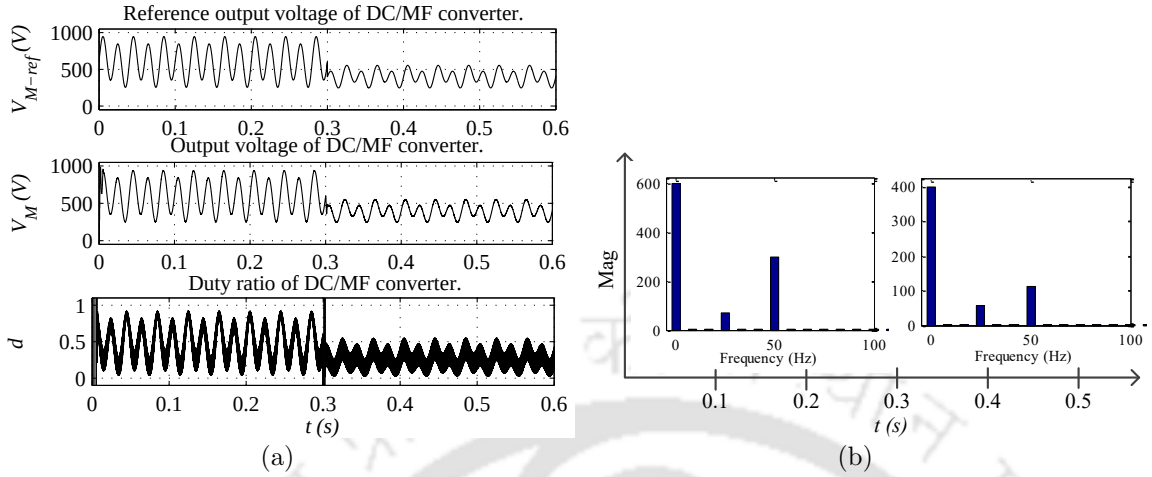

Figure 3.23: (a) Reference output voltage (V_{M-ref}), output voltage (V_M) and duty ratio (d) for case 1. (b) FFT analysis of output voltage (V_M) for case 1

$0-0.3\ s$ and 400 V DC+ 80 V 50 Hz (RMS)+ 40 V 25 Hz (RMS) for $0.3\ s-0.6\ s$. In Fig. 3.23 (a), the reference and actual output voltage are conferred with the duty ratio. It can be noticed that the duty ratio decreases at 0.3 s as the reference decreases and the actual output voltage of the DC/MF converter is tracking the reference voltage waveform throughout the $0-0.6\ s$.

Fast Fourier transformation (FFT) analysis is executed on the output voltage waveform to verify the presence of different frequency elements. In Fig. 3.23 (b), the FFT analysis is presented for $0-0.6\ s$ period. It can be noted that DC, 50 Hz, and 25 Hz frequency components are present in the output voltage waveform and all frequency voltages alter at 0.3 s as per change in reference voltage.

(ii) Case 2: Output voltage control with input voltage variation - For this case, the output voltage reference is fixed throughout the time but the input DC voltage changes at 0.3 s from 1000 V to 1200 V. Accordingly, the duty ratio decreases and the actual output voltage follows the reference throughout $0-0.6\ s$. In Fig 3.24 (a), the different output results are conferred for case 2.

(iii) Case 3: Output voltage control with load variation - Here, the resistive load is changed from 1 Ω to 5 Ω at 0.3 s keeping the output reference voltage fixed. It can be observed

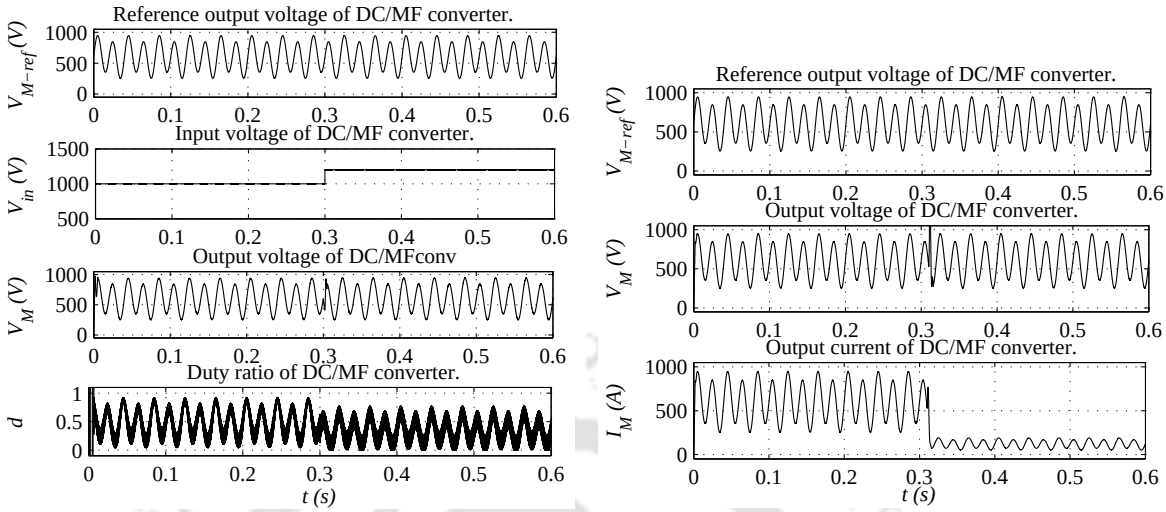

Figure 3.24: (a) Reference output voltage (V_{M-ref}), input voltage (V_{in}), output voltage (V_M) and duty ratio (d) for case 2. (b) Reference output voltage (V_{M-ref}), output voltage (V_M) and output current (I_M) for case 3.

from Fig. 3.24 (b) that the actual output voltage tracks the reference and the output current decreases five times as the load changes.

For all these cases, the PI controller is able to control the output voltage of the DC/MF converter. So the voltage control scheme is working and the PI controller is perfectly designed.

3.5.2 Average mode current Control

Here, the output current of the DC/MF converter is controlled and the inner loop of the average mode current control technique is used. For this, a type II compensator is designed and the parameters are shown in Table 3.3. First, the effect of change in reference output current on the output current of the DC/MF converter is investigated. It can be seen from Fig. 3.25 (a), that at 0.3 s the reference output current is changed from 15 A DC+ 5 A 50 Hz (RMS)+ 2 A 25 Hz (RMS) to 7 A DC+ 3 A 50 Hz (RMS)+ 1 A 25 Hz (RMS). As the output current reference decreases at 0.3 s, the duty ratio of the DC/MF converter also decreases to maintain the reference output current. It can be seen from the simulation results that the DC/MF converter maintains the output current as per the reference.

Next, the effect of change in input voltage on the output current of the DC/MF converter is investigated and conferred in Fig. 3.25 (b). The input voltage is changed from 1000 V to

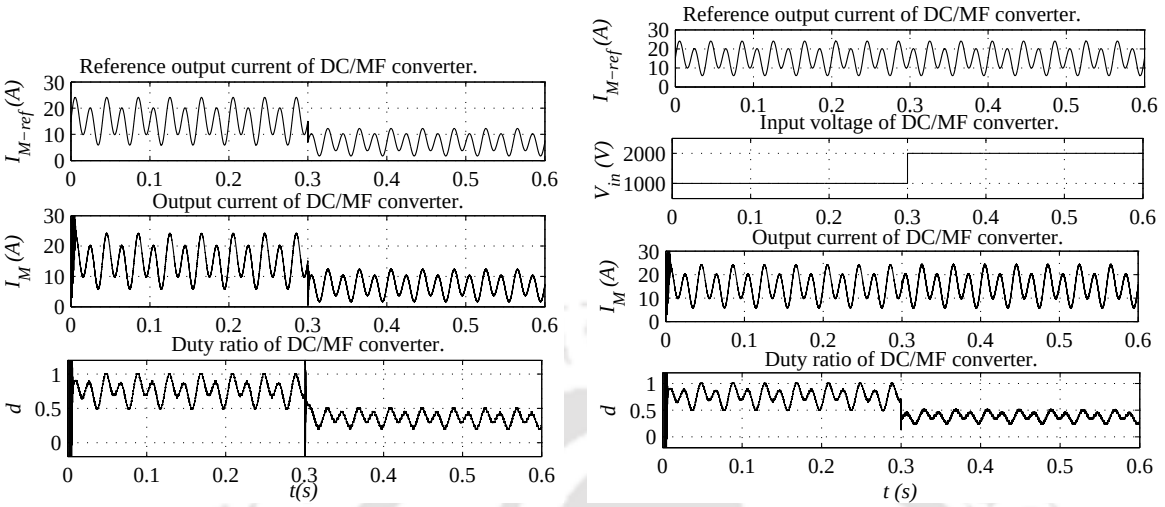

Figure 3.25: (a) Reference output current (I_{M-ref}), output current (I_M) and duty ratio (d) for change in reference voltage. (b) Reference output current(I_{M-ref}), input voltage (V_{in}), output current (I_M) and duty ratio (d) for change in input voltage.

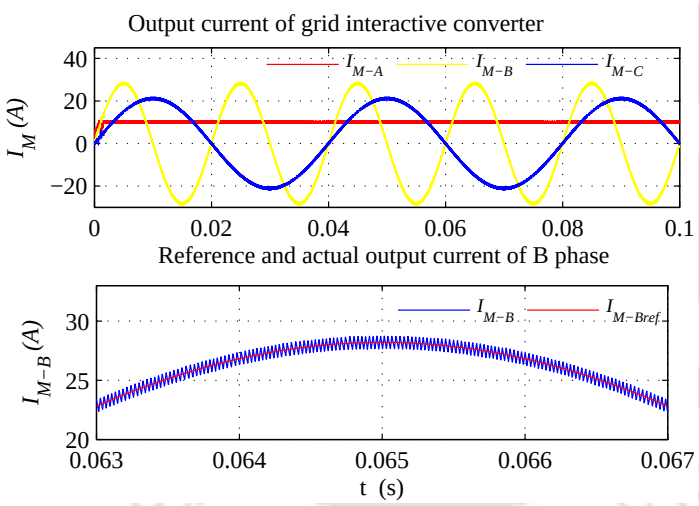

Figure 3.26: Three phase output currents (I_M) and zoomed version of B phase current (I_{M-B}) of grid interactive DC/MF converter.

2000 V at 0.3 s keeping the reference output current same. It can be noticed that the duty ratio is changed at 0.3 s to maintain the same output current. As input voltage increases, the duty ratio decreases at 0.3 s. So the designed compensator works perfectly and can maintain the output current with different input variations.

3.5.3 Hysteresis Control

A DC/MF converter is simulated with a resistive load and the output current of the converter is controlled by hysteresis control. It can be seen that the reference phase currents are not balanced and this type of operation is required for grid interactive converter to balance single phase loads. For this, the reference currents for phases A, B, and C are chosen as 10 A DC, 20 A 50 Hz (RMS), and 15 A 25 Hz (RMS) respectively. The output current of the DC/MF converter is conferred in Fig. 3.26. It can be seen that output currents match with the reference currents and DC/MF converter is able to generate different frequency currents in different phases. So the DC/MF converter can supply DC, 25 Hz, or 50 Hz single phase loads in an MFMG. The zoomed version of phase B current is also presented in Fig. 3.26. The output current of phase B varies between the hysteresis band and follows the reference current.

3.5.4 Conclusion

In this chapter, the architecture and DC/MF converter for MFMG are defined. The modelling of the converter is executed to find out the required TFs for controller design. A hardware prototype of the DC/MF converter is constructed and different open loop results of the converter are presented. It can be concluded from the open loop results that the converter structure is satisfactory. Different control strategies of the converter to work as grid side, grid feeding, grid forming, load side, and BESS side converter are introduced. To control the output voltage and output current for these operations, the voltage mode control, current mode control, and hysteresis control techniques are employed. Finally, the converter is simulated with closed loop controls and the output voltage and currents of the DC/MF converter are controlled. Closed loop results show that the designed controllers are working perfectly with the converter.

Note: Major part of this chapter is reproduced from my publications:

1. R. Dey and S. Nath, "Architecture and power converter for multifrequency microgrid," in *proceedings of IEEE National Power Electron. Conf.(NPEC)*, Dec. 2019, pp. 1–6.

2. R. Dey and S. Nath, "Grid interactive converter of multifrequency microgrid,"

in *proceedings of National Power Electronics Conference (NPEC)*, 2021, pp. 1–6.

4

Control and Management of Different Frequency Active Powers for Multifrequency Microgrid

Contents

4.1 Introduction

For any power system, if the source and load power do not match, the system becomes unstable and inoperative. Several active power balancing techniques for AC, DC, and hybrid microgrids are explained in the literature. Any MF system has a unique property over the conventional system. Different frequency active powers can be superimposed on the MF bus without mixing and consumers are able to choose any frequency power from the MF bus as per their needs. This frequency selective power distribution creates several power mismatch problems in MFMG which are not present in any AC, DC, or hybrid microgrid. For the operation of MFMG in grid connected and islanded mode, different frequency active powers need to be balanced for all these cases. This chapter analyzes the active power imbalance problems at different frequencies in detail. The problem of different frequency power imbalances in MFMG, due to frequency selective power transmission is analyzed for grid connected and islanded modes. Different active power unbalance cases are discussed and the conditions to balance active power at different frequencies are identified for an MF system for all the cases. It proposes control methods for both grid connected and islanded modes to balance different frequency active powers for all unbalanced cases in MFMG. The proposed methods are verified by simulation in Matlab Simulink environment of 7 bus MFMG, which consists of three different frequency sources and loads (DC, 25 Hz, 50 Hz) for both grid connected and islanded modes with three different cases. In this chapter first, the power management strategy of MFMG is described. Based on the management strategy different active power imbalance cases are found and for each case the active power balancing criteria is defined. Based on all the criteria, a flowchart is presented to balance different frequency active powers of MFMG. Finally, all supported simulation results are presented.

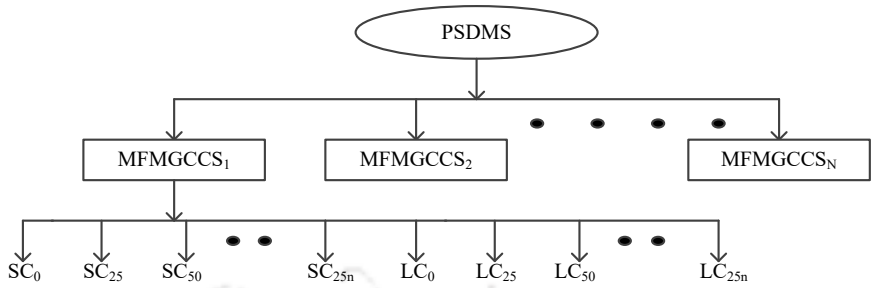

Figure 4.1: Block diagram of power management system of MFMG.

4.2 Power Management Strategy of Multifrequency Microgrid

First, the different frequency power management strategy of MFMG needs to be defined to discuss different power imbalance cases. Different frequency active powers of MFMG are regulated by a three-level hierarchical structure. The management system is presented in Fig. 4.1. Each individual source and load are connected to a source controller (SC) and load controller (LC) respectively. The third layer consists of different frequency source (SC) and load (LC) controllers which can measure and control the power flow of different loads and sources. To connect between all SCs and LCs, a multifrequency microgrid central controller system (MFMGCCS) is adopted. In grid connected mode, the LCs send different frequency active power consumption data, and SCs send the different frequency source power availability data. Based on the power generation capacity of each SC, MFMGCCS decides how much power ($P_{M-f-diff}$) the MFMG needs to export or import from the main grid to balance different frequency active powers at multifrequency (MF) bus. Based on this information, the grid side converter either export or import active power from grid to maintain the active power balance in the system. In islanded condition, the MFMGCCS sends the active power load demands to respective frequency SCs. According to that data, each SC sends the statistics that the source is able to fulfill the load demand or not ($P_{M-f-diff} = 0$ or $P_{M-f-diff} > 0$). If $P_{M-f-diff} = 0$, then that frequency active power is already balanced, and that frequency source is available for more power generation. If MFMGCCS receives $P_{M-f-diff} > 0$ for a particular SC then that frequency power is not balanced and it sends signals to other available SCs to increase

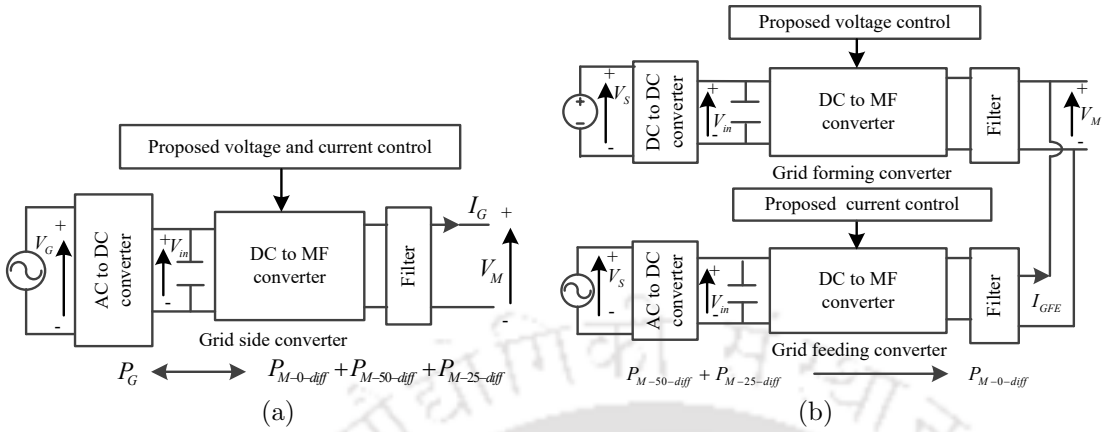

Figure 4.2: Active power balancing strategy of MFMG for (a) grid connected mode (b) islanded mode.

their power production equally to fulfill that frequency load demands. In the top layer, a power system distribution management system (PSDMS) is present which connects the microgrid to the main grid. It takes information from the main grid and decides whether the MFMGs should work in grid connected or islanded mode.

4.3 Problem of Active Power Balance of Multifrequency Microgrid

Different new active power imbalance cases evolve in MFMG due to frequency selectivity criteria. To tackle these situations, new power balancing algorithm is required. For that, different active power imbalance cases and the power balancing criteria for those cases need to be defined. In this section, the active power balance problems are analyzed separately for grid connected and islanded modes.

4.3.1 Grid Connected Mode

In grid connected mode, the MF bus voltage is maintained by the grid itself. Different frequency active powers of MFMG are also balanced by the grid. In the MFMG, if any frequency source power is lower than that frequency load power then the grid supplies the required frequency active power to MFMG. For this operation first, the active power differences between the sources and loads need to be calculated. The difference in active power for three different

Table 4.1: Different cases of active power imbalance in islanded mode of the MFMG

Case 1	$P_{M-0-diff} > 0$, $P_{M-25-diff} = 0$, $P_{M-50-diff} = 0$
Case 2	$P_{M-0-diff} = 0$, $P_{M-25-diff} > 0$, $P_{M-50-diff} = 0$
Case 3	$P_{M-0-diff} = 0$, $P_{M-25-diff} = 0$, $P_{M-50-diff} > 0$
Case 4	$P_{M-0-diff} > 0$, $P_{M-25-diff} = 0$, $P_{M-50-diff} > 0$
Case 5	$P_{M-0-diff} > 0$, $P_{M-25-diff} > 0$, $P_{M-50-diff} = 0$
Case 6	$P_{M-0-diff} = 0$, $P_{M-25-diff} > 0$, $P_{M-50-diff} > 0$

frequencies at MF bus is calculated as per equation 4.1.

$$P_{M-f-diff} = P_{M-f-L} - P_{M-f-S} \quad \text{for } f = \{DC, 25\ Hz, 50\ Hz\} \tag{4.1}$$

For MFMG, the different frequency active power balancing condition is presented in equation 4.2. According to this equation, the grid side converter needs to export or import the active power from the grid. For three frequencies (DC, 25 Hz, 50 Hz), the condition for power balance is also presented here.

$$P_G = \sum_{f=1}^{f=n} P_{M-f-L} - P_{M-f-S} = \sum_{f=1}^{f=n} P_{M-f-diff} = P_{M-0-diff} + P_{M-25-diff} + P_{M-50-diff} \tag{4.2}$$

So, grid side converter must have the ability to convert 50 Hz grid current to a combination of 0 Hz, 25 Hz, and 50 Hz load currents as per microgrid requirement and side by side it should maintain the MF bus voltage. So, a double loop control strategy needs to be implemented for grid side converter where the outer loop controls the output voltage and the inner loop controls the output current of the converter as shown in Fig. 4.2 (a).

4.3.2 Islanded Mode

In islanded mode, the grid got disconnected so, MFMG needs to be self sustained during this period. The grid interactive converter behaves like a grid forming converter and maintains the MF bus voltage and frequency. Other source side DC/MF converters behave like grid feeding converters. A source side control strategy is needed to balance different frequency active power load demands. The output currents of the grid feeding converters need to be controlled for this operation. For existing AC or DC microgrids, the active power balance conditions are given in

equation 4.3 [76]. Here the source bus and load bus power match with each other to achieve balance in active power.

$$P_{S-50} = P_{L-50}, \text{ or } P_{S-0} = P_{L-0} \tag{4.3}$$

However, in MFMG active power balance for each frequency at MF bus can be achieved without balancing individual frequency source and load bus power. Source side DC/MF converter can convert the source power to any other frequency power and send those to MF bus to fulfill other frequency load demands. Due to this unique advantage, the reliability of the sources increases, and critical loads can be supplied. Equations 4.4, and 4.5 present the criteria for active power balancing in islanded mode of MFMG, which state that the algebraic addition of all source bus power should match with the addition of all load bus power.

$$P_{S-f} \neq P_{L-f} \quad \text{for } f = \{1, 2, ...n\} \tag{4.4}$$

$$P_{S-1} + P_{S-2} + .. + P_{S-n} = P_{L-1} + P_{L-2} + .. + P_{L-n} \implies \sum_{f=1}^{f=n} P_{S-f} = \sum_{f=1}^{f=n} P_{L-f} \tag{4.5}$$

To analyze the problem of power balancing in islanded mode, an MFMG with three frequencies (DC, 50 Hz, 25 Hz) is examined in this thesis. However, the analysis can be extended to any number of frequencies which need not be multiple of each other. For a three frequency microgrid the active power balance conditions are presented in equations 4.6, and 4.7.

$$P_{S-0} + P_{S-25} + P_{S-50} = P_{L-0} + P_{L-25} + P_{L-50} \tag{4.6}$$

$$P_{S-0} \neq P_{L-0}, P_{S-25} \neq P_{L-25}, P_{S-50} \neq P_{L-50} \tag{4.7}$$

So, it is found that unlike AC or DC microgrid, there may be active power imbalances between individual frequency source bus and load bus. The individual frequency power mismatch between source bus and load bus can be balanced at MF bus by converting available frequency source power to required other frequency active powers by source side converter control.

Source side power can be reduced to any extent to match with load power ($P_{L-f} = P_{S-f}$) but all sources have some upper limit beyond which they can not be operated, which creates imbalance in different frequency active powers at MF bus. Depending on whether $P_{M-0-diff} > 0$

or = 0, $P_{M-25-diff} > 0$ or = 0, and $P_{M-50-diff} > 0$ or = 0, six power imbalance cases are possible and are given in Table 4.1. So, the grid feeding converters output currents need to be controlled to balance different frequency active powers for all the six cases. Here, only those cases are considered where atleast one source doesn't reach its maximum limit while fulfilling the load demand. So $P_{M-0-diff} > 0, P_{M-25-diff} > 0, P_{M-50-diff} > 0$ case is not considered.

The first case ($P_{M-0-diff} > 0$, $P_{M-25-diff} = 0$, $P_{M-50-diff} = 0$) situation is presented in Fig. 4.2 (b). The 50 and 25 Hz frequency powers are already balanced and these sources are available to produce more active power if required. The DC source reaches its maximum value but still could not supply the DC load demand. The required $P_{M-0-diff}$ needs to be supplied by the 50 and 25 Hz sources. For this operation, 50 and 25 Hz sources need to produce extra 50 and 25 Hz currents and source side converters need to convert those currents to DC current and send it to the MF bus.

4.4 Proposed Control Method for Active Power Balance

In this section, a control strategy is proposed to balance different frequency active powers of MFMG in grid connected and islanded modes. In grid connected mode, the grid side converter maintains the power balance whereas in islanded mode, the grid feeding converters maintain the power balance of MFMG.

In grid connected mode, the main grid is connected to the MFMG by a DC/MF converter. The output voltage and current of the grid side DC/MF converter need to be controlled. Here average mode current control strategy is employed for this operation as shown in Fig. 3.2 of previous chapter. The outer loop controls the output voltage to maintain The MF bus voltage magnitude and frequency. The output current is controlled by the inner loop. The grid side 50 Hz power can be converted to 0 Hz, 25 Hz, 50 Hz, or any other frequency powers if required. Here one flowchart is presented in Fig. 4.3 to calculate the reference current (I^*_{G2}) for an MFMG with n frequencies. First, it is checked that the microgrid is in grid connected mode or islanded mode. In grid connected mode, it is checked that the active power difference between source and load of different frequencies ($P_{M-f-diff}$) are +ve or zero. All active power

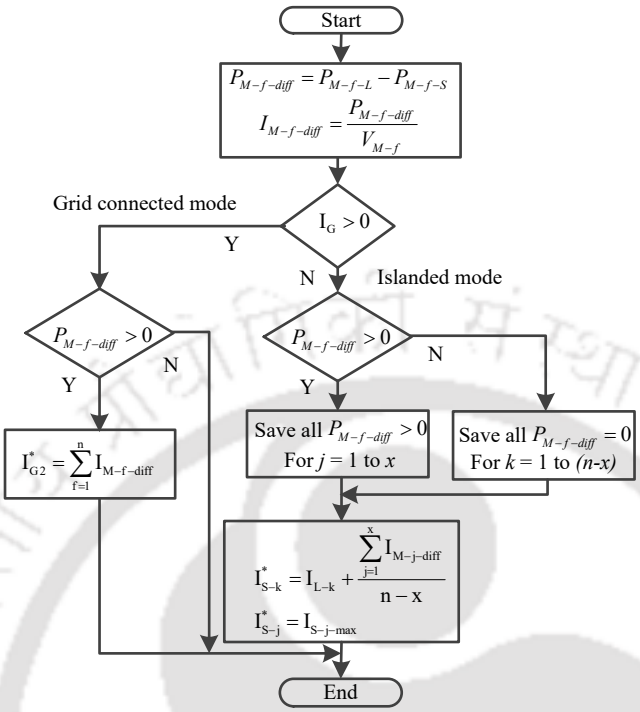

Figure 4.3: Flowchart to calculate the reference currents for grid side (I^*_{G2}) and grid feeding (I^*_{S-n}) converters for grid connected and islanded modes respectively to achieve active power balance.

differences are added and divided by grid voltage to obtain reference currents ($\sum_{f=1}^{f=n} I_{M-f-diff}$) for grid side converter. Here, 50 Hz grid power is converted to DC, 25 Hz, or 50 Hz active power to maintain active power balance in MFMG. If the active power difference is zero then active power is balanced and no action is needed for that frequency. If the controller works according to the proposed strategy then different frequency active powers got balanced and MFMG maintains the power balancing condition ($P_{M-0-diff} + P_{M-25-diff} + P_{M-50-diff} = P_G$) in grid connected mode.

In islanded mode, the MF bus voltage is maintained by the grid forming DC/MF converter. The voltage mode control technique is adopted here as shown in Fig. 3.3. The output currents of grid feeding converters are controlled to balance different frequency active powers of MFMG (Fig. 3.4). With load change, the source powers of MFMG need to be changed and matched with load powers to get the active power balance. MFMG source side DC/MF converter has one unique ability to convert the source frequency current to any other required load frequency currents. According to the power balance condition ($\sum P_{M-f-diff} = 0$), the reference currents

Table 4.2: Reference current equations of grid feeding converters for different cases to balance active power in islanded mode

Case number	Equation
Case 1	$I_{S-25} = I_{L-25} + \frac{I_{M-0-diff}}{2},\ I_{S-50} = I_{L-50} + \frac{I_{M-0-diff}}{2},\ I_{S-0} = I_{S-0-max}$
Case 2	$I_{S-0} = I_{L-0} + \frac{I_{M-25-diff}}{2}, I_{S-50} = I_{L-50} + \frac{I_{M-25-diff}}{2},\ I_{S-25} = I_{S-25-max}$
Case 3	$I_{S-0} = I_{L-0} + \frac{I_{M-50-diff}}{2},\ I_{S-25} = I_{L-25} + \frac{I_{M-50-diff}}{2},\ I_{S-50} = I_{S-50-max}$
Case 4	$I_{S-0} = I_{S-0-max},\ I_{S-25} = I_{L-25} + I_{M-0-diff} + I_{M-50-diff},\ I_{S-50} = I_{S-50-max}$
Case 5	$I_{S-0} = I_{S-0-max},\ I_{S-50} = I_{L-50} + I_{M-0-diff} + I_{M-25-diff},\ I_{S-25} = I_{S-25-max}$
Case 6	$I_{S-0} = I_{L-0} + I_{M-50-diff} + I_{M-25-diff},\ I_{S-25} = I_{S-25-max},\ I_{S-50} = I_{S-50-max}$

for all grid feeding converters (I^*_{S-j}, I^*_{S-k}) are calculated through a flowchart shown in Fig. 4.3 for an MFMG with n frequencies. First, one by one the active power differences between each frequency source and load are measured. Depending upon $P_{M-f-diff} > 0$ or $P_{M-f-diff} = 0$, different frequency sources are separately saved in two groups. For group $P_{M-f-diff} > 0$, these sources are at their maximum value but cannot supply the load demand. So, these sources are operated at maximum power and load takes the deficit power from other available sources equally. For group $P_{M-f-diff} = 0$, these frequency active powers are already balanced and sources are available to balance other frequency load power. The unbalanced frequency current differences are added to the reference output current of these sources to generate extra power to balance other frequency loads. All grid feeding converter's reference currents (I^*_{S-n}) are calculated with different equations for these two sets. Finally, the average current control method is employed to control the output current. This is explained by taking cases 1 and 4 as examples.

For case 1 ($P_{M-0-L} > P_{M-0-S}$, $P_{M-25-L} = P_{M-25-S}$ and $P_{M-50-L} = P_{M-50-S}$), 50 Hz and 25 Hz active powers are already balanced but DC power is not balanced. As the DC source is operated at maximum power, 50 and 25 Hz sources need to produce more power to balance the deficit DC load power. For this case, the value of n and x are 3 and 1. The equations for active power balance are presented here.

$$P_{M-25-diff} + P_{M-50-diff} = P_{M-0-diff} \tag{4.8}$$

According to the flowchart the current references for DC, 50 Hz and 25 Hz source side converters are,

$$I_{S-0} = I_{S-0-max},\ I_{S-50} = I_{L-50} + \frac{I_{M-0-diff}}{2},\ I_{S-25} = I_{L-25} + \frac{I_{M-0-diff}}{2} \tag{4.9}$$

Here $P_{M-0-diff}$ needs to be produced by 50 and 25 Hz sources. So $I_{M-0-diff}$ is divided equally and added with I_{L-50} and I_{L-25} to create current references for 50, and 25 Hz source side converters respectively. So the 50 Hz source side converter generates a mixture of 50 Hz and DC power whereas the 25 Hz source side converter generates a mixture of 25 Hz and DC power to balance the active powers at the MF bus. In case 4 ($P_{M-0-diff} > 0$, $P_{M-25-diff} = 0$, $P_{M-50-diff} > 0$), here only 25 Hz active power is balanced. The DC and 50 Hz sources are operated at their maximum ratings. The DC and 50 Hz active power imbalance current references are added with the 25 Hz converter current reference. For this case, the value of n and x are 3 and 2. The equations for active power balance are presented here.

$$P_{M-25-diff} = P_{M-0-diff} + P_{M-50-diff} \tag{4.10}$$

According to the flowchart the current reference for DC, 50 Hz and 25 Hz source side converters are,

$$I_{S-0} = I_{S-0-max},\ I_{S-50} = I_{L-50-max},\ I_{S-25} = I_{L-25} + I_{M-0-diff} + I_{M-50-diff} \tag{4.11}$$

Here, the 25 Hz source generates extra 25 Hz power and source side converter converts it to DC and 50 Hz power and sends it to the MF bus to balance DC and 50 Hz loads.

Using this technique, the reference currents of grid feeding converters for all six conditions are calculated and presented in Table 4.2. If condition $\sum_{f=1}^{f=n} P_{S-f} \neq \sum_{f=1}^{f=n} P_{L-f}$ arises in MFMG then different frequency source side active powers can be increased or decreased according to source capability to create $\sum_{f=1}^{f=n} P_{S-f} = \sum_{f=1}^{f=n} P_{L-f}$ condition and described strategy can be obtained for balancing active powers in islanding condition.

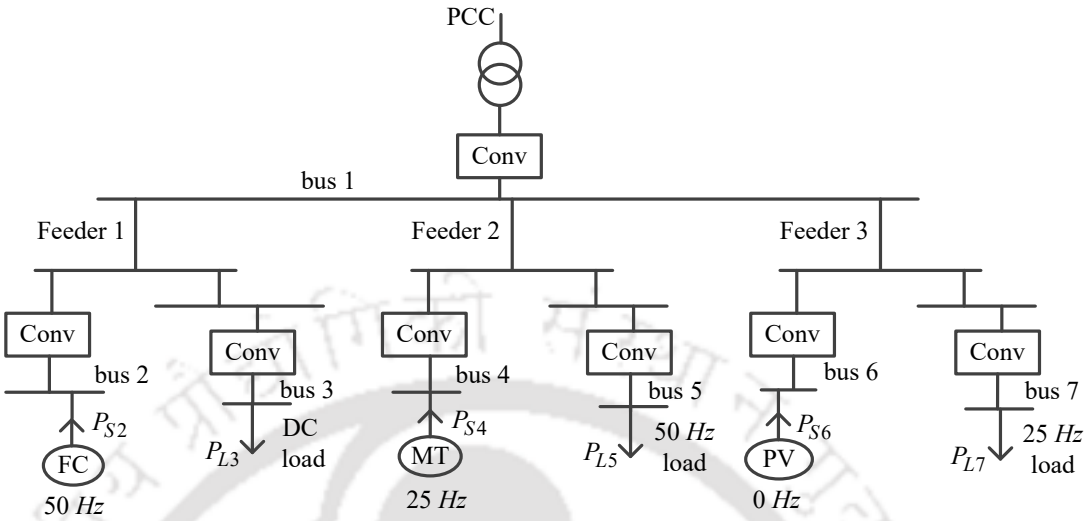

Figure 4.4: 7 bus structure of MFMG.

4.5 Simulation Results

Here a 7 bus MFMG is simulated which consists of three different frequency sources and loads to validate the control strategy on MFMG. The 7 bus MFMG structure is shown in Fig. 4.4. The DC, 25 Hz, and 50 Hz sources are connected to buses 2, 4, and 6. A switch is present at PCC to interchange between grid connected and islanded mode. Different sources send three different frequency currents of 0 Hz, 25 Hz, and 50 Hz to the MF bus. The source side converters are able to convert source side active power to other frequency required active powers for power balance of MFMG. Load side converters can choose any available power channel as per the requirement. The 7 bus MFMG is simulated in grid connected and islanded modes in Matlab Simulink. The circuit diagram of the simulation is presented in Fig. 4.5. The proposed active power balancing strategy is verified by changing the operating conditions of different sources and loads and creating different active power imbalance cases. Different filters, controllers, and compensators are designed separately for different converters and all system parameters are provided in Table 4.4.

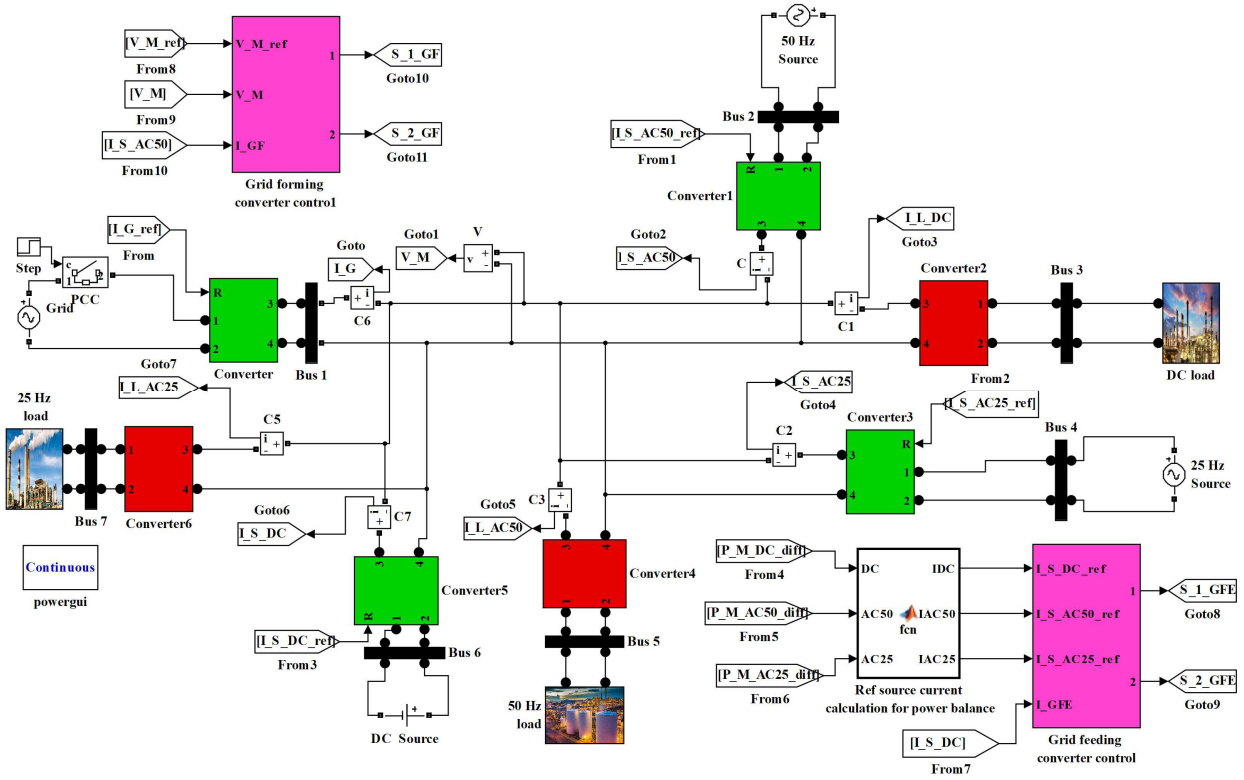

Figure 4.5: Simulation diagram of 7 bus MFMG.

Table 4.3: Case study of 7 bus MFMG

Type of source	Generation frequency	Voltage of source	Maximum capacity	Type of converter connected to source	Frequency selected by distributor	Bus no.
Grid	50 Hz	230 V	-	AC50/DC, DC/MF	50 Hz	1
PV	DC	1000 V	5 MW	DC/DC, DC/MF	DC	6
MT	25 Hz	300 V	3.5 MW	AC25/DC, DC/MF	25 Hz	4
FC	50 Hz	600 V	7 MW	AC50/DC, DC/MF	50 Hz	2

Type of load	Frequency of load	Voltage of load	Maximum capacity	Type of converter connected to load	Frequency chosen for power consumption	Bus no.
Load-bank	DC	110 V	10 MW	MF/DC, DC/DC		3
-	25 Hz	150 V	3 MW	MF/DC, DC/AC25		7
Motor	50 Hz	220 V	12 MW	MF/DC, DC/AC50	see Fig. 4.6 (b)	5

V_{MFB}: 500 V DC + 50 V AC 25 Hz (RMS) + 230 V AC 50 Hz (RMS)

Table 4.4: Simulation parameters of MFMG

Parameter	Value
L_G, C_G	1.5 mH, 750 μF
L_{GF}, C_{GF}	1 mH, 1000 μF
L_{GFE}	1 mH
L_L, C_L	0.2 mH, 400 μF
$K^P_{G-V}, K^I_{G-V}, K^P_{G-I}, K^I_{G-I}$	0.76, 8.2, 4.2, 26.5
K^P_{GF}, K^I_{GF}	0.02, 238
K^C_{GFE}	0.45

4.5.1 Grid Connected Mode

In grid connected mode, PCC is closed and grid is connected to MFMG by grid side converter. Here the microgrid sources try to fulfill the active power demand of same frequency load. If any frequency active power imbalance situation arises due to source power limitation then the grid tries to balance active power in that condition. Three different industrial loads in buses 3, 5, and 7 consume powers of different frequencies at different times of the day according to the load profiles shown in Fig. 4.6 (a). Total load demand in buses 3, 5, and 7 are 3.4 MW DC, 9.2 MW 50 Hz, 2.1 MW 25 Hz between 00:00 to 08:00, 5.6 MW 50 Hz, 6.3 MW DC, 2.3 MW 50 Hz between 08:00 to 16:00 and 2.4 MW 25 Hz, 2.5 MW 50 Hz, 2 MW 25 Hz between 16:00 to 24:00 respectively. Load profiles are assumed based on power availability, reliability, and quality. The frequency selection of different load bus is conferred in Fig. 4.6 (b). All three loads consume a mixture of different frequency active powers, so the frequency selectivity criteria is maintained.

Different frequency active power load demands are separately added to calculate total load demand ($P_{M-0-L} = P_{L3-0} + P_{L5-0} + P_{L7-0}$) and presented in Fig. 4.7 (a). It is found that the total load demand is 3.4 MW DC+ 9.2 MW 50 Hz+ 2.1 MW 25 Hz between 00:00 to 08:00, 6.3 MW DC+ 7.9 MW 50 Hz between 08:00 to 16:00 and 2.5 MW 50 Hz+ 4.4 MW 25 Hz between 16:00 to 24:00.

The total source power of MFMG for a day is presented in Fig. 4.7 (b). It can be noticed that between 08:00 to 16:00 DC source at bus 6 produces maximum power (5 MW) and is

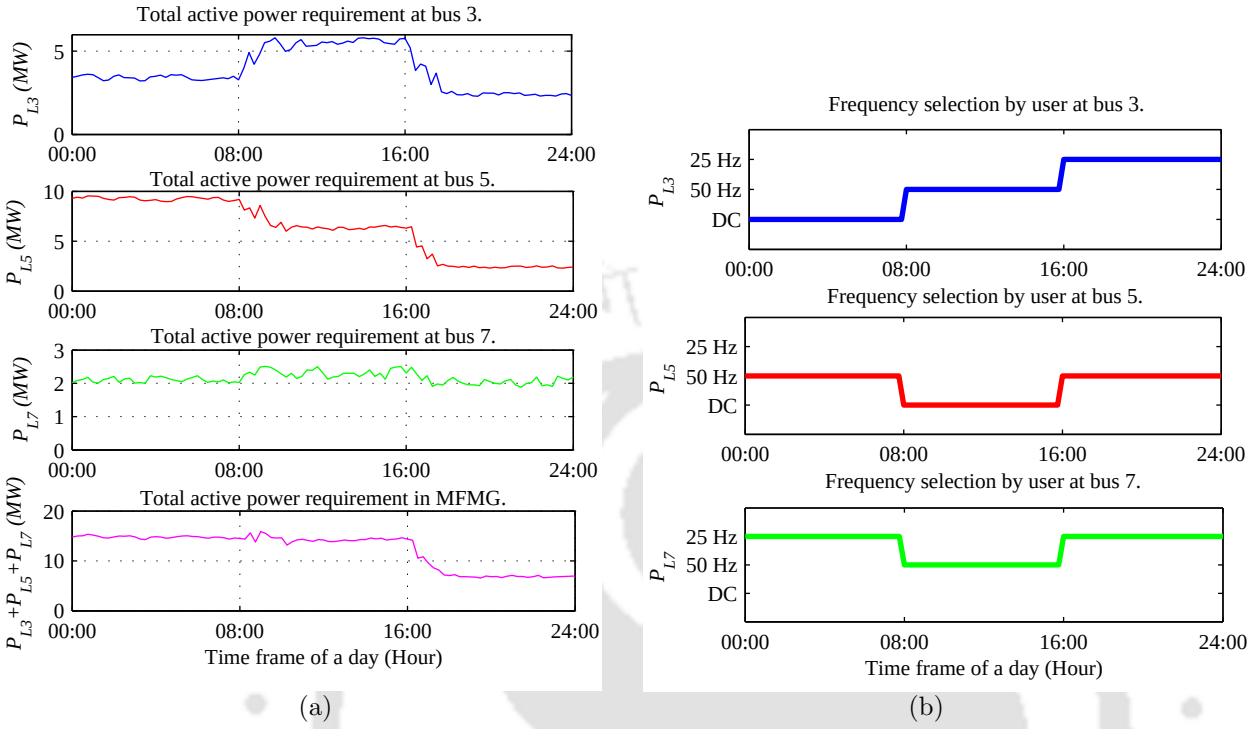

Figure 4.6: (a) Variation of active power load demands at bus 3 (P_{L3}), 5 (P_{L5}), and 7 (P_{L7}) throughout the day. (b) Different frequency active power selection by consumers at buses 3, 5, and 7 in different time frames.

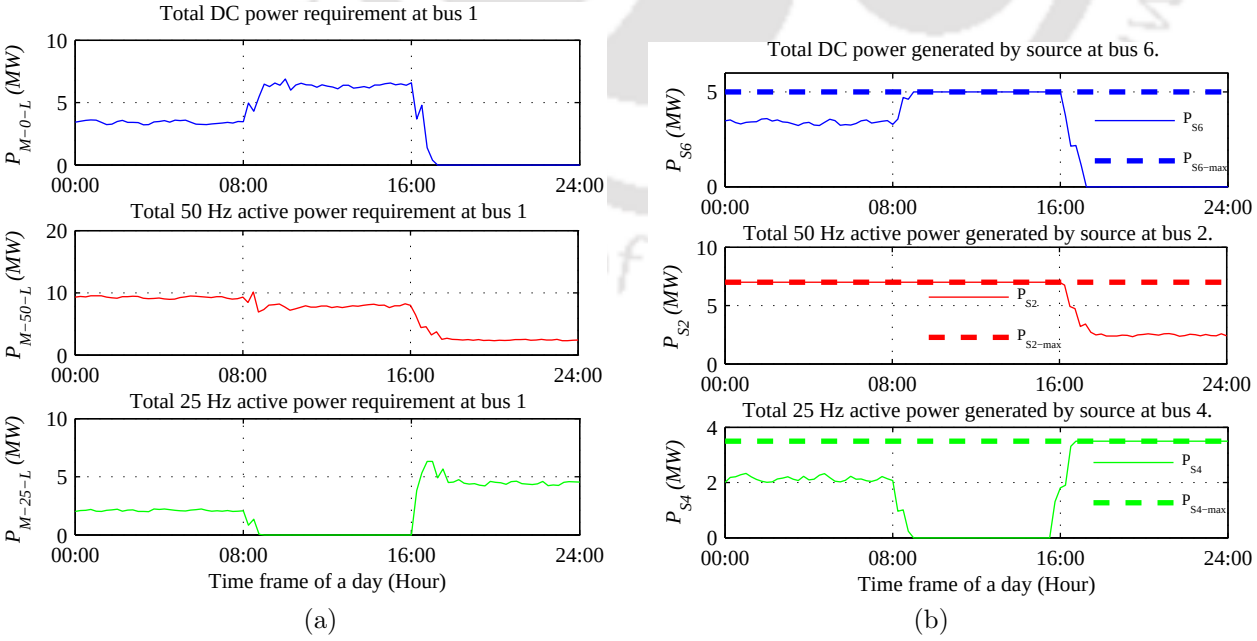

Figure 4.7: (a) Total DC (P_{M-0-L}), 50 Hz (P_{M-50-L}), and 25 Hz (P_{M-25-L}) active power load demands at bus 1 from the consumers of bus 3, 5, and 7. (b) Available DC (P_{S6}), 50 Hz (P_{S2}), and 25 Hz (P_{S4}) source active powers at bus 6, 2 and 4 in grid connected mode.

TH-2970_166102018

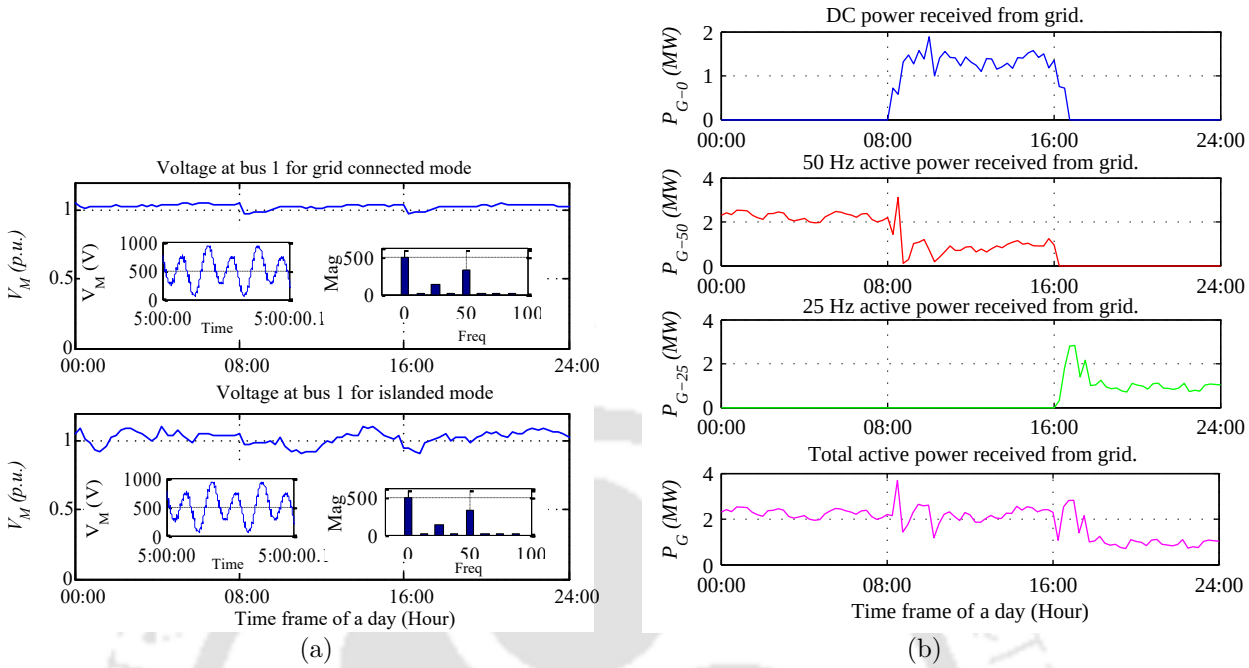

Figure 4.8: (a) MF bus (bus 1) voltage in grid connected and islanded mode. (b) Output 50 Hz active power of grid side converter (P_G) in grid connected mode which is converted to three different frequency active powers ($P_G = P_{G-0} + P_{G-50} + P_{G-25}$) and transmitted to bus 1.

still not able to meet the total DC load demand at the MF bus ($P_{M-0-diff} = 1.3\ MW$). The 50 Hz source present at bus 2 generates 7 MW between 00:00 to 16:00 and 2.5 MW power between 16:00 to 24:00. Between 00:00 to 16:00 the 50 Hz source is at its maximum limit but can not supply the total 50 Hz load demand ($P_{M-50-diff} = 2.2\ MW$ between 00:00 to 08:00 and $P_{M-50-diff} = 0.9\ MW$ between 08:00 to 16:00). The 25 Hz source at bus 4 generates maximum power (3.5 MW) between 16:00 to 24:00 but the total active load power of 25 Hz at the MF bus is not fully supplied ($P_{M-25-diff} = 0.9\ MW$). The grid side converter should provide the difference between source and load power at the MF bus for each frequency to balance active power properly.

The MF bus voltage is controlled by the grid side converter at 500 V DC+ 50 V 25 Hz+ 230 V 50 Hz. The MF bus (bus 1) voltage ($p.u.$) and its fast Fourier transform (FFT) analysis are conferred in Fig. 4.8 (a). From the FFT result it can be seen that the output voltage of grid side converter matches with the reference. It can be noticed that bus voltage doesn't get much affected by the load change and is controlled in a safe range throughout the simulated time. The MF bus voltage has some fluctuations ($\leq 10\%$). Due to this, there are fluctuations in

power waveforms. It can be smoothened out by improving the PI controller parameters of the grid forming converter. Due to the fluctuations, there is some power imbalance always present in the MFMG.

The flowchart in Fig. 4.3 calculates the reference output current for the grid side converter to balance the active power in MFMG. As the different frequency active power demands change periodically, the current reference of the grid side converter also changes and the DC/MF converter at the grid side can produce a combination of different frequency currents required to balance active powers at bus 1. From Fig. 4.8 (b), it can be observed that the converter produces 2.2 MW 50 Hz between 00:00 to 08:00, 1.3 MW DC+ 0.9 MW 50 Hz between 08:00 to 16:00 and 0.9 MW 25 Hz between 16:00 to 24:00. If the total source power is subtracted from total load power algebraically for each frequency, it matches with the total the grid side converter power ($P_{G-0} = P_{M-0-L} - P_{M-0-S}$, $P_{G-50} = P_{M-50-L} - P_{M-50-S}$, $P_{G-25} = P_{M-25-L} - P_{M-25-S}$) which are the active power balancing conditions for grid connected mode ($P_G = P_{G-0} + P_{G-25} + P_{G-50} = P_{M-0-diff} + P_{M-25-diff} + P_{M-50-diff}$). So, the power balancing algorithm works nicely for the total MFMG system in grid connected mode.

4.5.2 Islanded Mode

Next, the switch at PCC is open and MFMG is operated in islanded mode. In this case, different frequency load demands need to be fulfilled by the MFMG sources. First, all the sources try to fulfill the same frequency loads. Due to the source power limitation, different active power imbalance cases may happen. The active power references of the available sources are increased to balance different frequency active powers for all the cases. The loads at buses 3, 5, and 7 follow the load profiles shown in Fig. 4.6 (a) and according to Table 4.2, the reference currents for each source side grid feeding converter for different time frames are calculated.

The bus voltage is maintained by the grid forming converter at 500 V DC+ 50 V 25 Hz+ 230 V 50 Hz. The FFT analysis in Fig. 4.8 (a), shows that the output voltage of the converter follows the reference. The voltage controller in the grid forming converter works properly and maintains the MF bus voltage variations under a safe range.

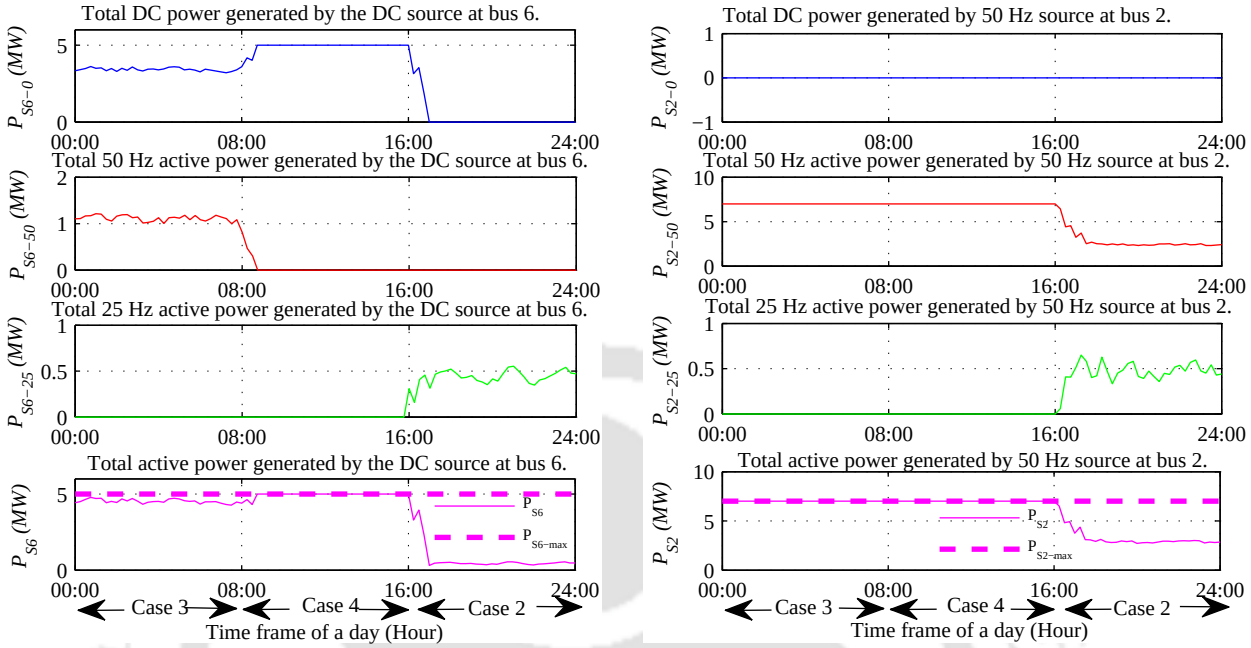

Figure 4.9: (a) Total DC source active power at bus 6 (P_{S6}) of MFMG in islanded mode which is converted to three different frequency active powers ($P_{S6} = P_{S6-0} + P_{S6-50} + P_{S6-25}$) and transmitted to bus 1. (b) Total 50 Hz source active power at bus 2 (P_{S2}) of MFMG in islanded mode which is converted to two different frequency active powers ($P_{S2} = P_{S2-50} + P_{S2-25}$) and transmitted to bus 1.

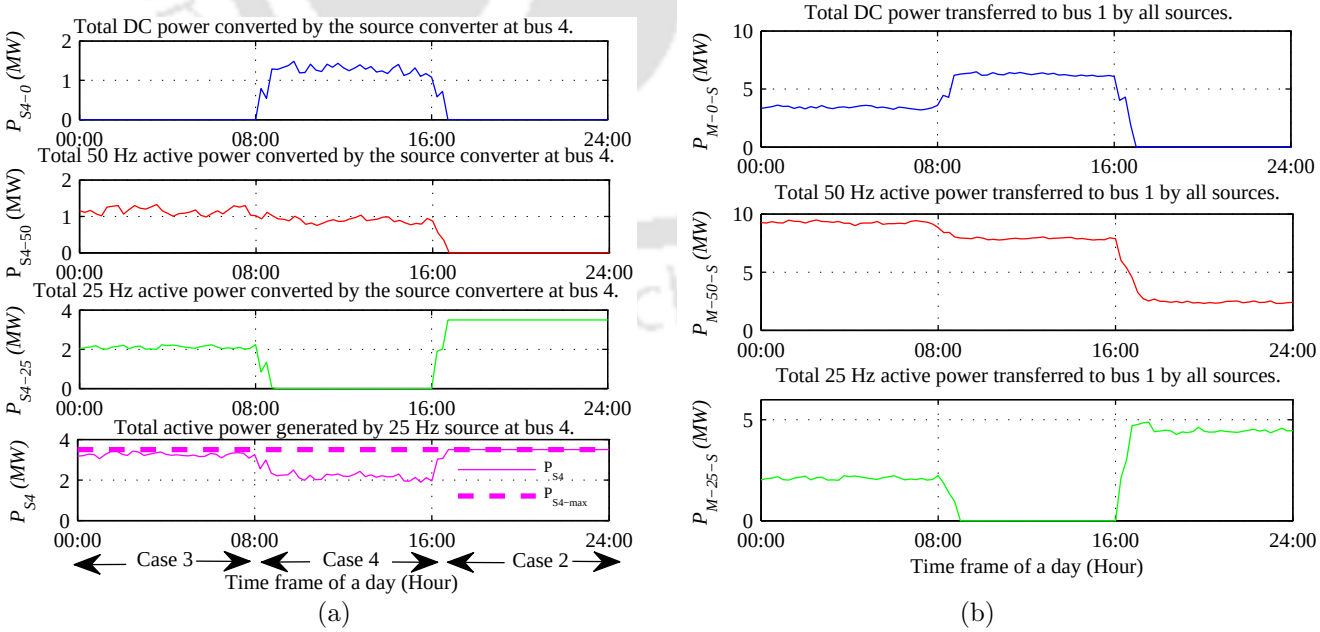

Figure 4.10: (a) Total 25 Hz source active power at bus 4 (P_{S4}) of MFMG in islanded mode which is converted to three different frequency active powers ($P_{S4} = P_{S4-0} + P_{S4-50} + P_{S4-25}$) and transmitted to bus 1. (b) Total DC (P_{M-0-S}), 50 Hz (P_{M-50-S}), and 25 Hz (P_{M-25-S}) active powers received at bus 1 from sources at bus 6, 2, and 4 in islanded mode.

By comparing the load (Fig. 4.7 (a)) and source data (Fig. 4.7 (b)) it is observed that different active power imbalance cases occur throughout the day. In between 00:00 to 08:00, the power differences of different frequencies are $P_{M-0-diff} = 0$, $P_{M-25-diff} = 0$, and $P_{M-50-diff} > 0$, which are the conditions for case 3. For this case, DC and 25 Hz active powers are already balanced but the 50 Hz source at bus 2 can't supply the total load demand. As per the flowchart, DC and 25 Hz sources at buses 6 and 4 should produce extra DC and 25 Hz power equally and source side converters convert those powers to the required 50 Hz power. It can be found form Fig. 4.9 (a), Fig. 4.9 (b), and Fig. 4.10 (a) that between 00:00 to 08:00 the total load demand of 50 Hz load is 9.2 MW. The 50 Hz source at bus 2 generates maximum 7 MW during this period. So, DC and 25 Hz sources at bus 6 and 4 generate extra 1.1 MW DC and 1.1 MW 25Hz power. Those active powers are converted to 50 Hz power by source side converter and sent to bus 1 for 50 Hz active power balance. Between 08:00 to 16:00 $P_{M-0-diff} > 0$, $P_{M-25-diff} = 0$, and $P_{M-50-diff} > 0$, so case 4 happens. For this case, only 25 Hz active power is balanced and both DC and 50 Hz sources are at their maximum capacity but still can't obtain full load power. So the 25 Hz source power at bus 4 should increase and the source side converter of the 25 Hz source converts that power to a mixture of required DC and 50 Hz active powers. It can be noticed that between 08:00 to 16:00 bus 4 sends extra 1.3 MW DC+ 0.9 MW 50 Hz active powers to bus 1 for active power balance. In the next time interval (16:00 to 24:00), case 2 happens. In this case, DC and 50 Hz active powers are balanced. The 25 Hz load demand at bus 1 is 4.4 MW. In this time period the 25 Hz source at bus 4 generates maximum 3.5 MW. The deficit 25 Hz power is 0.9 MW. So, DC and 50 Hz sources at bus 6 and 2 generate 0.45 MW DC and 0.45 MW 50 Hz powers and source side converters convert those to 25 Hz power and send that to bus 1 for active power balance of 25 Hz load.

Different frequency elements of all three source powers are algebraically added for each frequency individually ($P_{M-0-S} = P_{S6-0} + P_{S2-0} + P_{S4-0}$) to obtain total source power for each frequency at bus 1 which is presented in Fig. 4.10 (b). After controlling, it can be seen that the source power matches with load power for each frequency separately at bus 1

($P_{M-0-S} = P_{M-0-L}, P_{M-50-S} = P_{M-50-L}, P_{M-25-S} = P_{M-25-L}$). Finally, MFMG achieves active power balance conditions in islanded mode ($P_{L3} + P_{L5} + P_{L7} = P_{S2} + P_{S4} + P_{S6}$ whereas $P_{S2} \neq P_{L5}, P_{S6} \neq P_{L3}, P_{S4} \neq P_{L7}$). So the algorithm can balance every power imbalance case of the MFMG in islanded mode.

4.6 Conclusion

In the MF bus, different frequency active powers are present and customers of MFMG can choose any frequency available power from the MF bus. This increases reliability but creates several new active power imbalance cases for MFMG. In this chapter, a control method is introduced for grid side converter so that it can convert grid power to a mixture of different frequency powers to get active power balance in grid connected mode. For islanding mode, six different active and reactive power imbalance cases are defined and a control method is introduced for all grid feeding converters to balance power for every case. The strategy is verified by circuit simulation of 7 bus MFMG in Matlab Simulink. It can be seen from the results that the strategy balances different frequency active powers in grid connected and islanded modes. So the proposed strategy solves the active power balancing problems of MFMG. The grid side, grid forming, and grid feeding converter produce outputs as per the reference values so, all controllers of the converters are precisely designed.

Note: Major part of this chapter is reproduced from my publications:

1. R. Dey, S. Nath, "Control and management of different frequency active and reactive powers for multifrequency microgrid ," in *IEEE Access* (Submitted).

2. R. Dey and S. Nath, "A new active and reactive power control strategy for multifrequency microgrid in islanded mode," in *proceedings of 5th International Conf. on Smart Grid and Smart Cities (ICSGSC)*, 2021, pp. 45–49.

5

Control and Management of Different Frequency Reactive Powers for Multifrequency Microgrid

Contents

5.1 Introduction

To maintain the voltage level of a bus, the reactive power supply and demand should match with each other in any electrical system. The reliability and stability of a power system rely on reactive power management [71]. A consumer can select and consume any available frequency active power from the MF bus. Different power can be categorized by distance, cost, or availability. In an MFMG, a consumer chooses different frequency active powers at different time frames. As the input current of the load converter varies so reactive power demand also changes with change in active power. If active power demand increases for a certain frequency then reactive power demand also increases and vice versa. This frequency selective reactive power consumption creates several reactive power imbalance cases which are not present in traditional microgrids. All these cases need to be properly investigated and a reactive power balancing strategy needs to be proposed for MFMG to balance different frequency reactive powers in grid connected and islanded modes. In this chapter first, the issue of different frequency reactive power mismatch in MFMG is investigated for islanded and grid connected modes, and reactive power balancing conditions for these two modes are determined. Next, to solve the reactive power control problem for different frequencies, a new control strategy is introduced for the source side converter which works in both islanded and grid connected modes. Finally, an 9 bus MFMG is simulated in Matlab Simulink with the proposed strategies for different cases and all control strategies are verified through simulation results.

5.2 Problem of Reactive Power Balance of Multifrequency Microgrid

For proper operation of MFMG, different frequency reactive power control and management is necessary. Different new reactive power imbalance cases evolve in MFMG due to frequency selectivity criteria. To tackle these situations, a new power balancing algorithm is required. For that different reactive power imbalance cases and the power balancing criteria for those cases need to be defined. In this chapter, reactive power control problems are examined separately for

islanded and grid connected modes. Here an MFMG is chosen with four base frequencies (DC, 25 Hz, 50 Hz, and 100 Hz). The DC source does not produce any reactive power so, for the reactive power balancing strategy 25 Hz, 50 Hz, and 100 Hz reactive powers are considered.

5.2.1 Grid Connected Mode

In grid connected mode, the grid side converter maintains the bus voltage. In this mode, the grid can support MFMG by providing the required different frequency reactive powers. The reactive power generation of the grid side converter needs to be controlled based on the MFMG reactive power demand. Here, the main objective of the developed control is to set the reactive power production of each source in a way that the total reactive power injected at the grid matches the required set point of the transmission system operator (TSO). As the grid provides different frequency reactive powers based on the reactive power difference of each frequency source and load, to define the receive power balance criteria for this mode first, the reactive power difference between sources and loads needs to be defined. For any frequency, the difference between the source side and load side reactive power is defined by equation 5.1.

$$Q_{M-f-diff} = Q_{M-f-L} - Q_{M-f-S} \text{ for } f = \{25\ Hz, 50\ Hz, 100\ Hz\} \tag{5.1}$$

The reactive power balancing criteria of MFMG for grid connected mode is defined as,

$$Q_G = \sum_{f=1}^{f=n} Q_{M-f-L} - \sum_{f=1}^{f=n} Q_{M-f-S} = \sum_{f=1}^{f=n} Q_{M-f-diff} \tag{5.2}$$

For 25 Hz, 50 Hz, and 100 Hz reactive power the criteria becomes,

$$Q_G = Q_{M-25-diff} + Q_{M-50-diff} + Q_{M-100-diff} \tag{5.3}$$

So, the grid side converter balances the MF bus voltage and supplies the required reactive power to the bus. A new voltage and reactive power control strategy are required for grid side converter as shown in Fig. 5.1 (a). In some situation, if only the 25 Hz reactive power is balanced then the grid produce extra 50 Hz reactive power and the grid side converter convert that to the required amount of 50 and 100 Hz reactive powers and send those to the MF bus

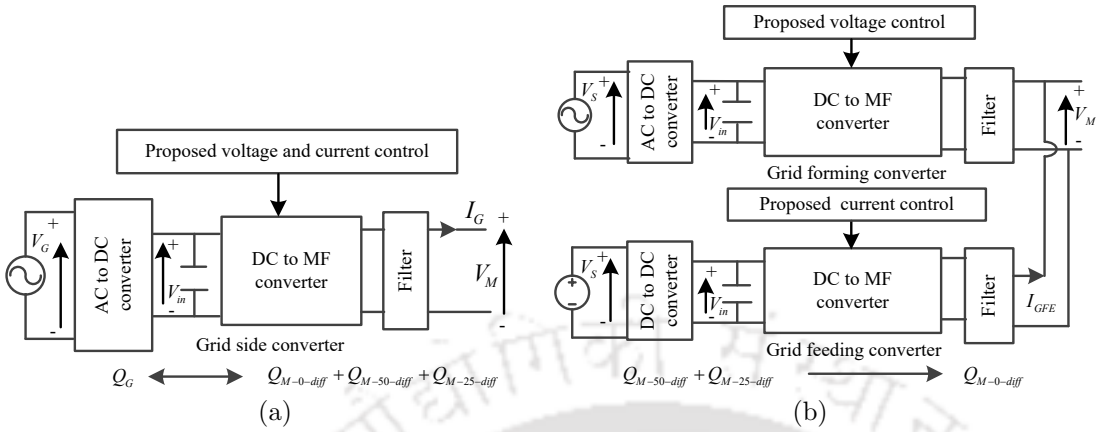

Figure 5.1: Reactive power balancing strategy of MFMG for (a) grid connected mode (b) islanded mode.

Table 5.1: Different cases of reactive power imbalance in islanded mode

Case1	$Q_{M-25-diff} > 0, Q_{M-50-diff} = 0, Q_{M-100-diff} = 0$
Case2	$Q_{M-25-diff} = 0, Q_{M-50-diff} > 0, Q_{M-100-diff} = 0$
Case3	$Q_{M-25-diff} = 0, Q_{M-50-diff} = 0, Q_{M-100-diff} > 0$
Case4	$Q_{M-25-diff} > 0, Q_{M-50-diff} = 0, Q_{M-100-diff} > 0$
Case5	$Q_{M-25-diff} > 0, Q_{M-50-diff} > 0, Q_{M-100-diff} = 0$
Case6	$Q_{M-25-diff} = 0, Q_{M-50-diff} > 0, Q_{M-100-diff} > 0$

for reactive power balance.

5.2.2 Islanded Mode

In islanded mode, the grid is disconnected and MFMG needs to be self-sustained. The bus voltage is controlled by grid forming converter. A source side reactive power control strategy is required to control the grid feeding converters to inject the assigned value of reactive powers. For this first, the reactive power balancing criteria for islanded mode is defined and compared with AC microgrid.

$$Q_{S-50} = Q_{L-50} \tag{5.4}$$

Here, total reactive power consumption at the load bus should match with total reactive power generation at the source bus. But in MFMG, reactive power balance for the overall system can be attained without balancing load and source bus reactive powers for individual frequency. So the system reliability increases and the critical loads can be supplied for any power outrage case. In equations 5.5, 5.6, the condition to control reactive powers in the MFMG is presented.

The algebraic summation of different frequency source side reactive power generations should be equal to the summation of different frequency load side reactive power consumptions.

$$Q_{S-f} \neq Q_{L-f} \quad \text{for } f = \{1, 2, ...n\} \tag{5.5}$$

$$Q_{S-1} + Q_{S-2} + ... + Q_{S-n} = Q_{L-1} + Q_{L-2} + ... + Q_{L-n}$$
$$\implies \sum_{f=1}^{f=n} Q_{S-f} = \sum_{f=1}^{f=n} Q_{L-f} \tag{5.6}$$

For an MFMG with three different frequencies (25 Hz, 50 Hz, 100 Hz), the reactive power balance condition is,

$$Q_{S-25} + Q_{S-50} + Q_{S-100} = Q_{L-25} + Q_{L-50} + Q_{L-100},$$
$$Q_{S-25} \neq Q_{L-25}, Q_{S-50} \neq Q_{L-50}, Q_{S-100} \neq Q_{L-100} \tag{5.7}$$

All sources and loads of MFMG are connected by power electronics converters. So any frequency source reactive power can be converted to different frequency reactive powers by the source side converter and sent those powers to the MF bus to fulfill the variable frequency reactive power demands. Due to this unique advantage, different frequency reactive powers can be balanced at MF bus without balancing the source and load bus reactive power individually for each frequency. The reactive power differences between individual frequency source and load (25, 50, and 100 Hz) at the MF bus are presented in equation (5.1). As all sources have some power generation limit, the total load demand of reactive power may not be supplied in islanded mode ($Q_{L-f} > Q_{S-f}$). If $Q_{M-f-diff} = 0$, then, that frequency reactive power is balanced and the source is available to generate more reactive power. If $Q_{M-f-diff} > 0$, then that frequency reactive power is not balanced and the residual load reactive power is taken from all other available sources equally. Depending upon these conditions whether $Q_{M-25-diff} > 0$ or $= 0$, $Q_{M-50-diff} > 0$ or $= 0$, and $Q_{M-100-diff} > 0$ or $= 0$, total six reactive power imbalance cases can occur in MFMG which are shown in Table 5.1. Only those cases have been selected where at least one source doesn't reach its maximum limit. So, $Q_{M-25-diff} > 0$, $Q_{M-50-diff} > 0$, $Q_{M-100-diff} > 0$ case is not considered. So in islanded mode, a source side control strategy is

required where the available sources increase their reactive power generations and the source side converters convert those powers to the required frequency load reactive power to balance different frequency reactive powers for these six cases.

The first case of Table 5.1 is presented in Fig. 5.1 (b). Here $Q_{M-25-diff} > 0$ but $Q_{M-50-diff} = 0$ and $Q_{M-100-diff} = 0$. In this case, 50 and 100 Hz reactive powers are balanced but 25 Hz reactive power is not balanced. The 25 Hz source is operated at its maximum limit of reactive power but is unable to supply the 25 Hz load reactive power. So the reactive power generation of 50 and 100 Hz should increase equally. Source side converters need to convert these 50 and 100 Hz reactive powers to 25 Hz reactive power and send that to the MF bus.

5.3 Proposed Control Method for Reactive Power Balance

In this section, a reactive power balance strategy is explained for MFMG in grid connected and islanded modes. A combination of AC/DC and DC/MF converters is used as the grid side converter in MFMG. Here both the output voltage and current need to be controlled so, the average mode current control technique is used. The 50 Hz grid reactive power can be converted to any other frequency reactive power by the back to back converter structure. Here, one current reference is created from the output of the PI controller of the voltage control loop. Another current reference is created from the reactive power balancing equation of grid connected mode ($Q_G = \sum_{f=1}^{f=n} Q_{M-f-diff}$). The direct and quadrature axis reference current are calculated by the equation 5.8.

$$I^*_{G2-d} = \frac{2(Q_{G-diff}V_{G-q})}{3(V^2_{G-d} + V^2_{G-q})},\ I^*_{G2-q} = -\frac{2(Q_{G-diff}V_{G-d})}{3(V^2_{G-d} + V^2_{G-q})} \tag{5.8}$$

Finally, these two current references are added and compared to the actual output current of the grid side converter and the error signal is passed through a PI controller to generate the modulating signal. The PI controller design is properly described in chapter 3. With this control strategy, the output current of the grid side converter is properly controlled to mitigate any reactive power balancing issue in MFMG. This strategy is properly described in Fig. 3.2.

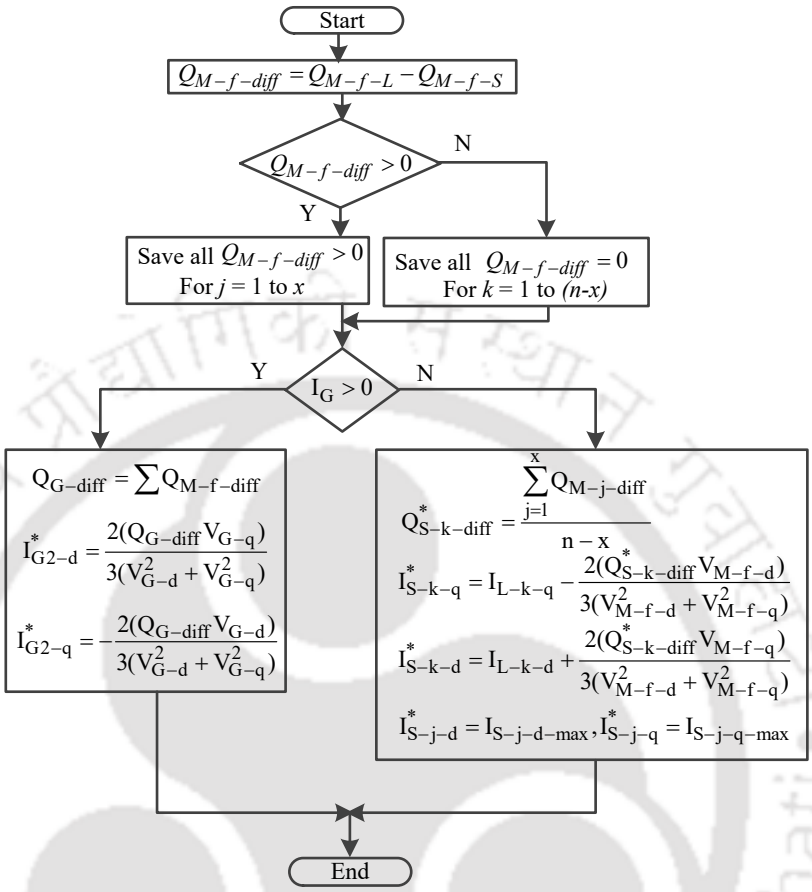

Figure 5.2: Flowchart to calculate the reference currents for grid feeding (I^*_{S-n}) and grid side (I^*_{G2}) converters for islanded and grid connected modes respectively to achieve reactive power balance.

In islanding mode, the grid forming converter maintains the MF bus voltage. The control of the grid forming converter is already explained for the active power balancing case. Every source of MFMG is connected by the grid feeding converters. The output currents of these converters are adjusted to achieve reactive power balance. In MFMG, the source side converters have the ability to convert source frequency reactive power to other frequency reactive powers if required. So, if one particular frequency source reaches its maximum limit, then other frequency sources can produce extra reactive power, and power electronic converters convert that to the required frequency format and send it back to the MF bus to balance reactive power.

Here, a control strategy is designed to maintain different frequency reactive power balance in MFMG in islanded mode. The flowchart of the control strategy is presented in Fig. 5.2. First, the reactive power difference between the source and load of every individual frequency

is checked. Based on $Q_{M-f-diff} > 0$ or $Q_{M-f-diff} = 0$, all sources are divided into two groups. If $Q_{M-f-diff} > 0$, then these frequency sources are at their maximum value but load reactive power demands are not fulfilled. For this group, all sources are operated at their maximum reactive power value and the loads take the deficit power from other sources. For group $Q_{M-f-diff} = 0$, these frequency reactive powers are already balanced and sources are available to balance other frequency reactive loads. The output current references of these sources are increased as per other frequency load demands. According to this logic, the direct and quadrature axis reference currents of grid feeding converters are calculated by equation. To generate the three phase reference current, dq/abc conversion is done. This reference current is compared with the output current of the converter and the error signal is sent to a PI controller. The controller design is explained in chapter 3. Here the inner loop current control of the average mode current control method is used to control the output current the of DC/MF converter.

For case 1, the 25 Hz reactive power is not balanced but 50 and 100 Hz reactive powers are balanced. As the 25 Hz source is operated at its maximum value so, the deficit amount of 25 Hz reactive power is supplied by 50 and 100 Hz sources. It can be noticed from the flowchart that the required 25 Hz reactive power is split equally between 50 and 100 Hz sources. Here the value of x and n are 1 and 3. The reactive power balance equation for this case is presented in equation 5.9.

$$Q_{M-50-diff} + Q_{M-100-diff} = Q_{M-25-diff} \tag{5.9}$$

All direct and quadrature axis currents for 25, 50, and 100 Hz grid feeding converters are calculated for case 1 and conferred here.

$$I_{S-25-d} = I_{S-25-d-max}, I_{S-25-q} = I_{S-25-q-max} \tag{5.10}$$

$$I_{S-50-d} = I_{L-50-d} + \frac{2(\frac{Q_{M-25-diff}}{2} V_{M-50-q})}{3(V_{M-50-d}^2 + V_{M-50-q}^2)} \tag{5.11}$$

$$I_{S-50-q} = I_{L-50-q} - \frac{2(\frac{Q_{M-25-diff}}{2} V_{M-50-q})}{3(V_{M-50-d}^2 + V_{M-50-q}^2)} \tag{5.12}$$

$$I_{S-100-d} = I_{L-100-d} + \frac{2(\frac{Q_{M-25-diff}}{2} V_{M-100-q})}{3(V_{M-100-d}^2 + V_{M-100-q}^2)} \tag{5.13}$$

$$I_{S-100-q} = I_{L-100-q} - \frac{2(\frac{Q_{M-25-diff}}{2} V_{M-100-q})}{3(V_{M-100-d}^2 + V_{M-100-q}^2)} \tag{5.14}$$

A mixture of 25 and 50 Hz reactive powers is generated by the 50 Hz source converter whereas a mixture of 25 and 100 Hz reactive powers is generated by the 100 Hz source side converter to balance different frequency reactive powers for the first case in the MFMG. For case 5, the 100 Hz reactive power is balanced but 25 and 50 Hz reactive powers are not balanced. Here, 25 and 50 Hz sources are operated at their maximum values so the 100 Hz source's reactive power generation is increased and that power is converted to a mixture of 25 and 50 Hz reactive powers. Here the value of x and n are 2 and 3. The reactive power balance equation for this case is -

$$Q_{M-100-diff} = Q_{M-25-diff} + Q_{M-50-diff} \tag{5.15}$$

All direct and quadrature axis currents for 25, 50, and 100 Hz grid feeding converters are calculated for case 5 and shown here.

$$I_{S-25-d} = I_{S-25-d-max}, I_{S-25-q} = I_{S-25-q-max} \tag{5.16}$$

$$I_{S-50-d} = I_{S-50-d-max}, I_{S-50-q} = I_{S-50-q-max} \tag{5.17}$$

$$I_{S-100-d} = I_{L-100-d} + \frac{2(Q_{M-25-diff} V_{M-100-q})}{3(V_{M-100-d}^2 + V_{M-100-q}^2)} + \frac{2(Q_{M-50-diff} V_{M-100-q})}{3(V_{M-100-d}^2 + V_{M-100-q}^2)} \tag{5.18}$$

$$I_{S-100-q} = I_{L-100-q} - \frac{2(Q_{M-25-diff} V_{M-100-q})}{3(V_{M-100-d}^2 + V_{M-100-q}^2)} - \frac{2(Q_{M-50-diff} V_{M-100-q})}{3(V_{M-100-d}^2 + V_{M-100-q}^2)} \tag{5.19}$$

Here 100 Hz source generates a mixture of 25, 50, and 100 Hz reactive powers to balance different frequency reactive powers. Using this method, all grid feeding converters current references can be calculated for all six cases and the reactive power balancing condition ($\sum_{f=1}^{f=n} Q_{S-f} = \sum_{f=1}^{f=n} Q_{L-f}$) can be achieved for each case.

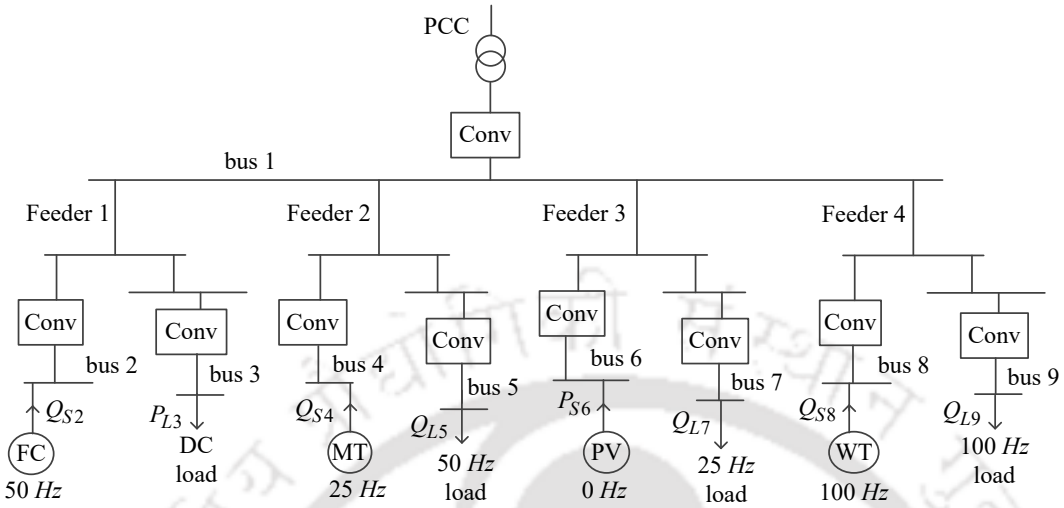

Figure 5.3: 9 bus structure of MFMG.

5.4 Simulation Results

The loads in MFMG can choose different frequency active powers in different time frames. With change in active power, reactive power also changes and different new reactive power imbalance cases are created in MFMG. In this section, the proposed control strategy to mitigate all these unbalance cases is verified by Matlab Simulation. For reactive power presentation, one 100 Hz source and one 100 Hz load are connected with the previous bus structure and the 9 bus MFMG (Fig. 5.3) is simulated with four different frequency (DC, 25 Hz, 50 Hz, 100 Hz) sources and loads. The main grid can be disconnected from MFMG by the switch at PCC. All sources and loads are connected to the MF bus by DC/MF converters. These power electronics converters can convert any frequency source reactive power to other required frequency reactive powers. Different frequency source data are presented in Table 5.2.

5.4.1 Grid Connected Mode

For this mode, the switch at PCC is closed and the grid is connected with MFMG. The bus voltage is maintained by the grid side converter. In this mode, the total reactive power demand of MFMG is supplied by the MFMG sources and grid. Due to the maximum reactive power production limit, several reactive power unbalance cases happen in grid connected mode which

Table 5.2: Case study of 9 bus MFMG

Type of source	Generation frequency	Voltage of source	Maximum capacity	Type of converter connected to source	Frequency selected by distributor	Bus no.
Grid	50 Hz	230 V	-	AC50/DC, DC/MF	50 Hz	1
MT	25 Hz	300 V	2 $MVAR$	AC25/DC, DC/MF	25 Hz	4
FC	50 Hz	600 V	3.5 $MVAR$	AC50/DC, DC/MF	50 Hz	2
WT	100 Hz	200 V	2.5 $MVAR$	AC100/DC, DC/MF	100 Hz	8

Type of load	Frequency of load	Voltage of load	Maximum capacity	Type of converter connected to load	Frequency chosen for power consumption	Bus no.
-	25 Hz	150 V	2 $MVAR$	MF/DC, DC/AC25	see Fig. 5.4 (b)	7
Motor	50 Hz	220 V	5 $MVAR$	MF/DC, DC/AC50		5
-	100 Hz	110 V	2.2 $MVAR$	MF/DC, DC/AC100		9

V_{MFB}: 500 V DC + 50 V AC 25 Hz (RMS) + 230 V AC 50 Hz (RMS) + 100 V AC 100 Hz (RMS)

are balanced by the grid. For every time period, the reactive power differences are calculated for different frequency sources and loads and those data are transmitted to the transmission system operator. Accordingly, the reactive power output of the grid side converter is changed to supply the different frequency reactive powers. The different frequency reactive power demands from the grid are presented in Fig. 5.4 (a) for a day. The reactive power difference between the 25 Hz source and load (Q_{G-25}) is 0.3 $KVAR$ in between 00:00-08:00, and 0.8 $KVAR$ in between 08:00-16:00. The reactive power difference between the 50 Hz source and load (Q_{G-50}) is 0.25 $KVAR$ in between 16:00-24:00. The reactive power difference between the 100 Hz source and load (Q_{G-100}) is 0.3 $KVAR$ in between 00:00-08:00, and 0.25 $KVAR$ in between 16:00-24:00. The flowchart (Fig. 5.2) calculates the output reference current of the grid side converter to balance these cases. It can be seen from Fig. 5.4 (a) that in between 00:00-08:00, the grid produces 0.6 $KVAR$ reactive power which is converted to 0.3 $KVAR$ 25 Hz+ 0.3 $KVAR$ 100 Hz reactive powers and sends those powers to the MF bus for reactive power balance at MF bus. Similarly in between 08:00-16:00, the grid produces 0.8 $KVAR$ reactive power and in between 16:00-24:00, grid produces 0.5 $KVAR$ reactive power which is converted to required frequency reactive power. So for every time period, the grid supplies the deficient amount of different frequency reactive powers and maintains reactive power balancing criteria ($Q_G = \sum_{f=1}^{f=n} Q_{M-f-diff}$). So

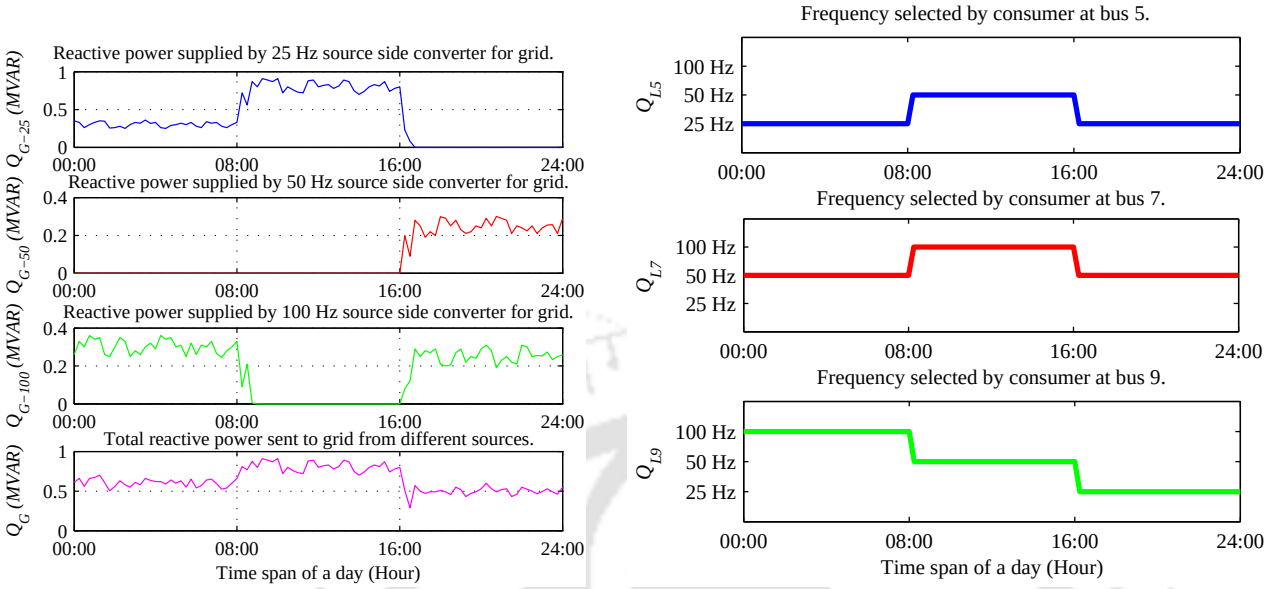

Figure 5.4: (a) Reactive power at grid side converter (Q_G) in grid connected mode which consists of three different frequency reactive powers ($Q_G = Q_{G-25} + Q_{G-50} + Q_{G-100}$). (b) Different frequency reactive power selection by consumers at buses 5, 7, and 9 in different time frames.

the reactive power balancing strategy works flawlessly in grid connected mode.

5.4.2 Islanded Mode

Next, the MFMG is simulated in islanded mode. In this mode, MFMG needs to be self supported and different frequency reactive power demands are fulfilled by the MFMG sources. First, the sources try to supply the same frequency reactive power loads but due to source side reactive power limitation, some frequency load reactive power demands are not fulfilled. So the reactive power references of the available sources are increased to compensate these frequency reactive powers. It can be seen from Fig. 5.3, that three different frequency loads are connected in bus 7 (25 Hz), bus 5 (50 Hz), and bus 9 (100 Hz). These loads absorb different frequency active and reactive powers as per frequency selectivity criteria. The frequency selection is presented in Fig. 5.4 (b). The reactive power load demands for load in buses 7, 5, and 9 are shown in Fig. 5.5 (b), which are 1.2 $MVAR$ 25 Hz, 4.4 $MVAR$ 50 Hz, 1.7 $MVAR$ 100 Hz at 00:00 to 08:00 interval, 1.8 $MVAR$ 50 Hz, 3.2 $MVAR$ 100 Hz, 2 $MVAR$ 50 Hz at 08:00 to 16:00 interval, and 1.6 $MVAR$ 25 Hz, 1.2 $MVAR$ 50 Hz, 0.6 $MVAR$ 25 Hz at 16:00 to 24:00 interval. All three loads take different frequency reactive powers alternatively at different time

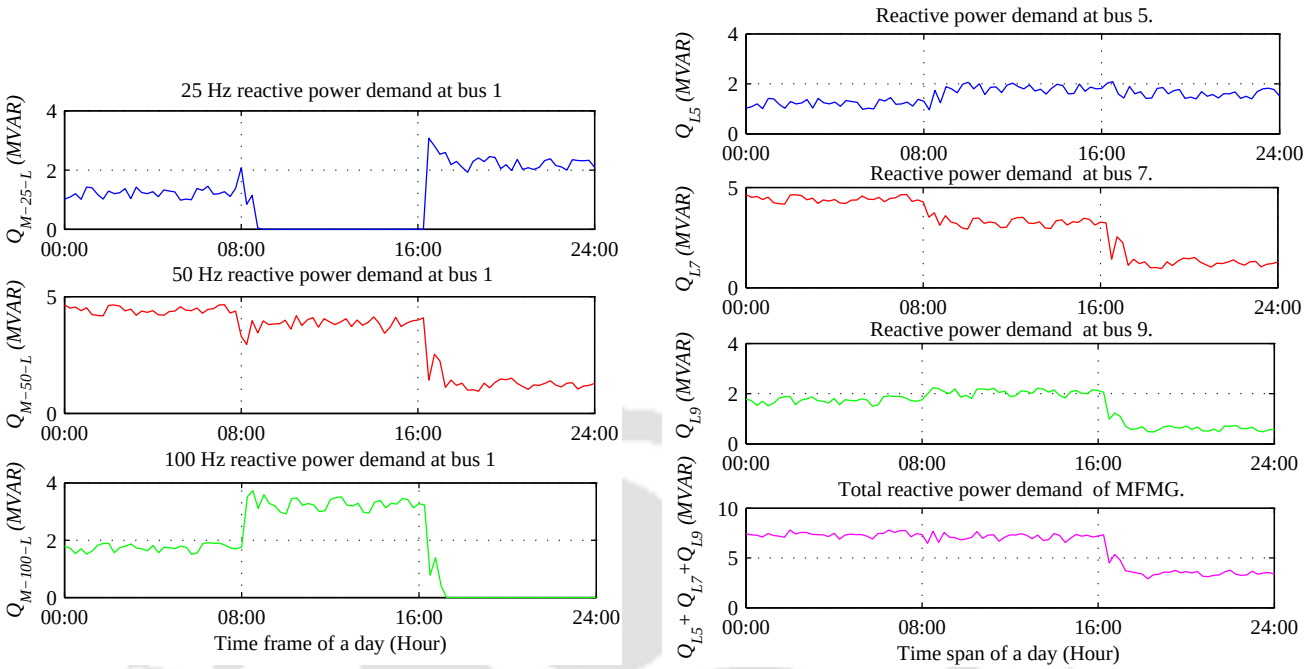

Figure 5.5: (a) Total 25 Hz (Q_{M-25-L}), 50 Hz (Q_{M-50-L}), and 100 Hz ($Q_{M-100-L}$) reactive power load demands at bus 1 from the consumers of bus 5, 7, and 9. (b) Variation of reactive power load demands at bus 5 (Q_{L5}), 7 (Q_{L7}), and 9 (Q_{L9}) throughout the day.

periods.

Same frequency reactive load powers are individually added for each time period and the total reactive power demand for a particular frequency at the MF bus is calculated ($Q_{M-25-L} = Q_{L5-25} + Q_{L7-25} + Q_{L7-25}$) which is referred in Fig. 5.5 (a). At 00:00 to 08:00 interval, total reactive power load demand is 1.2 $MVAR$ 25 Hz +4.4 $MVAR$ 50 Hz +1.7 $MVAR$ 100 Hz. The 25 and 100 Hz sources produce the required amount of reactive power but the 50 Hz source produces maximum 3.5 $MVAR$ in this time period. Here the reactive power differences for different frequencies are, $Q_{M-25-diff} = 0$, $Q_{M-50-diff} = 0.9$ $MVAR$, and $Q_{M-100-diff} = 0$, which are the circumstances for case 2. According to the flowchart presented in Fig. 5.2, 25 and 100 Hz sources at buses 4 and 8 generate extra 0.45 $MVAR$ reactive power each. Source side converters convert those reactive powers to 50 Hz reactive power and send them to bus 1 to control reactive power of 50 Hz. In between 08:00 to 16:00, the total reactive power load demand is 3.8 $MVAR$ 50 Hz +3.2 $MVAR$ 100 Hz. Here, both 50 and 100 Hz sources reach their maximum limit and produce 3.5 $MVAR$ 50 Hz and 2.5 $MVAR$ 100 Hz

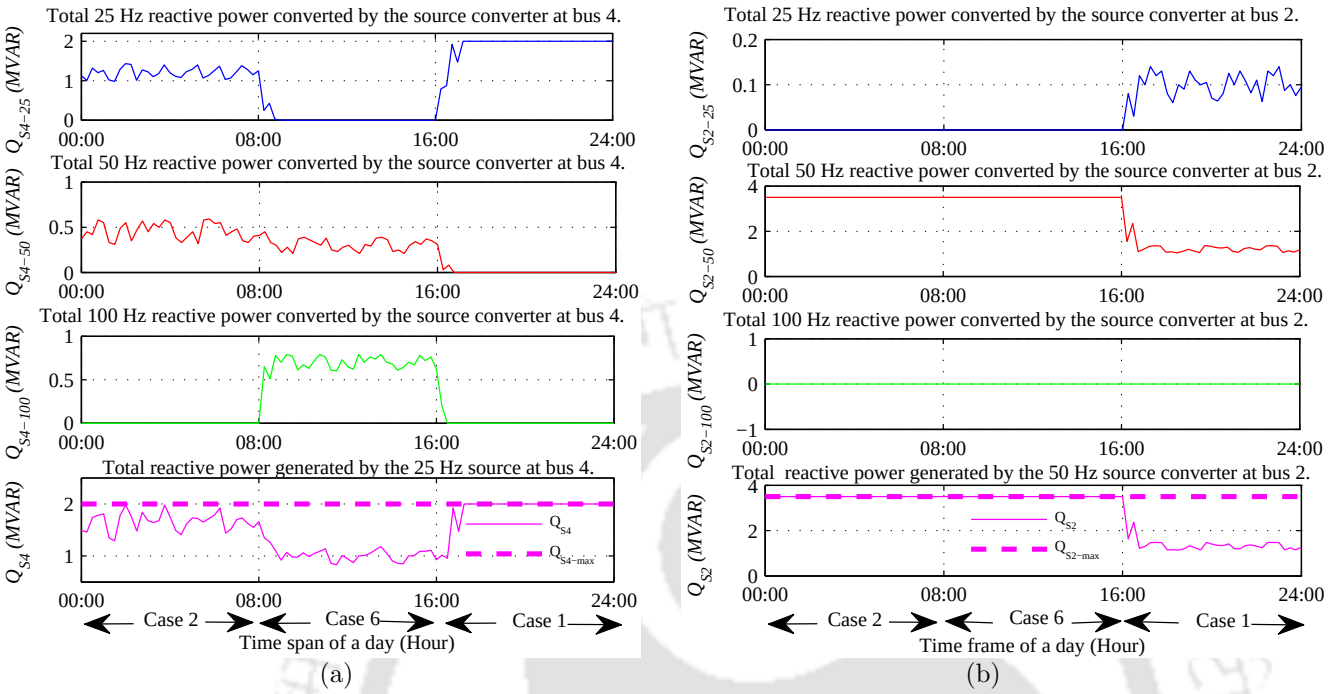

Figure 5.6: (a) Total 25 Hz source reactive power at bus 4 (Q_{S4}) of MFMG in islanded mode which is converted to three different frequency reactive powers ($Q_{S4} = Q_{S4-25} + Q_{S4-50} + Q_{S4-100}$) and sent to bus 1. (b)Total 50 Hz source reactive power at bus 2 (Q_{S2}) of MFMG in islanded mode which is converted to three different frequency reactive powers ($Q_{S2} = Q_{S2-25} + Q_{S2-50} + Q_{S2-100}$) and sent to bus 1.

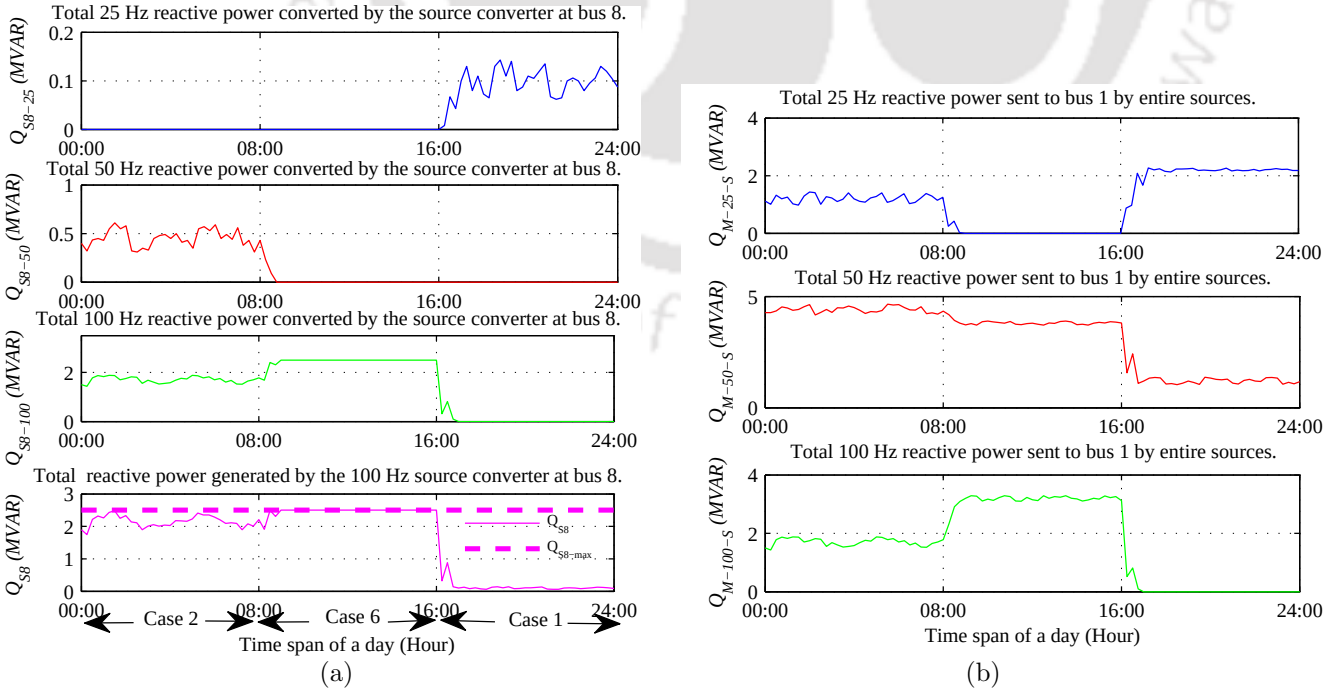

Figure 5.7: (a) Total 100 Hz source reactive power at bus 8 (Q_{S8}) of MFMG in islanded mode which is converted to three different frequency reactive powers ($Q_{S8} = Q_{S8-25} + Q_{S8-50} + Q_{S8-100}$) and sent to bus 1. (b) Total 25 Hz (Q_{M-25-S}), 50 Hz (Q_{M-50-S}), and 100 Hz ($Q_{M-100-S}$) reactive powers obtained at bus 1 from sources of bus 2, 4, and 8 in islanded mode.

reactive powers respectively. For this situation, the reactive power differences are, $Q_{M-25-diff} = 0$, $Q_{M-50-diff} = 0.3\ MVAR$, and $Q_{M-100-diff} = 0.7\ MVAR$ so, case 6 happens. In this time interval, 25 Hz source at bus 4 generates extra 1 $MVAR$ reactive power. The source converter at bus 4 converts this reactive power to 0.3 $MVAR$ 50 Hz +0.7 $MVAR$ 100 Hz and sends it to bus 1. At 16:00 to 24:00 intervals, the total reactive power load demand becomes 2.2 $MVAR$ 25 Hz +1.2 $MVAR$ 50 Hz. The 50 Hz source produces the required 50 Hz reactive power but the 25 Hz source at bus 4 generates maximum 2 $MVAR$. Here the reactive power difference equations are, $Q_{M-25-diff} = 0.2\ MVAR$, $Q_{M-50-diff} = 0$, and $Q_{M-100-diff} = 0$, which are the conditions for case 1. As per the flowchart, this $Q_{M-25-diff}$ is equally produced by 50 and 100 Hz sources and sent to bus 1 to achieve reactive power balance. The output reactive powers of the source side converters of bus 4, 2, and 8 are shown in Fig 5.6, and 5.7 (a) respectively.

The total source power at bus 1 is obtained by algebraically addition of each frequency component of all source powers ($Q_{M-25-S} = Q_{S2-25} + Q_{S4-25} + Q_{S6-25}$) and conferred in Fig. 5.7 (b). It can be observed that source and load reactive power of individual frequency match with each other after control ($Q_{M-25-S} = Q_{M-25-L}$, $Q_{M-50-S} = Q_{M-50-L}$, $Q_{M-100-S} = Q_{M-100-L}$) at MF bus. Finally, MFMG attains the reactive power balancing conditions for islanded mode ($Q_{L5} + Q_{L7} + Q_{L9} = Q_{S2} + Q_{S4} + Q_{S8}$, whereas $Q_{L5} \neq Q_{S2}$, $Q_{L7} \neq Q_{S4}$, $Q_{L9} \neq Q_{S8}$).

5.5 Conclusion

In MFMG, different frequency powers are superimposed on the MF bus and the consumers have a special ability to choose among the available powers alternatively at different time frames. This frequency selective power consumption creates variable reactive power demands at the load side and several new reactive power imbalance situations develop. In this chapter, all these cases are defined for islanded and grid connected modes. For three different frequency reactive powers, a total of six imbalance cases are identified for islanded mode and a reactive power balancing strategy is proposed by controlling the grid feeding converters. In grid connected mode, the control of the grid side converter is carried in such a way that grid can give reactive power to

MFMG to improve power quality and stability. To validate these strategies, simulation of a 9 bus MFMG is executed for islanded and grid connected modes. It can be concluded from the results that different frequency reactive power control is achieved for all the cases and MFMG fulfills the reactive power balancing conditions for islanded and grid connected modes. So, all controllers and compensators are properly designed and the new control schemes are working flawlessly.

Note: Major part of this chapter is reproduced from my publications:

1. R. Dey, S. Nath, "Control and management of different frequency active and reactive powers for multifrequency microgrid ," in *IEEE Access* (Submitted).

2. R. Dey and S. Nath, "A new active and reactive power control strategy for multifrequency microgrid in islanded mode," in *proceedings of 5th International Conf. on Smart Grid and Smart Cities (ICSGSC)*, 2021, pp. 45–49.

6

Multifrequency Microgrid with Energy Storage System

Contents

6.1 Introduction

Solar and wind power varies throughout the day. In the noon time the solar irradiation is maximum and in the night time no solar power is available. Wind power of a wind turbine depends upon the wind speed which varies throughout the day. So without help of an energy storage system, the solar and wind sources cannot supply a sensitive load which needs reliable power. The addition of ESS with MFMG increases the reliability and stability of the system. The integration and operation of ESS with MFMG are explained in this chapter. It can be seen that with the presence of ESS, MFMG can operate in two extra power imbalance cases. For all active power imbalance cases for islanded and grid connected modes, the power balancing criteria are defined here. Finally, one algorithm is designed to coordinate between the ESS and other frequency sources of MFMG to balance different frequency load power demands for optimum power generation through communication under a cooperative framework. The framework is constructed based on the assumption that any load prefers to absorb power from the closest source for minimum power loss and cost. The categorization of different source load pairs is done based on the physical distance by different frequencies and accordingly the algorithm is structured. As different frequency active powers do not mix with each other and can be separated at the load side, this operation is possible. A circuit model of 8 bus MFMG is simulated in Matlab Simulink to validate the algorithm for different power imbalance cases. In this chapter, the coordinated power management strategy of MFMG is described. Based on the strategy, it has been found that two new active power imbalance cases occur due to the integration of ESS. Next, all these new cases are explored, and accordingly power balancing criteria of MFMG with ESS is defined. Based on all the criteria, an algorithm is proposed to balance different frequency active powers of MFMG with ESS. Finally, the algorithm is verified through simulation results.

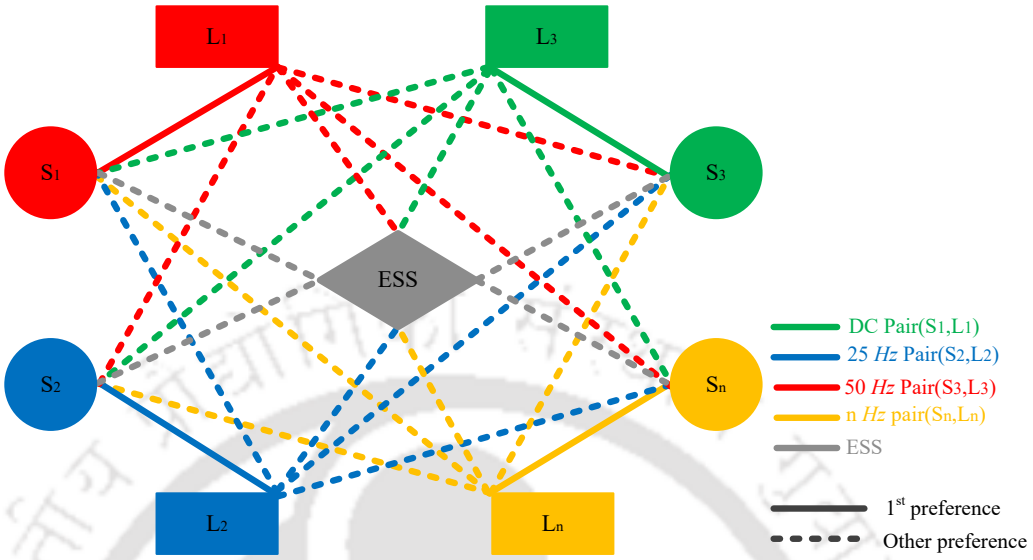

Figure 6.1: Coordinated power management structure of MFMG.

6.2 Coordinated Power Management of Multifrequency Microgrid

In this chapter, the MFMG power management strategy with ESS is formed based on the coordinated structure which needs to be defined first. The coordinated power management structure of MFMG is presented in Fig. 6.1. Different frequency sources, loads, and an ESS are connected with each other by an MF bus. Total 'n' different frequency active powers are transmitted through the MF bus by creating different power channels. It is considered that the load tries to absorb power from the closest source to reduce power loss and cost. If the closest source power is unavailable then the load takes the required power from other available sources equally. Based on these conditions, a pair is formed with one source and one load based on the physical distance. Each source-load pair is operated in a distinctive frequency to differentiate that pair from the rest of the system. All loads and sources of MFMG are controlled by power electronic converters so, this operation is achievable irrespective of the load and source frequency. From Fig. 6.1, it can be noticed that S_1 and L_1 are functioned as DC source load pair, S_2 and L_2 are functioned as 25 Hz source load pair, and similarly S_n and L_n are functioned as 'n' Hz source load pair. The logic behind the power management is that the DC load (L_1)

Table 6.1: Physical distances between different frequency sources and loads

Source	Load	Distance (km)	Pair selection
PV	EV	0.1	DC pair
PV	DL	2	
PV	IL	2.5	
WT	EV	3	
WT	DL	0.05	25 Hz pair
WT	IL	3.2	
MT	EV	1.8	
MT	DL	1.5	
MT	IL	0.8	50 Hz pair

should absorb power from the DC source (S_1). If DC source power is not available then DC load will absorb power from other available sources ($S_2, S_3, ...S_n$) equally. For implementation of this strategy in a traditional microgrid which has 'n' number of sources and 'm' number of loads a total of $(m * n)$ number of dedicated connections are needed. For MFMG, only one MF bus dedicatedly connects all the sources and loads through different power channels which reduces the installation and maintenance cost of the system. To increase the reliability of MFMG, an ESS is connected to the MF bus. Based on the source availability and load demand, the ESS is charged or discharged to maintain the different frequency active power balance of MFMG. In extreme situations, the ESS can supply the critical loads of MFMG. The MFMG architecture is presented in Fig. 3.1 (b) in chapter 3. Three different frequency (DC, 25 Hz, 25 Hz) sources and loads are present in the architecture. The physical distances between different frequency sources and loads are present in Table 6.1, which is chosen based on the calculation presented in [77]. Based on the physical distance, the PV and EV are chosen as DC pair, the WT and DL are chosen as 25 Hz pair, and the MT and IL are chosen as 50 Hz pair.

6.3 Active Power Balance Problem of Multifrequency Microgrid with Energy Storage System

In any system, the active power balance is necessary to maintain the bus frequency and stability. In MFMG, different frequency active powers are present on the MF bus and customers

are able to select any of the available powers. Due to the frequency selectivity criteria, different new active power imbalance cases are generated in MFMG. Based on the coordinated strategy (Fig. 6.1), different power imbalance cases are analyzed and accordingly power balancing criteria are defined for MFMG with ESS. To balance the different frequency active powers of MFMG, the sources and ESS need to be controlled precisely. All sources and ESS are controlled by power electronic converters so any frequency source power can be transformed to other frequency load powers and sent to the MF bus. For any source-load pair, if load demand is higher than the maximum power generation of the source then other available sources can produce extra power to fulfill that load demand. Here, the active power balancing problem is investigated separately for islanded mode and grid connected mode.

6.3.1 Islanded Mode

In islanded mode the switch at PCC opens, and the grid is disconnected from the MFMG. Here, the MFMG needs to be self-sufficient and the total load demand is delivered by the sources and ESS. For a traditional AC or DC microgrid, if the source power is higher then the ESS is charged and if the load power is higher, then the ESS is discharged. For traditional microgrids, the ESS power needs to match the difference between the source and load powers of that frequency for power balancing. The active power balancing condition for the DC and AC microgrid is given in equation 6.1.

$$P_{BESS} = P_{M-0-S} - P_{M-0-L},\ P_{BESS} = P_{M-50-S} - P_{M-50-L} \tag{6.1}$$

In MFMG, the ESS is connected by a by-directional MF/DC and DC/DC converter. The MF/DC converter can convert any frequency power to DC power and vice-versa. So, by proper power conversion, a single ESS unit can store different frequency active powers. In islanding mode first, the sources try to balance different frequency load demands of MFMG. If the paired source-load power is not balanced then that load takes the required power from other available sources. If no source is available to supply that load demand, then the load takes power from the ESS. So for MFMG, the ESS is charged when the total source power is higher than the total

Table 6.2: Different cases of active power imbalance of the MFMG with ESS in islanded mode

Case 1	$P_{M-0-diff} = 0,\ P_{M-25-diff} = 0,\ P_{M-50-diff} = 0$
Case 2	$P_{M-0-diff} > 0,\ P_{M-25-diff} = 0,\ P_{M-50-diff} = 0$
Case 3	$P_{M-0-diff} = 0,\ P_{M-25-diff} > 0,\ P_{M-50-diff} = 0$
Case 4	$P_{M-0-diff} = 0,\ P_{M-25-diff} = 0,\ P_{M-50-diff} > 0$
Case 5	$P_{M-0-diff} > 0,\ P_{M-25-diff} = 0,\ P_{M-50-diff} > 0$
Case 6	$P_{M-0-diff} > 0,\ P_{M-25-diff} > 0,\ P_{M-50-diff} = 0$
Case 7	$P_{M-0-diff} = 0,\ P_{M-25-diff} > 0,\ P_{M-50-diff} > 0$
Case 8	$P_{M-0-diff} > 0,\ P_{M-25-diff} > 0,\ P_{M-50-diff} > 0$

load demand and the ESS is discharged when the total load demand is higher than the total source power. The active power balancing criteria for an MFMG system with ESS is presented in equation 6.2 which states that the ESS power should match with the difference between the algebraic sum of different load and source bus powers.

$$P_{BESS} = \sum_{f=1}^{n} P_{M-f-S} - \sum_{f=1}^{n} P_{M-f-L} \tag{6.2}$$

Here the MFMG contains three different frequencies (DC, 25 Hz, 50 Hz) so, the active power balancing condition becomes,

$$P_{BESS} = P_{M-0-S} + P_{M-25-S} + P_{M-50-S} - P_{M-0-L} - P_{M-25-L} - P_{M-50-L} \tag{6.3}$$

For each source-load pair, the active power difference is defined as,

$$P_{M-f-diff} = P_{M-f-L} - P_{M-f-S} \quad \text{for } f = DC, 25\ Hz, 50\ Hz \tag{6.4}$$

In another way, it can be said that the different frequency active powers of MFMG are balanced if the ESS power is equal to the algebraic sum of different source load pair active power differences.

$$P_{BESS} = \sum_{f=1}^{n} P_{M-f-diff} \quad \text{for } f = DC, 25\ Hz, 50\ Hz \tag{6.5}$$

Based on the source-load pair power differences, total eight cases of active power imbalance can occur in MFMG with ESS. For three different frequency sources, loads and without ESS, total six power unbalance cases (case 2- case 7) are already defined. It is observed that with ESS,

the active power can be balanced for two more cases (case 1, case 8), where previously power balance was not possible. So, reliability of the system increases by connecting the ESS with MFMG. All these cases are presented in Table 6.2. A new active power balancing technique needs to be designed to balance power for all these eight cases.

From Table 6.2, it can be seen that the power imbalance situation for case 1 is $P_{M-0-diff} = 0$, $P_{M-25-diff} = 0$, $P_{M-50-diff} = 0$. For this situation, all different frequency source-load pairs in MFMG are balanced. Still, the sources have to generate extra power to charge up the ESS. The power imbalance condition for case 4 is $P_{M-0-diff} = 0$, $P_{M-25-diff} = 0$, $P_{M-50-diff} > 0$. Here DC and 25 Hz active power pairs are balanced. The 50 Hz source reaches its maximum capacity and still can not fulfill the 50 Hz load power demand. Here, the available sources (DC, 25 Hz) need to generate extra DC and 25 Hz active power equally. Source side converters will transform those powers to the required 50 Hz active power ($P_{M-50-diff}$) and send that to the MF bus to maintain the active power balance of the total system. As the DC and 25 Hz sources are available after balancing the total load demand, the ESS is charged for this case. Case 8 has an imbalance condition of $P_{M-0-diff} > 0$, $P_{M-25-diff} > 0$, $P_{M-50-diff} > 0$. For this case, all sources of MFMG are at their maximum capacity, yet can't fulfill their paired load demands. Here the ESS is discharged and the required load power is supplied by the ESS to balance different frequency active powers.

6.3.2 Grid Connected Mode

In grid connected mode, the switch at PCC is closed and the grid is connected to the MFMG. The grid controls the bus voltage and balances different frequency active powers in MFMG. As the grid power cost is lower than the storage power, the ESS is never discharged in grid connected mode. The lithium-ion battery is operated in mid-SOC range ($20\% - 80\%$) to maintain a good state of health [78]. So, the ESS is only charged in grid connected mode and if SOC climbs to 80% then the ESS is disconnected from the system. Here, the objective of the control strategy is to set the grid active power reference in a way that it fulfills all source-load pair active power mismatches and charges the ESS. The active power balancing criteria of the

MFMG with ESS in grid connected mode is presented in equation 6.6.

$$P_G = \sum_{f=1}^{n} P_{M-f-diff} + P_{BESS} \tag{6.6}$$

The grid is connected to the MF bus by a back to back converter structure of AC/DC and DC/MF converters. This combination of converters transforms the 50 Hz grid power to different frequency active powers and sends those to the MF bus for the active power balance of MFMG. The MFMG architecture (Fig. 3.1(b)), contains three different frequency sources and loads. Equation 6.7 represents the active power balancing criteria for grid connected mode of MFMG with ESS.

$$P_G = P_{M-0-diff} + P_{M-25-diff} + P_{M-50-diff} + P_{BESS} \tag{6.7}$$

Which states that the algebraic sum of all source-load pair power imbalances and ESS power should be equal to grid power for power balance in grid connected mode.

6.4 Algorithm for Active Power Balance of Multifrequency Microgrid with Energy Storage System

Based on the power balance criteria, an algorithm is designed under varying different frequency loads for islanded and grid connected modes. The main objective behind the algorithm is that in islanded mode, any load always tries to take active power from the paired source. If paired source power is not available then the load takes power from other available sources of MFMG. If no other source is available then the load takes power from the ESS and if ESS power is also not available then load shedding needs to be done. In islanded mode, if $P_{ST} > P_{LT}$ then ESS takes the extra source power to store. If $P_{LT} > P_{ST}$ then ESS discharges and delivers different frequency required active powers to the loads. If ESS is fully charged then the sources should be controlled to decrease the active power generation. In grid connected mode, the grid balances different frequency active power imbalances of MFMG and charges the ESS. The flowchart for the proposed algorithm is conferred in Fig. 6.2. The algorithm is composed of ten steps.

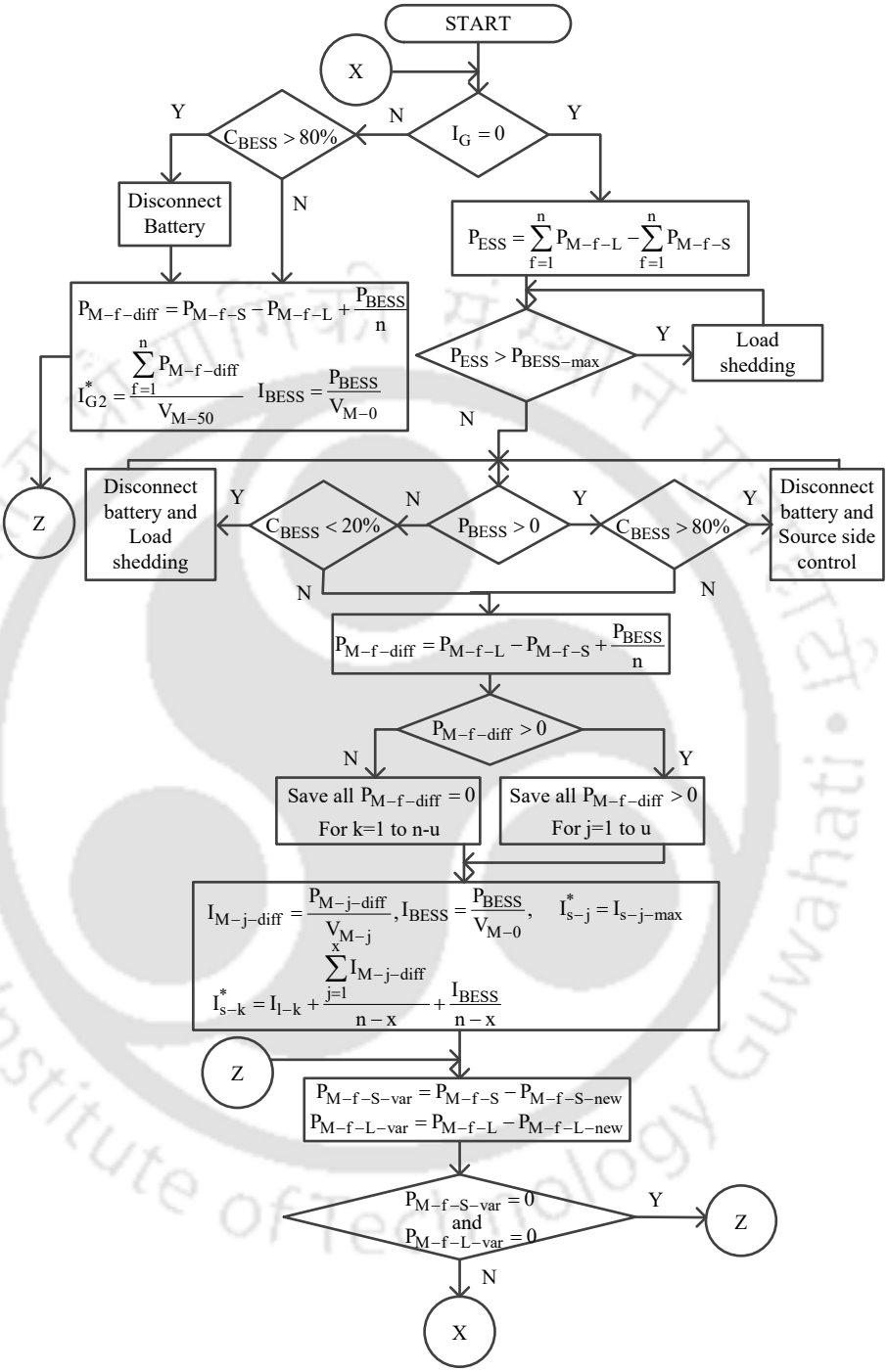

Figure 6.2: Flowchart to achieve active power balance of MFMG with ESS.

- Step 1: Check the mode of operation of MFMG -

$$I_G = 0 \begin{cases} Yes & \text{Then MFMG is in islanded mode and jump to step 4.} \\ No & \text{Then MFMG is in grid connected mode and goto next step.} \end{cases}$$

- Step 2: Check the charging status of the battery -

$$C_{BESS} > 80\% \begin{cases} Yes & \text{Maximum SOC limit is reached so, charging is off and battery is disconnected and goto next step.} \\ No & \text{Then goto next step.} \end{cases}$$

- Step 3: Find out the power difference of different frequency source-load pairs at MF bus ($P_{M-f-var}$), compute the output current reference for grid side converter (I^*_G) and battery side converter (I^*_{BESS}) and jump to step 10.

$$P_{M-f-diff} = P_{M-f-S} - P_{M-f-L} + \frac{P_{BESS}}{n},\ I^*_{G2} = \frac{\sum_{f=1}^{n} P_{M-f-diff}}{V_{M-50}},\ I^*_{BESS} = \frac{P_{BESS}}{V_{M-0}}$$

- Step 4: Find out the power difference of different frequency source-load pairs at MF bus and check the battery power is available or not -

$$P_{ESS} = \sum_{f=1}^{n} P_{M-f-L} - \sum_{f=1}^{n} P_{M-f-S}$$

$$P_{ESS} > P_{BESS-max} \begin{cases} Yes & \text{Then some loads are shedded and go back to step 4.} \\ No & \text{Then goto next step.} \end{cases}$$

- Step 5: Check mode of operation of the battery as-

$$P_{BESS} > 0 \begin{cases} Yes & \text{Battery takes power, in charging mode and goto next step.} \\ No & \text{Battery supplies power, in discharging mode and jump to step 9.} \end{cases}$$

- Step 6: Check the charging status of the battery -

$$C_{BESS} > 80\% \begin{cases} Yes & \text{Maximum SOC is reached so, charging is off and battery is disconnected and control the sources to generate less power and go back to step 5.} \\ No & \text{Then goto next step.} \end{cases}$$

- Step 7: Check the different frequency active power differences between source-load pairs and battery at MF bus and goto next step.

$$P_{M-f-diff} = P_{M-f-L} - P_{M-f-S} + \frac{P_{BESS}}{n}$$

- Step 8: Check -

$P_{M-f-diff} > 0$ {

Yes This frequency load demand is not fulfilled but paired source is already at the maximum capacity so the load takes the required power from other available sources and the paired source is operated at maximum power, and jump to step 10.

$I^*_{s-j} = I_{s-j-av}$

No This frequency load demand is fulfilled and paired source is not at maximum limit so it delivers power to other frequency loads and charges battery then jump to step 10.

$I^*_{s-k} = I_{l-k} + \frac{\sum_{f=1}^{n} P_{M-f-diff}}{n-x} + \frac{I_{BESS}}{n-x}$

- Step 9: Check the discharging status of the battery -

$C_{BESS} < 20\%$ {

Yes Then discharging off and disconnect battery and some loads are shedded and go back to step 5.

No Then go back to step 7 if all references are calculated then goto next step.

$P_{BESS} = \sum_{f=1}^{n} P_{M-f-L} - \sum_{f=1}^{n} P_{M-f-S},\ I^*_{BESS} = \frac{P_{BESS}}{V_{M-0}}$

- Step 10: Check the source and load active powers have changed or not -

$$P_{M-f-S-var} = P_{M-f-S} - P_{M-f-S-new},\ P_{M-f-L-var} = P_{M-f-L} - P_{M-f-L-new}$$

Table 6.3: Comparison of proposed strategy with existing literature

References	[79], [61], [80], [81].	This work.
Bus voltage frequency	50 Hz (AC) [80], [81], DC [79], 50 Hz and DC (Hybrid) [61].	DC+ 25 Hz+ 50 Hz (MF).
Active Power imbalance cases	Two cases for AC or DC [80], [81], [79], and four cases for hybrid microgrid [61].	Eight cases for MFMG.
Active power balancing strategy	Centralized d-q power control in [80], fuzzy logic control in [81], positive and negative sequence components control in [79],V-F control in [61].	Centralized d-q power control.
Active power sharing strategy	Based on cost in [79], based on source rating [61].	Based on distance between source and load to reduce active power loss and cost.
Converter control strategy	Inverter current control in [80], fuzzy control in [81], Combined feedforward and feedback control in [79], and droop control in [61].	Voltage mode and average current control.
Source side power categorization	Not possible.	Source side powers can be categorized depending upon their availability, reliability, cost, or distance of the source from load and pass through different frequency power channels of MF bus without mixing.
Consumer power selection	Not possible.	Consumers have the ability to choose between different frequency powers from MF bus based on their needs.

$$P_{M-f-S-var}/P_{M-f-L-var} = 0 \begin{cases} Yes & \text{Total active power is balanced.} \\ No & \text{Go back to step 1.} \end{cases}$$

A brief comparison of the work presented in the thesis with respect to the state-of-the-art is presented in Table 6.3 to understand the innovative contribution.

6.5 Simulation Results

To evaluate the algorithm, an 8 bus MFMG is simulated in islanded mode and grid connected mode in the Matlab Simulink environment. One BESS unit at bus 8 is added with the bus structure (Fig. 4.4) used in chapter 4, and the new structure is formed. The description of the sources and loads of the MFMG are given in Table 6.4 which are used in the simulation. It can be seen from the architecture that different sources, loads, and battery energy storage system (BESS) are connected to the MF bus by different converters and LC filters. The filter

Table 6.4: Case study of 8 bus MFMG with ESS

Source/ Load	Operating frequency	Voltage	Maximum capacity	Type of converter connected	Bus no.
Grid	50 Hz	230 V	-	AC50/DC, DC/MF	1
PV	DC	300 V	100 kW	DC/DC, DC/MF	6
WT	25 Hz	150 V	80 kW	AC25/DC, DC/MF	4
MT	50 Hz	230 V	60 kW	AC50/DC, DC/MF	2
EV	DC	110 V	60 kW	MF/DC, DC/DC	3
DL	25 Hz	230 V	70 kW	MF/DC, DC/AC25	7
IL	50 Hz	230 V	80 kW	MF/DC, DC/AC50	5
BESS	DC	475 V	50 kW	MF/DC, DC/DC	8

V_{MFB}: 500 V DC + 50 V AC 25 Hz (RMS) + 230 V AC 50 Hz (RMS)

Table 6.5: Filter parameters of MFMG

Parameter	Value
L_G, C_G	1.5 mH, 750 μF
L_{GF}, C_{GF}	1 mH, 1000 μF
L_{GFE}	1 mH
L_L, C_L	0.2 mH, 400 μF
L_B, C_B	0.5 mH, 600 μF

Table 6.6: Controller parameters for different converters of MFMG

Converter name	Proportional Gain (K_P)	Integral Gain (K_I) in S^{-1}
Grid side	$K^P_{G-V} = 1.8$, $K^P_{G-I} = 3.6$	$K^I_{G-V} = 78.4$, $K^I_{G-I} = 62.6$
Grid forming	$K^P_{GF} = 1.2$	$K^I_{GF} = 45$
Grid feeding	$K^P_{GFE} = 18.7$	$K^I_{GFE} = 345$
BESS	$K^P_B = 18.3$, $K^R_B = 20$	$K^I_B = 165$, $K^S_B = 76$

parameters which are used for the simulation are presented in Table 6.5. The PI controllers of grid side, grid feeding, grid forming, and BESS converters are designed and those values are shown in Table 6.6. The different frequency load varies throughout the time frame of the day. Due to this several new active power imbalance cases are created. The algorithm is applied to control the MFMG sources and BESS to balance the active powers for all these cases. In this section, the simulation results are presented for islanded mode and grid connected mode separately.

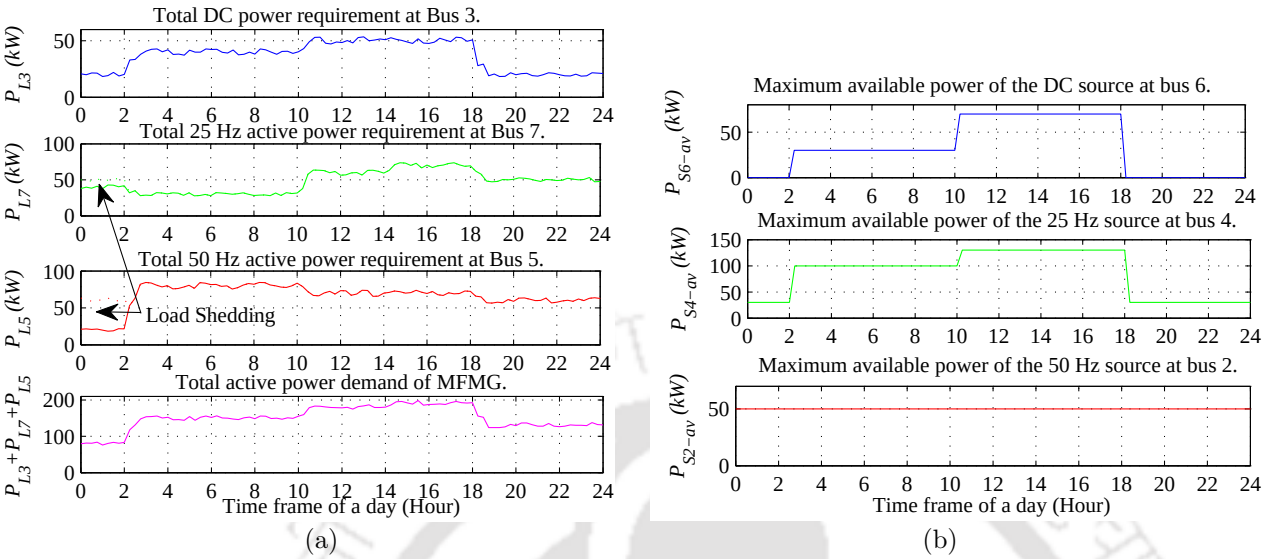

Figure 6.3: (a) Total load side DC (P_{L3}), 25 Hz (P_{L7}) and 50 Hz (P_{L5}) active power requirement in bus 3, 7, and 5. (b) Available source side DC (P_{S6-av}), 25 Hz (P_{S4-av}) and 50 Hz (P_{S2-av}) active power in bus 6, 4, and 2 in different time frames.

6.5.1 Islanded Mode

In this mode grid is disconnected from MFMG so, total load demand is supplied by the sources and BESS. Due to frequency selective power absorption, different active power imbalance cases are created. The algorithm calculates the reference output current for the source and battery side converters to balance different frequency active powers for these cases.

An electric vehicle (EV) charging station (DC), industrial load (50 Hz), and domestic load (25 Hz) are connected to buses 3, 5, and 7 respectively where the domestic (DL) and industrial loads (IL) are non-sensitive load and can be shredded if required. The daily load profiles are shown in Fig. 6.3 (a). The load demands vary as per their nature throughout the day. During 18:00-24:00, total load demand (130 kW) is higher than total source power (80 kW). So the battery is discharged to supply the required load power. The SOC of the battery reaches 20% at 24:00 and the battery is disconnected from the MFMG. To balance the active powers between the sources and loads, some portions of the IL and DL are shredded in between 00:00-02:00. The IL is decreased by 40 kW and the DL is decreased by 10 kW. From 02:00-18:00, total source power (P_{ST}) is higher than the load power (P_{LT}). So MFMG is able to deliver total load power and charge the BESS.

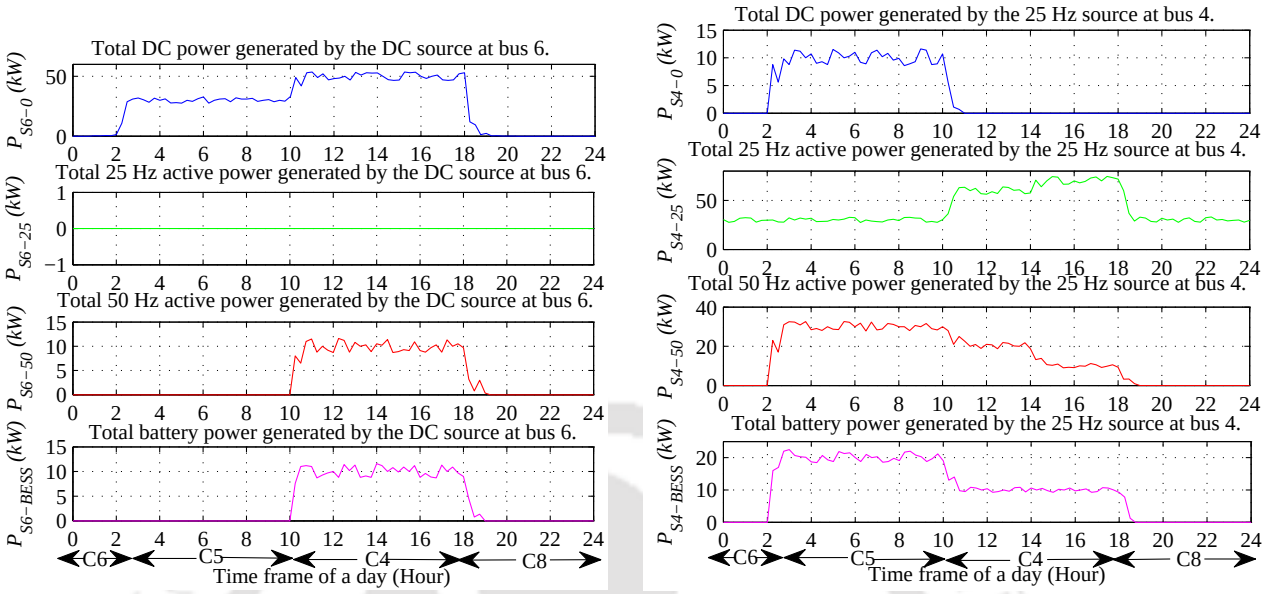

Figure 6.4: (a) Total DC power is converted to DC (P_{S6-0}), 25 Hz (P_{S6-25}), 50 Hz (P_{S6-50}), and battery power ($P_{S6-BESS}$) by DC source (bus 6) converter and sent to MF bus. (b) Total 25 Hz active power is converted to DC (P_{S4-0}), 25 Hz (P_{S4-25}), 50 Hz (P_{S4-50}), and battery power ($P_{S4-BESS}$) by 25 Hz source (bus 4) converter and sent to MF bus.

A photo voltaic (PV) source (DC), two wind turbine (WT) units (25 Hz), and one micro turbine (MT) unit (50 Hz) are connected in buses 6, 4, and 2 respectively. One WT behaves as grid interactive converter and balances the MF bus voltage. The maximum source powers profile for a day is conferred in Fig. 6.3 (b). The PV source generates power only during the day time and in between 10:00-18:00, it generates the maximum amount of power. The WT sources generate a variable amount of power throughout the day depending on the wind speed. The MT unit is governed by fossil fuel and is available throughout the day.

The source powers are properly controlled based on their availability throughout the day. The proposed control strategy is implemented at source and ESS side converters. It can be noticed that four active power imbalance cases occur and for these cases, the power balancing strategy is applied. The output current of the source side and battery side converter is calculated from the algorithm for different cases and accordingly, the current control method is applied in these grid feeding converters. As per the requirement, the source currents are increased and the source side converter converts that power to the required frequency load powers. Source power at bus 6 (DC), bus 4 (25 Hz), and bus 2 (50 Hz) are presented in Fig. 6.4 (a), Fig. 6.4 (b),

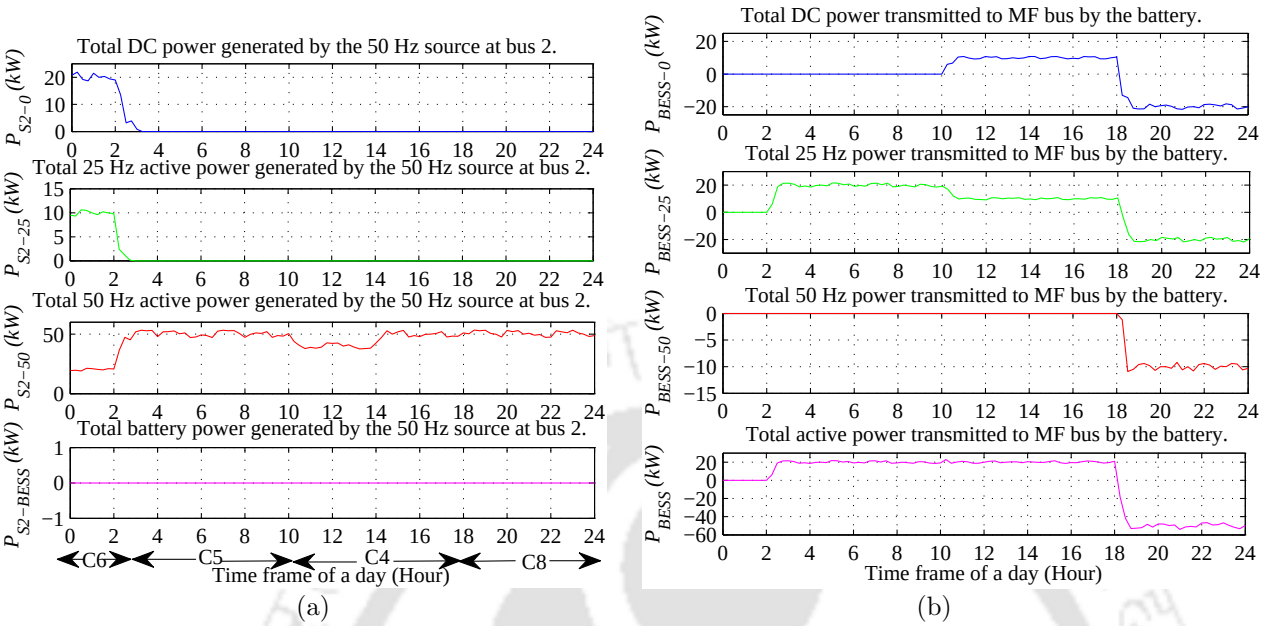

Figure 6.5: (a) Total 50 Hz active power is converted to DC (P_{S2-0}), 25 Hz (P_{S2-25}), 50 Hz (P_{S2-50}), and battery power ($P_{S2-BESS}$) by 50 Hz source (bus 2) converter and sent to MF bus. (b) Total active power exchange of the battery with MF bus which contains three different frequencies ($P_{BESS} = P_{BESS-0} + P_{BESS-25} + P_{BESS-50}$).

and Fig. 6.5 (a) respectively for different time of a day. The active power differences between different source-load pairs are $P_{M-0-diff} > 0$, $P_{M-25-diff} = 0$, and $P_{M-50-diff} > 0$, so case 5 occurs. For this case, the 25 Hz load demand is balanced by the paired source but DC and 50 Hz sources are unable to fulfill their paired load demands. So the available 25 Hz source (S_4) power is increased by 40 kW, which is converted to 10 kW DC and 30 kW 50 Hz active powers and are sent to the MF bus. After balancing the total load demand, 25 Hz source power is still available so the battery is charged and absorbs 20 kW power from the 25 Hz source. It can be noticed that between 10:00-18:00, the active power difference between different source-load pairs are, $P_{M-0-diff} = 0$, $P_{M-25-diff} = 0$, and $P_{M-50-diff} > 0$ (case 4). Here, the DC and 25 Hz load demand is balanced by the paired sources but 50 Hz pair power is not balanced. So according to the algorithm, the DC and 25 Hz sources generate extra power to fulfill the load demand of 25 Hz load. The 50 Hz load (L_5) takes total 20 kW active power equally from the DC (S_6) and 25 Hz source (S_4). As the DC and 25 Hz sources are still available after the active power balancing, so the BESS takes 10 kW DC and 10 kW 25 Hz power. From 18:00-24:00, the source-load pair power differences are $P_{M-0-diff} > 0$, $P_{M-25-diff} > 0$, and

Table 6.7: Different source and load powers of MFMG with ESS in islanded condition

$Time(H)$	$P_{S6}(kW)$	$P_{S4}(kW)$	$P_{S2}(kW)$	$P_{ST}(kW)$	$P_{L3}(kW)$	$P_{L7}(kW)$	$P_{L5}(kW)$	$P_{LT}(kW)$	$P_{ESS}(kW)$	Case no.
0-2	0	30	50	80	20	40	20	80	0	Case 6
2-4	30	90	50	170	40	30	80	150	-20	Case 5
4-6	30	90	50	170	40	30	80	150	-20	Case 5
6-8	30	90	50	170	40	30	80	150	-20	Case 5
8-10	30	90	50	170	40	30	80	150	-20	Case 5
10-12	70	90	40	200	50	60	70	180	-20	Case 4
12-14	70	90	40	200	50	60	70	180	-20	Case 4
14-16	70	90	50	210	50	70	70	190	-20	Case 4
16-18	70	90	50	210	50	70	70	190	-20	Case 4
18-20	0	30	50	80	20	50	60	130	50	Case 8
20-22	0	30	50	80	20	50	60	130	50	Case 8
22-24	0	30	50	80	20	50	60	130	50	Case 8

$P_{M-50-diff} > 0$, so case 8 happens. Here, all the three sources (DC, 25 Hz, 50 Hz) are at their maximum limit but can't fulfill their paired load demands. As no other source is available, the loads take power from the BESS. The battery discharges and generates 50 kW active power to balance all load demands. After 6 hours at 24:00, the SOC level of the battery reaches 20% and it is disconnected from the MFMG. In between 00:00-02:00, the 25 Hz (DL) and 50 Hz (IL) loads are shredded and the active power differences are $P_{M-0-diff} > 0$, $P_{M-25-diff} > 0$, and $P_{M-50-diff} = 0$ (case 6). The load demand of the 50 Hz pair is fulfilled and the 50 Hz source is available to supply other frequency load demands. Different frequency sources and loads powers for islanded mode throughout the day are presented in Table 6.7.

Based on the operating scenarios, the BESS is charged or discharged. If total load power of the MFMG is lower than the source power ($\sum_{f=1}^{n} P_{M-f-L} - \sum_{f=1}^{n} P_{M-f-S} < 0$) then BESS absorbs the extra source power and is charged. If total load power is higher than the source power ($\sum_{f=1}^{n} P_{M-f-L} - \sum_{f=1}^{n} P_{M-f-S} > 0$) then BESS provides the required active power and discharges. So for case 1 - case 7, the battery is charged and in case 8, the battery is discharged. In Fig. 6.5 (b), the different frequency battery power components are presented. By adding all the components, the total battery power is obtained. From 02:00-10:00, the battery absorbs 20 kW power from the 25 Hz source and is charged. In between 10:00-18:00, the battery absorbs 10 kW power from the DC source and 10 kW power from the 25 Hz source. As the total source power is decreased at night time, in between 18:00-24:00 the battery is discharged and supplies 50 kW active power. Which is converted to 20 kW DC + 20 kW 25 Hz + 10 kW 50 Hz power by the battery side converter and is sent to the MF bus. At 24:00, the battery is

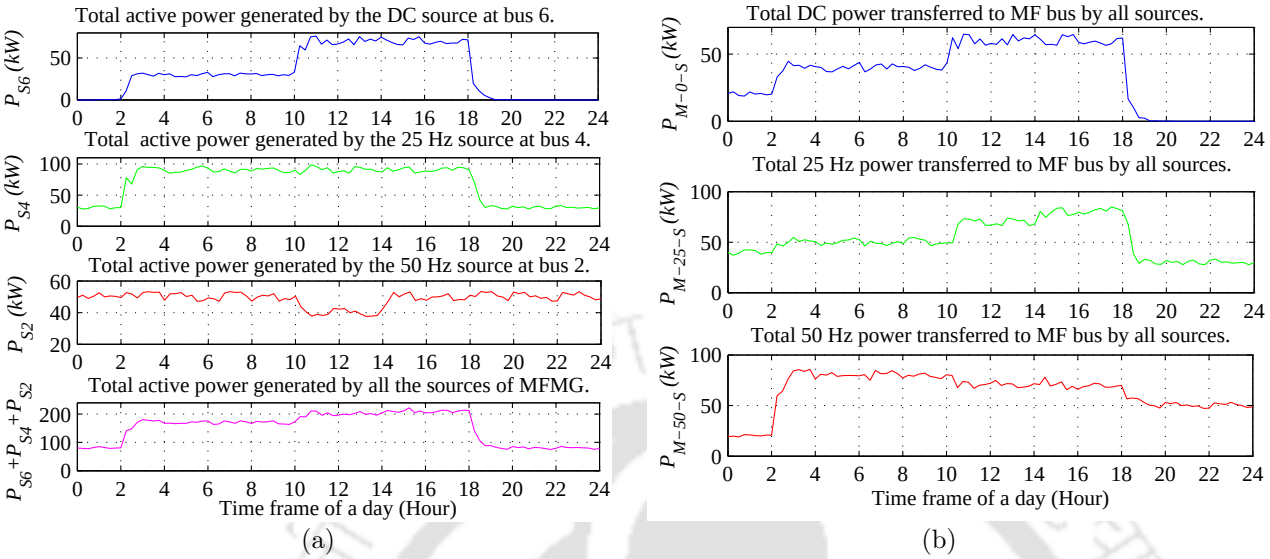

Figure 6.6: (a) Active power generation of the sources at bus 6 (P_{S6}), 4 (P_{S4}), and 2 (P_{S2}) in islanded mode. (b) Total DC (P_{M-0-S}), 25 Hz (P_{M-25-S}), and 50 Hz (P_{M-50-S}) active powers received at MF bus (bus 1) from different sources of MFMG.

fully discharged and it is disconnected from the MF bus between 00:00-02:00.

Different frequency elements of the source powers at bus 6 (P_{S6}= P_{S6-0}+ P_{S6-25}+ P_{S6-50}+ $P_{S6-BESS}$), 4, and 5 are added and the total source power of those buses are presented in Fig. 6.6 (a). Total source power of the MFMG is computed by adding these bus powers (P_{ST}= P_{S6}+ P_{S4}+ P_{S2}). It can be observed from the simulation results that the algorithm maintains the active power balancing criteria in islanded mode (P_{BESS}= P_{ST}- P_{LT}). So the algorithm can maintain the active power balancing criteria in any power imbalance cases.

The active powers of MFMG are balanced if different frequency incoming powers at MF bus match with the outgoing powers. To examine the power balancing criteria, the different frequency incoming active powers are compared with the different frequency outgoing powers at the MF bus. For this total incoming DC (P_{M-0-S}= P_{S6-0}+ P_{S4-0}+ P_{S2-0}+ $P_{S6-BESS}$), 25 Hz and 50 Hz active powers are calculated and conferred in Fig. 6.6 (b). It can be observed from Fig. 6.6 (b), Fig. 6.5 (b), and Fig. 6.3 (a) that every incoming frequency power matches with that frequency outgoing power at MF bus. So, $P_{M-0-S} = P_{L3} + P_{BESS-0}$, $P_{M-25-S} = P_{L7} + P_{BESS-25}$, $P_{M-50-S} = P_{L5} + P_{BESS-50}$ and $P_{S6} \neq P_{L3}$, $P_{S4} \neq P_{L7}$, $P_{S2} \neq P_{L5}$. So it is stated from the results that if the MFMG obeys the power balancing criteria then the

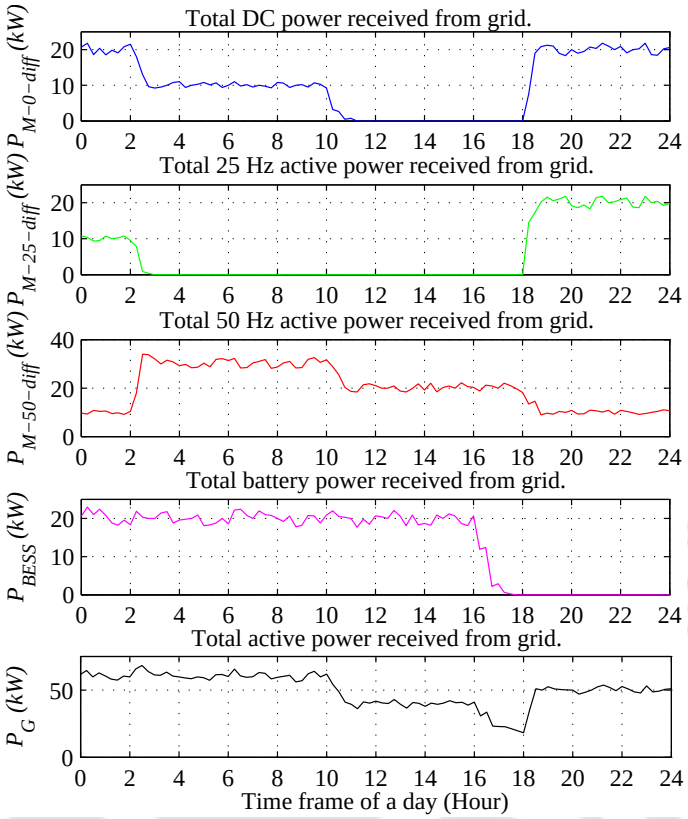

Figure 6.7: Output power of the grid side converter (P_G) which is converted to different frequency active powers (P_G= $P_{M-0-diff}$+ $P_{M-25-diff}$+ $P_{M-50-diff}$+ P_{BESS}) and transmitted to bus 1.

different frequency active powers are balanced at MF bus. So, the criteria is well defined.

6.5.2 Grid Connected Mode

Next, the MFMG is simulated in grid connected mode. As per the algorithm, here grid balances different frequency source-load pair active power differences and charges the battery. The total grid connected time is chosen as 24 hours for simulation purpose. In this case, the BESS only takes power from the main grid and is charged. The BESS is disconnected from the circuit when the SOC level climbs to 80%.

Simulation results for grid connected MFMG with different operating conditions are presented in Fig. 6.7. Between 00:00-02:00, $P_{M-0-diff} = 20\,kW$, $P_{M-25-diff} = 10\,kW$, $P_{M-50-diff} = 10\,kW$, and $P_{BESS} = 20\,kW$. As per the algorithm, the grid supplies a total of 60 kW active power which is converted to the different frequency required load power by grid side converter.

In between 10:00-16:00, the grid delivers 40 kW active power (20 kW 50 Hz + 20 kW BESS power). At 16:00, the battery is disconnected from the MF bus as the battery SOC level climbs to 80%. From 16:00-18:00, the grid produces 20 kW power to balance the 50 Hz load. Between 18:00-24:00, the grid generated 50 kW power which is transformed to 20 kW DC, 20 kW 25 Hz, and 10 kW 50 Hz active powers to balance the loads. It can be seen from simulation results that the algorithm maintains the active power balancing condition ($P_G = \sum_{f=1}^{n} P_{M-f-diff} + P_{BESS}$) for grid connected mode so the algorithm works perfectly.

6.6 Conclusion

Due to the presence of multiple frequency active powers on the MF bus, the integration of ESS with MFMG is challenging but possible. With ESS, MFMG can be operated in two more power imbalance cases, so the reliability of the system increases. For all these cases, a control algorithm is proposed to coordinate between the sources and the battery to achieve different frequency active power balance of MFMG. Different power imbalance case studies are performed in the Simulink environment to elaborate on the effectiveness of the algorithm. In every case, the algorithm achieves the power balancing criteria and controls ESS in a way to balance different frequency active powers of MFMG. In grid connected mode, the ESS is charged and the grid maintains the active power balance of MFMG as per the algorithm. So it can be concluded that the algorithm is properly designed for both islanded and grid connected modes. The source side converters and the BESS converter properly follow the algorithm so, all controllers of these converters are perfectly designed.

Note: Major part of this chapter is reproduced from my publications:

1. R. Dey and S. Nath, "Cooperative active power management in multifrequency microgrid with an energy storage system based on distance of source to load," *IEEE Access*, vol. 10, pp. 120398 –120411, May 2022. doi: 10.1109/ACCESS.2022.3177208.

7

Conclusion and Future Scope

Contents

7.1 Conclusion

Any MF system has several advantages and many new features over conventional systems. MFMG can use these new features and bring many advantages over AC, DC, or hybrid microgrid. First, the basic laws behind the formation of MFMG are studied in this thesis. The orthogonal power flow theory for different frequency active and reactive powers for a single phase and three phase MF systems are mathematically proved. It can be seen that different frequency active and reactive powers are orthogonal to each other and can flow on a single conductor without mixing through different power channels. At the load side, a new control technique is introduced so that the consumer can choose any available frequency power from the MF bus. It can be observed from simulation results that consumers can choose any available frequency power and shift between different power channels throughout the day. So both orthogonal power flow theory and frequency selectivity criteria can be applied to any MF system. Based on these theories the MFMG can be constructed which has several advantages over traditional microgrids like higher efficiency, higher flexibility, and lower size.

The basic architecture of the MFMG is proposed in this thesis with three different frequency sources, loads, and battery. The DC/MF converter is used as a building block of the MFMG architecture. The control strategies of DC/MF converter to act as grid side, grid feeding, grid forming, load side, and battery side converter are properly explained. The DC/MF converter structure is proposed and the modelling of the DC/MF converter is executed through the state space analysis method. The converter structure is verified by open loop hardware and simulation results. It can be seen from the results that the output voltage of the DC/MF converter changes as per change in input voltage, duty ratio, and load. So the modelling of the converter is satisfactory and the converter is able to generate MF voltage from DC voltage. Based on the small signal model, transfer functions for different controllers are designed for closed loop voltage and current control of the DC/MF converter. To verify the control strategies and controller designs, a DC/MF converter model is simulated in the close loop in Matlab Simulink. The simulation results show that the converter is able to control the output voltage and current

with several input variations. So it can be concluded that all controllers and control strategies are perfectly designed. The DC/MF converter acts as grid side, grid forming, grid feeding, and load side converter of MFMG and can be used as a building block of MFMG architecture.

In MFMG, the orthogonal power flow theory and frequency selectivity criteria create several new active and reactive power imbalance situations. In this thesis, all these cases are investigated for islanded and grid connected modes. For three different frequency powers, total six power imbalance cases are identified for islanded mode and power balancing criteria is defined for all the cases. Based on the criteria, a power balancing strategy is proposed to balance different frequency active and reactive powers by controlling the output currents of grid feeding converters. In grid connected mode, the control of the grid side converter is carried in such a way that grid balances the different frequency powers of MFMG to improve power quality and stability. To validate these strategies, a simulation model of MFMG is prepared and simulation of this model is executed for islanded and grid connected modes in the Matlab Simulink environment taking three different power imbalance cases. It can be noticed from the results that different frequency active and reactive power balance is achieved for all three cases. So it can be concluded that the active and reactive power balancing criteria for all the cases are well defined. The proposed active and reactive power balancing strategies are working fine and generate the required output current references for grid side and grid feeding converters. The grid side and grid feeding converters generate the required output current as per the reference so, all controllers and compensators are working properly.

To increase the stability and reliability of MFMG, an ESS is integrated with MFMG. The battery side converter control strategy is explained and it has been found that several new power imbalance cases are created due to the addition of the ESS unit. To balance the different frequency active powers with ESS, an algorithm is proposed which coordinates between different frequency sources and ESS and generates references for grid side, grid feeding, and battery side converters. Next, different power imbalance case studies are performed in the Simulink environment to elaborate on the effectiveness of the algorithm. In islanded mode, the algorithm achieves the power balancing for every power imbalance case and accordingly the

ESS is charged or discharged. In grid connected mode, the power balancing is achieved and the grid balances the different frequency active power differences and charges the ESS. From all the simulation results it can be concluded that the power balancing algorithm is properly designed for grid connected and islanded modes. The battery side converter is able to exchange different frequency active powers with the MF bus as per the requirement, so the control strategy of the battery side converter is suitable.

7.2 Future Scope

The future scopes of the thesis which are worth to explore are-

- The power balancing algorithm which is proposed in the thesis is based on the physical distance between the source and load to minimize the power loss. In the future, different other aspects like cost, reliability, and availability of the sources may be considered and accordingly, new algorithms can be proposed. The same power balancing strategy can be applied to microgrid clusters where some microgrids act like loads and other microgrids act as sources.

- In MFMG, all sources and loads are dedicatedly connected by the MF bus through different power channels. So any load can take power from any available source and source recognition is possible. With all the new features, the sensitivity analysis of the MFMG is another important topic to explore.

- Frequency selective power transmission of MFMG can create an open market at the distribution side. Different powers can be categorized based on cost, availability, or quality of the sources. Different generation companies can broadcast their powers using different assigned frequency channels and consumers can select any of those channels and can shift between different channels throughout the day depending on their needs. The future power market can be constructed based on this concept.

- In the future, the real time simulation of MFMG can be done on OPAL-RT simulator. The proposed control strategy for grid side, grid feeding, grid forming, and load side

converter can be implemented on that. The power balancing strategies can be verified by using this simulator.

References

[1] D. Semnov, G. Mirzaeva, C. D. Townsend, and G. C. Goodwin, "An ac microgrid architecture and control strategy to achieve stability with any type of load," in *proceedings of IEEE Southern Power Electronics Conference (SPEC)*, 2017, pp. 1–6.

[2] D. Kumar, F. Zare, and A. Ghosh, "Dc microgrid technology: System architectures, ac grid interfaces, grounding schemes, power quality, communication networks, applications, and standardizations aspects," *IEEE Access*, vol. 5, pp. 12 230–12 256, June 2017.

[3] Z. Yuan, S. W. de Haan, J. B. Ferreira, and D. Cvoric, "A facts device: Distributed power-flow controller (dpfc)," *IEEE Transactions on Power Electronics*, vol. 25, no. 10, pp. 2564–2572, May 2010.

[4] K. V. Chandrika and P. Venkatesh, "Simulation of distributed interline power flow controller (dipfc) for power quality improvement in distribution system," *International Electrical Engineering Journal (IEEJ)*, vol. 5, no. 12, pp. 1673–1679, 2014.

[5] M. Rezkallah, A. Chandra, B. Singh, and S. Singh, "Microgrid: Configurations, control and applications," *IEEE Transactions on Smart Grid*, vol. 10, no. 2, pp. 1290–1302, Oct. 2019.

[6] J. J. Justo, F. Mwasilu, J. Lee, and J.-W. Jung, "Ac-microgrids versus dc-microgrids with distributed energy resources: A review," *Renewable and Sustainable Energy Review*, vol. 24, pp. 387–405, 2013.

[7] M. Ganjian-Aboukheili, M. Shahabi, Q. Shafiee, and J. M. Guerrero, "Seamless transition of microgrids operation from grid-connected to islanded mode," *IEEE Transactions on Smart Grid*, vol. 11, no. 3, pp. 2106–2114, Oct. 2020.

[8] H. Lotfi and A. Khodaei, "Ac versus dc microgrid planning," *IEEE Transactions on Smart Grid*, vol. 8, no. 1, pp. 296–304, Aug. 2015.

[9] H. Han, X. Hou, J. Yang, J. Wu, M. Su, and J. M. Guerrero, "Review of power sharing control strategies for islanding operation of ac microgrids," *IEEE Transactions on Smart Grid*, vol. 7, no. 1, pp. 200–215, June 2015.

[10] M. Faisal, M. A. Hannan, P. J. Ker, A. Hussain, M. B. Mansor, and F. Blaabjerg, "Review of energy storage system technologies in microgrid applications: Issues and challenges," *IEEE Access*, vol. 6, pp. 35 143–35 164, May 2018.

[11] S. K. Sahoo, A. K. Sinha, and N. Kishore, "Control techniques in ac, dc, and hybrid ac–dc microgrid: A review," *IEEE Journal of Emerging and Selected Topics in Power Electronics*, vol. 6, no. 2, pp. 738–759, June 2017.

[12] L. He, Y. Li, J. M. Guerrero, and Y. Cao, "A comprehensive inertial control strategy for hybrid ac/dc microgrid with distributed generations," *IEEE Transactions on Smart Grid*, vol. 11, no. 2, pp. 1737–1747, Mar. 2020.

[13] S. Beheshtaein, R. M. Cuzner, M. Forouzesh, M. Savaghebi, and J. M. Guerrero, "Dc microgrid protection: A comprehensive review," *IEEE Journal of Emerging and Selected Topics in Power Electronics*, pp. 1–1, Mar. 2019.

[14] J. Rocabert, A. Luna, F. Blaabjerg, and P. Rodrguez, "Control of power converters in ac microgrids," *IEEE Transactions on Power Electronics*, vol. 27, no. 11, pp. 4734–4749, May 2012.

[15] A. Gupta, S. Doolla, and K. Chatterjee, "Hybrid acdc microgrid: Systematic evaluation of control strategies," *IEEE Transactions on Smart Grid*, vol. 9, no. 4, pp. 3830–3843, July 2018.

[16] P. Bajpai and S. Singh, "An electric power trading model for indian electricity market," in *proceedings of 2006 IEEE Power Engineering Society General Meeting.* IEEE, 2006, pp. 5–pp.

[17] A. Saranya, P. Verma, T. Vidyamani, and K. S. Swarup, "Data analytics for statistical characterization of prices and empirical resource investment planning in indian electricity market," in *proceedings of 2018 20th National Power Syst. Conf. (NPSC).* IEEE, 2018, pp. 1–6.

[18] S. Brüske, G. De Carne, and M. Liserre, "Multi-frequency power transfer in a smart transformer based distribution grid," in *proceedings of IECON 2014-40th Annual Conference of the IEEE Industrial Electronics Society*, Oct. 2014, pp. 4325–4331.

[19] K. Terada, "Application and economical evaluation of the superposed ac and dc power transmission system," *Electrical Engineering Japan*, vol. 98, no. 1, 1978.

[20] R. Alaei and S. A. Khajehoddin, "The operation of a power transmission line with injected third harmonic voltage," *IEEE Transactions on Power Delivery*, vol. 32, no. 1, pp. 226–233, Nov. 2016.

[21] S. Brske, G. Buticchi, and M. Liserre, "Multifrequency single-phase islanded grids," *IEEE Transactions on Industrial Electronics*, vol. 65, no. 12, pp. 9528–9538, Mar. 2018.

[22] P. A. Madduri, J. Poon, J. Rosa, M. Podolsky, E. A. Brewer, and S. R. Sanders, "Scalable dc microgrids for rural electrification in emerging regions," *IEEE Journal of Emerging and Selected Topics in Power Electronics*, vol. 4, no. 4, pp. 1195–1205, May 2016.

[23] P. Wang, X. Liu, C. Jin, P. Loh, and F. Choo, "A hybrid ac/dc micro-grid architecture, operation and control," in *proceedings of IEEE Power and Energy Society General Meeting*, 2011, pp. 1–8.

[24] M. Ahmed, L. Meegahapola, M. Datta, and A. Vahidnia, "A novel hybrid ac/dc microgrid architecture with a central energy storage system," *IEEE Transactions on Power Delivery*, vol. 37, no. 3, pp. 2060–2070, Aug. 2022.

[25] M. Ahmed, L. Meegahapola, A. Vahidnia, and M. Datta, "Stability and control aspects of microgrid architecturesa comprehensive review," *IEEE Access*, vol. 8, pp. 144 730–144 766, Aug. 2020.

[26] S. Akshatha, C. Arun, V. Abhijith, and B. Fernandes, "A unified ac-dc microgrid architecture for distribution of ac and dc power on the same line," in *proceedings of IEEE Appllied Power Electronics Conference and Exposition (APEC)*, Mar. 2017, pp. 430–433.

[27] L. Gu and K. Jin, "A three-phase isolated bidirectional ac/dc converter and its modified svpwm algorithm," *IEEE Transactions on Power Electronics*, vol. 30, no. 10, pp. 5458–5468, Dec. 2015.

[28] R. Carballo, R. Nunez, V. H. Kurtz, and F. Botteron, "Design and implementation of a three-phase dc-ac converter for microgrids based on renewable energy sources," *IEEE Latin America Transactions*, vol. 11, no. 1, pp. 112–118, Feb. 2013.

[29] J. Khodabakhsh, E. Mohammadi, and G. Moschopoulos, "Pmsg-based wind energy conversion systems integration into dc microgrids with a novel compact converter," *IEEE Access*, vol. 8, pp. 83 583–83 595, May 2020.

[30] R. Majumder, "A hybrid microgrid with dc connection at back to back converters," *IEEE Transactions on Smart Grid*, vol. 5, no. 1, pp. 251–259, June 2014.

[31] L. Wang, X. Fu, and M.-C. Wong, "Operation and control of a hybrid coupled interlinking converter for hybrid ac/low voltage dc microgrids," *IEEE Transactions on Industrial Electronics*, vol. 68, no. 8, pp. 7104–7114, June 2021.

[32] X. Guo, L. Wang, Y. Zhao, G. Wang, G. Liu, and Q. Zhong, "Reliability-oriented selection for grid-connected converters: A low voltage direct current microgrid case study," *IEEE Access*, vol. 8, pp. 205 836–205 847, Nov. 2020.

[33] J. Banda and K. Siri, "Improved central-limit control for parallel-operation of dc-dc power converters," in *proceedings of PESC'95-Power Electronics Specialist Conference IEEE*, vol. 2, June 1995, pp. 1104–1110.

[34] X. Meng, N. Zhou, Q. Wang, and J. M. Guerrero, "A nonlinear, bounded and lipchitz continuous distributed active power sharing control method for islanded ac microgrids," *IEEE Access*, vol. 7, pp. 36 843–36 853, Feb. 2019.

[35] E. Luo, P. Cong, H. Lu, and Y. Li, "Two-stage hierarchical congestion management method for active distribution networks with multi-type distributed energy resources," *IEEE Access*, vol. 8, pp. 120 309–120 320, June 2020.

[36] M. S. Golsorkhi and D. D. C. Lu, "A control method for inverter-based islanded microgrids based on v-i droop characteristics," *IEEE Transactions on Power Delivery*, vol. 30, no. 3, pp. 1196–1204, Sep. 2015.

[37] M. D. Cook, G. G. Parker, R. D. Robinett, and W. W. Weaver, "Decentralized mode-adaptive guidance and control for dc microgrid," *IEEE Transactions on Power Delivery*, vol. 32, no. 1, pp. 263–271, June 2017.

[38] D. Chen, L. Xu, and L. Yao, "Dc voltage variation based autonomous control of dc microgrids," *IEEE Transactions on Power Delivery*, vol. 28, no. 2, pp. 637–648, Feb. 2013.

[39] A. Kirakosyan, E. F. El-Saadany, M. S. E. Moursi, A. H. Yazdavar, and A. Al-Durra, "Communication-free current sharing control strategy for dc microgrids and its application for ac/dc hybrid microgrids," *IEEE Transactions on Power Systems*, vol. 35, no. 1, pp. 140–151, June 2020.

[40] J.-O. Lee, Y.-S. Kim, and S.-I. Moon, "Novel supervisory control method for islanded droop-based ac/dc microgrids," *IEEE Transactions on Power Systems*, vol. 34, no. 3, pp. 2140–2151, Dec. 2019.

[41] L. N. Khanh, J.-J. Seo, Y.-S. Kim, and D.-J. Won, "Power-management strategies for a grid-connected pv-fc hybrid system," *IEEE Transactions on Power Delivery*, vol. 25, no. 3, pp. 1874–1882, May 2010.

[42] H. Mahmood, D. Michaelson, and J. Jiang, "Reactive power sharing in islanded microgrids using adaptive voltage droop control," *IEEE Transactions on Smart Grid*, vol. 6, no. 6, pp. 3052–3060, Apr. 2015.

[43] A. Mortezaei, M. G. Simes, M. Savaghebi, J. M. Guerrero, and A. Al-Durra, "Cooperative control of multi-masterslave islanded microgrid with power quality enhancement based on conservative power theory," *IEEE Transactions on Smart Grid*, vol. 9, no. 4, pp. 2964–2975, Nov. 2018.

[44] A. Shaker, A. Safari, and M. Shahidehpour, "Reactive power management for networked microgrid resilience in extreme conditions," *IEEE Transactions on Smart Grid*, pp. 3940–3953, Mar. 2021.

[45] Z. Liu, J. Yang, Y. Zhang, T. Ji, J. Zhou, and Z. Cai, "Multi-objective coordinated planning of active-reactive power resources for decentralized droop-controlled islanded microgrids based on probabilistic load flow," *IEEE Access*, vol. 6, pp. 40 267–40 280, July 2018.

[46] H.-J. Yoo, T.-T. Nguyen, and H.-M. Kim, "Consensus-based distributed coordination control of hybrid ac/dc microgrids," *IEEE Transactions on Sustainable Energy*, vol. 11, no. 2, pp. 629–639, Feb. 2020.

[47] N. Eghtedarpour and E. Farjah, "Power control and management in a hybrid ac/dc microgrid," *IEEE Transactions on Smart Grid*, vol. 5, no. 3, pp. 1494–1505, Apr. 2014.

[48] X. Li and S. Wang, "Energy management and operational control methods for grid battery energy storage systems," *CSEE Journal of Power and Energy Systems*, vol. 7, no. 5, pp. 1026–1040, June 2021.

[49] G. O. Suvire, M. G. Molina, and P. E. Mercado, "Improving the integration of wind power generation into ac microgrids using flywheel energy storage," *IEEE Transactions on Smart Grid*, vol. 3, no. 4, pp. 1945–1954, Sep. 2012.

[50] J. Wu, X. Xing, X. Liu, J. M. Guerrero, and Z. Chen, "Energy management strategy for grid-tied microgrids considering the energy storage efficiency," *IEEE Transactions on Industrial Electronics*, vol. 65, no. 12, pp. 9539–9549, Mar. 2018.

[51] F. A. Inthamoussou, J. Pegueroles-Queralt, and F. D. Bianchi, "Control of a supercapacitor energy storage system for microgrid applications," *IEEE Transactions on Energy Conversion*, vol. 28, no. 3, pp. 690–697, May. 2013.

[52] A. Berrueta, A. Soto, J. Marcos, i. de la Parra, P. Sanchis, and A. Ursa, "Identification of critical parameters for the design of energy management algorithms for li-ion batteries operating in pv power plants," *IEEE Transactions on Industry Applications*, vol. 56, no. 5, pp. 4670–4678, June 2020.

[53] Q. Wu, R. Guan, X. Sun, Y. Wang, and X. Li, "Soc balancing strategy for multiple energy storage units with different capacities in islanded microgrids based on droop control," *IEEE Journal of Emerging and Selected Topics in Power Electronics*, vol. 6, no. 4, pp. 1932–1941, Jan. 2018.

[54] N. L. Daz, J. C. Vasquez, and J. M. Guerrero, "A communication-less distributed control architecture for islanded microgrids with renewable generation and storage," *IEEE Transactions on Power Electronics*, vol. 33, no. 3, pp. 1922–1939, Apr. 2018.

[55] J. Jiang, S. Peyghami, C. Coates, and F. Blaabjerg, "A decentralized reliability-enhanced power sharing strategy for pv-based microgrids," *IEEE Transactions on Power Electronics*, vol. 36, no. 6, pp. 7281–7293, Nov. 2021.

[56] R. Al Badwawi, W. R. Issa, T. K. Mallick, and M. Abusara, "Supervisory control for power management of an islanded ac microgrid using a frequency signalling-based fuzzy logic controller," *IEEE Transactions on Sustainable Energy*, vol. 10, no. 1, pp. 94–104, Apr. 2019.

[57] X. Lu, K. Sun, J. M. Guerrero, J. C. Vasquez, and L. Huang, "Double-quadrant state-of-charge-based droop control method for distributed energy storage systems in autonomous dc microgrids," *IEEE Transactions on Smart Grid*, vol. 6, no. 1, pp. 147–157, Sep. 2015.

[58] X. Lin, R. Zamora, and C. A. Baguley, "A fully filter-based decentralized control with state of charge balancing strategy for battery energy storage systems in autonomous dc microgrid applications," *IEEE Access*, vol. 9, pp. 15 028–15 040, Jan. 2021.

[59] K. D. Hoang and H.-H. Lee, "Accurate power sharing with balanced battery state of charge in distributed dc microgrid," *IEEE Transactions on Industrial Electronics*, vol. 66, no. 3, pp. 1883–1893, May 2019.

[60] X. Li, Z. Li, L. Guo, J. Zhu, Y. Wang, and C. Wang, "Enhanced dynamic stability control for low-inertia hybrid ac/dc microgrid with distributed energy storage systems," *IEEE Access*, vol. 7, pp. 91 234–91 242, July 2019.

[61] P. C. Loh, D. Li, Y. K. Chai, and F. Blaabjerg, "Autonomous control of interlinking converter with energy storage in hybrid ac-dc microgrid," *IEEE Transactions on Industry Applications*, vol. 49, no. 3, pp. 1374–1382, Mar. 2013.

[62] X. Pan, L. Zhang, J. Xiao, F. H. Choo, A. K. Rathore, and P. Wang, "Design and implementation of a communication network and operating system for an adaptive integrated hybrid ac/dc microgrid module," *CSEE Journal of Power and Energy Systems*, vol. 4, no. 1, pp. 19–28, Mar. 2018.

[63] Z. Liu, H. Fan, C. Mao, D. Wang, and Z. Sang, "Tie-line power control of islanded microgrid cluster based on coordinated operation of thermostatically controlled load and battery," in *proceedings of 11th International Conference on Power and Energy Systems (ICPES)*, 2021, pp. 506–512.

[64] Z. Yuan, S. W. de Haan, J. B. Ferreira, and D. Cvoric, "A facts device: Distributed power-flow controller (dpfc)," *IEEE Transactions on power electronics*, vol. 25, no. 10, pp. 2564–2572, May 2010.

[65] Z. Pantic, K. Lee, and S. M. Lukic, "Multifrequency inductive power transfer," *IEEE Transactions on Power Electronics*, vol. 29, no. 11, pp. 5995–6005, Jan. 2014.

[66] J. A. Ferreira, "Nestled secondary power loops in multilevel modular converters," in *proceedings of IEEE Control and Model for Power Electronics (COMPEL),15th Workshop*, 2014, pp. 1–9.

[67] S. Brüske, G. Buticchi, and M. Liserre, "Multifrequency single-phase islanded grids," *IEEE Transactions on Industrial Electronics*, vol. 65, no. 12, pp. 9528–9538, Mar. 2018.

[68] V. Chitransh, A. Shetty, A. K. Das, J. O. Ojo, M. Veerachary, B. G. Fernandes, and J. A. Ferreira, "Evaluation of multi-frequency power electronic converters: Concept, architectures and realization," *IEEE Journal of Emerging and Selected Topics in Power Electronics*, pp. 1–1, Aug. 2020.

[69] V. Chitransh and M. Veerachary, "Multi-frequency power system for renewable source integration in smart grid," *IET Power Electronics*, vol. 12, no. 7, pp. 1800–1808, 2019.

[70] M. Gagic, I. Pecelj, Z. Qin, and J. Ferreira, "Control of load interfacing power electronics converter in multifrequency systems," in *proceedings of IEEE 10th International Conference on Power Electronics and ECCE Asia (ICPE 2019-ECCE Asia)*, May 2019, pp. 1574–1580.

[71] R. V. A. Neves, R. Q. Machado, V. A. Oliveira, X. Wang, and F. Blaabjerg, "Multitask fuzzy secondary controller for ac microgrid operating in stand-alone and grid-tied mode," *IEEE Transactions on Smart Grid*, vol. 10, no. 5, pp. 5640–5649, Dec. 2019.

[72] V. Z. Manusov and V. V. Khripkov, "Comparative analysis of mathematical models for the coefficient of conductor resistance increase due to higher harmonics," in *2018 XIV International Scientific-Technical Conference on Actual Problems of Electronics Instrument Engineering (APEIE)*. IEEE, 2018, pp. 133–136.

[73] R. D. Middlebrook and S. Cuk, "A general unified approach to modelling switching-converter power stages," in *proceedings of IEEE Power Electronics Specialists Conference*, 1976, pp. 18–34.

[74] R. H. Tan and L. Y. H. Hoo, "Dc-dc converter modeling and simulation using state space approach," in *proceedings of IEEE Conference on Energy Conversion (CENCON)*, 2015, pp. 42–47.

[75] T. Dars Fernandes, C. Galup-Montoro, and M. C. Schneider, "Analysis and design of the three-inverter schmitt trigger for supply voltages down to 50 mv," *IEEE Transactions on Circuits and Systems II: Express Briefs*, vol. 68, no. 7, pp. 2302–2306, July. 2021.

[76] J. M. Guerrero, P. C. Loh, T.-L. Lee, and M. Chandorkar, "Advanced control architectures for intelligent microgrids part ii: Power quality, energy storage, and ac/dc microgrids," *IEEE Transactions on Industrial Electronics*, vol. 60, no. 4, pp. 1263–1270, Apr. 2013.

[77] A. Eales, A. Alsop, D. Frame, S. Strachan, and S. Galloway, "Assessing the market for solar photovoltaic (pv) microgrids in malawi," *Hapres Journal of Sustainability Research*, vol. 2, no. 1, Feb. 2020.

[78] I. Buchmann, "Bu-808: How to prolong lithium-based batteries," *How to Prolong Lithium-Based Batteries-Battery University, Cadex Electronics Inc., batteryuniversity. com/learn/article/how_to_prolong_lithium_based_batteries*, 2003.

[79] M. Kumar, S. Srivastava, and S. Singh, "Control strategies of a dc microgrid for grid connected and islanded operations," *IEEE Transactions on Smart Grid*, vol. 6, no. 4, pp. 1588–1601, 2015.

[80] R. Ahshan, S. A. Saleh, and A. Al-Badi, "Performance analysis of a dq power flow-based energy storage control system for microgrid applications," *IEEE Access*, vol. 8, pp. 178 706–178 721, Sep. 2020.

[81] M. Faisal, M. A. Hannan, P. J. Ker, and M. N. Uddin, "Backtracking search algorithm based fuzzy charging-discharging controller for battery storage system in microgrid applications," *IEEE Access*, vol. 7, pp. 159 357–159 368, Nov. 2019.

LIST OF PUBLICATIONS

Journal Publications:

Published

1. R. Dey and S. Nath, "Cooperative active power management in multifrequency microgrid with an energy storage system based on distance of source to load," in *IEEE Access*, vol. 10, pp. 120398 –120411, May 2022. doi: 10.1109/ACCESS.2022.3177208.

Submitted

1. R. Dey, S. Nath, "Control and management of different frequency active powers for multifrequency microgrid ," in *Sustainable Energy Grid and Networks, ELSEVIER.*

Conference Publications:

Published

1. R. Dey and S. Nath, "Orthogonality of different frequency reactive powers in multifrequency system," *2021 National Power Electronics Conference (NPEC)*, Bhubaneswar, India, 2021, pp. 1–6, doi: 10.1109/NPEC52100.2021.9672536.

2. R. Dey and S. Nath, "Grid interactive converter of multifrequency microgrid," *2021 National Power Electronics Conference (NPEC)*, Bhubaneswar, India, 2021, pp. 1–6, doi: 10.1109/NPEC52100.2021.9672542.

3. R. Dey and S. Nath, "A new active and reactive power control strategy for multifrequency microgrid in islanded mode," *2021 5th International Conference on Smart Grid and Smart Cities (ICSGSC)*, Tokyo, Japan, 2021, pp. 45–49, doi: 10.1109/ICSGSC52434.2021.9490493.

4. R. Dey and S. Nath, "A new power distribution concept for multifrequency microgrid," *2021 IEEE 12th Energy Conversion Congress Exposition - Asia (ECCE-Asia)*, Singapore, Singapore, 2021, pp. 491–496, doi: 10.1109/ECCE-Asia49820.2021.9479014.

5. R. Dey and S. Nath, "Architecture and power converter for multifrequency microgrid," *2019 IEEE National Power Electron. Conf.(NPEC)*, Tiruchirappalli, India, Dec. 2019, pp. 1–6, doi: 10.1109/NPEC47332.2019.9034700.

6. R. Dey and S. Nath, "A simplified charge balancing algorithm for modular multilevel converter," *2017 IEEE PES Asia-Pacific Power and Energy Engineering Conference (APPEEC)*, Bangalore, India, 2017, pp. 1–6, doi: 10.1109/APPEEC.2017.8308940.